Unclassified
SECURITY CLASSIFICATION OF THIS PAGE (When Data Entered)

AD A051954

REPORT DOCUMENTATION PAGE

READ INSTRUCTIONS BEFORE COMPLETING FORM

1. REPORT NUMBER: 1
2. GOVT ACCESSION NO.
3. RECIPIENT'S CATALOG NUMBER

4. TITLE (and Subtitle): CROSS SPECTRAL ANALYSIS OF ACOUSTIC SIGNALS.
5. TYPE OF REPORT & PERIOD COVERED: Interim rept.
6. PERFORMING ORG. REPORT NUMBER

7. AUTHOR(s): Allan L. Gutjahr, Charles R. Holmes
8. CONTRACT OR GRANT NUMBER(s): N00014-75-C-0169

9. PERFORMING ORGANIZATION NAME AND ADDRESS: New Mexico Institute of Min. & Tech. Research & Development Div. Campus Station Socorro New Mexico, 87801
10. PROGRAM ELEMENT, PROJECT, TASK AREA & WORK UNIT NUMBERS: 12 14

11. CONTROLLING OFFICE NAME AND ADDRESS: Office of Naval Research, 800 n. Quincy Street, 613: MAC, Arlington, Virginia, 22217
12. REPORT DATE: Mar[illegible]78
13. NUMBER OF PAGES: 104

14. MONITORING AGENCY NAME & ADDRESS (if different from Controlling Office): Office of Naval Research, Resident Repr. Univ. of Arizona, Rm. 421, Space Sci. Bl[illegible] Tucson, Arizona, 85721
15. SECURITY CLASS (of this report): unclassified
15a. DECLASSIFICATION/DOWNGRADING SCHEDULE

16. DISTRIBUTION STATEMENT (of this Report): distribution is unlimited

DISTRIBUTION STATEMENT A
Approved for public release;
Distribution Unlimited

17. DISTRIBUTION STATEMENT (of the abstract entered in Block 20, if different from Report): same

DDC RECEIVED

18. SUPPLEMENTARY NOTES

19. KEY WORDS (Continue on reverse side if necessary and identify by block number)
cross-spectral analysis
acoustics of thunder

20. ABSTRACT (Continue on reverse side if necessary and identify by block number)
This report presents a detailed analytical treatment of a cross-spectral technique for the use of the acoustic signals of thunder for lightning location. The report also contains application of this technique to location of C-4 and Prima-Cord explosive shots and to lightning location.

AD No. DDC FILE COPY

DD FORM 1 JAN 73 1473 EDITION OF 1 NOV 65 IS OBSOLETE
S/N 0102-014-6601

Unclassified
SECURITY CLASSIFICATION OF THIS PAGE (When Data Entered)

CROSS-SPECTRAL ANALYSIS OF ACOUSTIC SIGNALS

Allan L. Gutjahr, mathematics department
Charles R. Holmes, physics department
New Mexico Institute of Mining and Technology

I. INTRODUCTION

The spectrum of thunder contains a considerable amount of information about the thunder signal as well as information about the lightning which is presumed to be the cause of the thunder. Holmes, et al. (1971), McCrory (1969), and Few (1968, 1969), among others, have analyzed the acoustic signal generated by thunder. Although the shape of the spectrum is not completely known, various aspects of the spectrum are discussed in the papers mentioned above.

The main purposes of this paper are to discuss the use of thunder for lightning location, to discuss estimation of the quantities that occur in the digital analysis of signals and to present the statistical analysis of the estimated quantities.

Most of the procedures presented here are available in the literature, but they are either described rather generally or in great mathematical detail. In either case they are often inaccessible to the practitioner who is not both a statistician and electrical engineer. In addition, the available discussions are scattered throughout the various publications, so that the problems encountered by the user are accentuated by differences in notation and terminology.

Hence, this is also an attempt to give a consistent treatment of all of the aspects mentioned above.

The following is an overview and table of contents of the paper.

I. Introduction.

II. Review of past work. This section will include a discussion of the physical models which form the basis for the work carried out in lightning location and spectral analysis. In addition, a critique of the past work in lightning location will be included.

III. Cross-spectral analysis and lightning location. This section will contain an exposition of the method of cross-spectral analysis and its use in lightning location. The location procedures and confidence intervals will also be discussed.

IV. Application of cross-spectral analysis to location of prima-cord and c-4 shots.

V. Application of cross-spectral analysis to lightning location.

The appendices will include more detailed explanations of the procedures of sections II and III. In particular, they will contain discussions of the various computer routines used, and further explanations of the formulas and procedures.

The appendices are:

A. Spectral Analysis

B. Cross-spectral Analysis

C. Variance and Covariance Calculations

D. Spherical Location Procedure

E. Plane Location Procedure

F. Additional Remarks on Spectra and Covariances

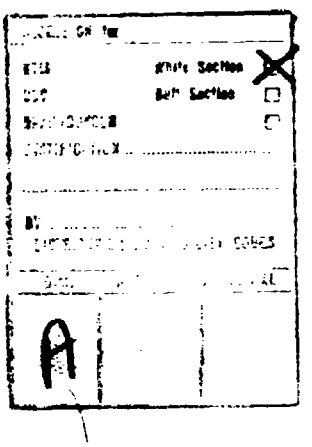

II. REVIEW OF PAST WORK AND THE PHYSICAL MODEL

The phenomenon of lightning and its relation to thunder is discussed extensively in Uman (1969), Few (1968), and McCrory (1969). We will present a brief review of the models proposed by these authors, with particular emphasis on those aspects that are relevant to our work in lightning location.

Thunder is associated with the lightning path. Various theories have been offered as to how this association occurs. One modern theory offers the explanation that thunder is due to rapid heating in the lightning channel. This rapid heating causes a shock wave which propagates radially outward. As the shock wave moves out, the shock-front pressure decreases and eventually the wave becomes a sound wave, which, after modification by the environment, becomes the audible thunder.

The lightning channel from which the thunder emanates is formed by a stepped-leader process. The name stepped-leader is derived from the fact that as the lightning channel is built from a cloud to the ground, say, it seems to move in steps of varying length, with pauses between the steps. The average step length is about 50 meters and the average duration of each step is about 50 μ-sec. Usually the resulting channel is branched. After the channel reaches the ground a rapidly moving return stroke occurs, moving from the ground to the cloud and propagating along the branches. There may be subsequent return strokes associated with dart-leaders. The dart-leaders move from the cloud to the ground along the main lightning channel and the ensuing return strokes also follow

only the main channel. It is the return strokes which cause the rapid heating, and consequently the thunder, in the model described above. Because the return stroke moves very rapidly, the source of the thunder occurs almost simultaneously along the entire channel.

The description above is for the simplest discharge to ground (called a discrete stroke - a discrete flash contains several such discrete strokes). There are also strokes (known as continuous strokes) where there is a continuing current to ground immediately after a return stroke and corresponding hybrid flashes, which consist of series of continuous strokes.

Few (1969) puts forth a "string-of-pearls" model of lightning, wherein the lightning channel supposedly behaves as a string of cylindrical sources of acoustical energy. Each cylindrical source will appear as a spherical source at large distances, where the spherical source has a radius such that it emits the same energy as the original cylindrical source.

From the theory for spherical shock waves one can then obtain a relation between distance and the dominant frequency (McCrory (1971)), and consequently one can predict where the peaks in the spectral density of thunder should occur.

Various studies of the power spectra of thunder have been carried out by Few (1968), Few, et al. (1967), McCrory (1971) and Holmes, et al. (1971). The earlier studies of Few, et al. (1967), indicated a peak in the spectrum at about 200 HZ, but more accurate estimates of the spectrum by McCrory (1971)

and Holmes, et al. (1971) show that the peaks are lower than this -- for ground flashes they measured peaks (after correction for wind-noise) in the 40 to 80 HZ range. Some attenuation occurs due to propagation through the medium, with the higher frequency portions of thunder suffering the greatest attenuation.

Accounting for the attenuation and the non-stationary nature of the spectrum of thunder, (i.e. its time dependence) Holmes, et al. (1971) and McCrory (1971), found that the power spectrum had peaks at low frequencies and that these peaks were inconsistent with the theory that thunder was caused totally by the acoustic mechanism described above. As a possible explanation, these investigators put forth the theory that a second mechanism was in operation -- this mechanism was proposed originally by Wilson (1920) and studied further by Colgate (1967) and Colgate and McKee (1969). This accounts for low frequencies by proposing an electrostatic reaction due to the collapse of the region of charge storage within the cloud at the time of lightning discharge. This indeed would account for the low frequency content of the spectrum and also is in accord with the fact that low frequencies were observed in the later part of the thunder signal.

The lightning channel is quite tortuous, even on a small scale. This tortuosity can introduce additional ripples on the spectrum as proposed by McCrory (1971). In addition, the fact that the received signal is the sum of several signals from different portions of the channel can

also introduce ripples on the spectrum. McCrory estimates this latter filtering effect, which he calls phase noise, and concludes that the tortuosity of the channel is more important than the time structure in explaining the hash or ripples that appear on the spectrum.

The exact nature of a lightning channel is still not known. Some authors have claimed that the horizontal portion of the channel which is within the cloud can be quite large in comparison to the vertical portion that is observed (Uman (1969)). Few has attempted to reconstruct the channel by recording thunder signals at different locations and then tracing back to the source by using co-variance analysis on the signals. Since our objective is to do a similar reconstruction and since the method relies rather heavily on Few's work we next give an extensive review of his procedure.

By considering the hydrodynamical conditions right after a lightning discharge, Few obtained the equations

$$(\frac{\partial}{\partial t} + v \cdot \nabla)\rho + \rho(\nabla \cdot v) = 0 \tag{1}$$

$$(\frac{\partial}{\partial t} + v \cdot \nabla)v + g\vec{z} + \rho^{-1} \nabla P = 0 \tag{2}$$

$$(\frac{\partial}{\partial t} + v \cdot \nabla)P + \gamma P(\nabla \cdot v) = 0. \tag{3}$$

ρ is the density, P the pressure, v the velocity vector of the sound wave, $\vec{z}$ is a unit vector in the z (vertical) direction, g the force of gravity and γ is the ratio of the specific heat of the gas at constant pressure to the specific heat at constant volume. The equations (1), (2), and (3) correspond

respectively, to conservation of mass, momentum and energy.

If the quantities v, ρ and P are written as a steady state term plus a perturbed term we have, after renormalizing,

$$v(r,t) = v_0(r) + c\, v_1(r,t) \tag{4}$$

$$\rho(r,t) = \rho_0(r)[1 + \rho_1(r,t)] \tag{5}$$

$$P(r,t) = P_0(r)[1 + P_1(r,t)]. \tag{6}$$

If (4) through (6) are substituted into the previous equations and if the perturbed terms are set equal to 0, one obtains

$$(\frac{\partial}{\partial t} + v_0 \cdot \nabla)\rho_1 - (c/H)(v_1 \cdot \vec{z}) + c\,\nabla \cdot v_1 = 0 \tag{7}$$

$$(\frac{\partial}{\partial t} + v_0 \cdot \nabla)v_1 + (g/c)\rho_1 \vec{z} + (c/\gamma)\nabla \cdot P_1 - c(\gamma H)^{-1} P_1 = 0 \tag{8}$$

$$(\frac{\partial}{\partial t} + v_0 \cdot \nabla)P_1 - (c/H)v_1 \cdot \vec{z} + (c/\gamma)\nabla \cdot v_1 = 0. \tag{9}$$

c is the adiabatic speed of sound and H is the scale height of the atmosphere. These results are obtained by first solving the steady state equations.

Finally expanding ρ_1, P_1 and v_1 in wave-number space we have

$$\rho_1(r,t) = \iiint_{-\infty}^{\infty} \rho_{10}(k)e^{i[k\cdot(r-v_0t) - \omega t]}\, dk_1dk_2dk_3 \tag{10}$$

$$P_1(r,t) = \iiint_{-\infty}^{\infty} P_{10}(k)e^{i[k\cdot(r-v_0t) - \omega t]}\, dk_1dk_2dk_3 \tag{11}$$

$$v_1(r,t) = \iiint_{-\infty}^{\infty} v_{10}(k)e^{i[k\cdot(r-v_0t) - \omega t]}\, dk_1dk_2dk_3. \tag{12}$$

In equations (10) - (12) ω is the angular frequency. If these equations are substituted into equation (7) through (9), 4 homogeneous equations involving P_{10}, ρ_{10} and horizontal and vertical components of v_{10} are obtained. If this system is to have a unique solution, the determinant of the coefficients must be zero. The resulting determinant involves ω, k and $\omega_g \equiv (\gamma - 1)g/(\gamma H)$. If ω_g, which is quite small, is ignored, one obtains the result that $\omega^2 = c^2\, k \cdot k$. Finally, ignoring gravity terms, one has

$$v_{10} = k\, \|k\|^{-1}\, P_{10}\, \gamma^{-1}. \tag{13}$$

Consequently, P_{10} completely determines the solutions of equations (7) through (9).

$P_{10}(k)$, and in fact $P_{10}(k,t)$, where time dependence is permitted, could be estimated by using an array of microphones to obtain the thunder signals at several locations simultaneously and then using a 4-dimensional Fast Fourier Transform to calculate $P_{10}(k,t)$. This might be of some use since $P_{10}(k,t)$ could be used to study the dependence of the spectrum on distance.

In place of (10) through (12) one could also assume that P_1, ρ_1, and v_1 are spatially and temporally statistically homogeneous (Tatarski (1961)) and then obtain results similar to those above by using a Fourier-Stieltjes representation. In this case, P_{10} would be a function of k and t.

The additional assumption that the pressure wave is a plane wave yields

$$v_{10}(r,t) = k\, \|k\|^{-1}\, (P_0(r)/\rho_0(r))\, P_1(r,t). \tag{14}$$

Then writing $P_{10}(k)$ in three mutually perpendicular coordinates where the coordinate system is oriented so that a unit vector is along k_1, the first coordinate of k, we have

$$P_{10}(k) = P_{11}(k_1)\ \delta(k_2)\ \delta(k_3) \tag{15}$$

and

$$P_1(r,t) = \int_{-\infty}^{\infty} P_{11}(k_1) e^{ik\cdot(r-tv_0)}\ e^{-i\omega t}\ dk_1. \tag{16}$$

Here δ denotes the delta function (that is, the coordinate system is oriented in the direction of the plane wave).

Few then assumes that the cross-covariance between $P_1(r_1,s)$ and $P_1(r_2,t)$ only depends on the differences t-s and r_2-r_1, which is an assumption of cross-stationarity. This assumption is not explicitly stated by Few but indeed it is the heart of the cross-covariance technique. If $P_1(r_2,t) = P_1(r_1,t+\tau)$, (i.e. if the pressure wave at r_2 lags the pressure wave of r_1 by τ units) then one can estimate τ, which is assumed to be constant, by calculating the cross-covariance between $P_1(r_2,t)$ and $P_1(r_1,t)$ and using the point where the cross-covariance is maximum as the desired estimate of the time lag.

The planarity of the wave and the geometry of the situation lead to the following equation for α, the direction between $r_2 - r_1 - v_0\tau$ and k:

$$\cos\alpha = \frac{c\tau}{\left|r_2 - r_1 - v_0\tau\right|}\ . \tag{17}$$

v_0 is the wind velocity and usually is neglected.

If this method is applied to signals received at three

microphones placed in a triangular array, and if lightning follows the string-of-pearls model, then the wave can be traced back to find the location of the source. An additional measurement of the time of onset of the lightning is also required -- this can be obtained optically or by field-change measurements. Several segments of the signals are used to get several points on the lightning channel.

The assumptions that the cross-covariance only depends on the lag between the received signals and that the received pressure wave is locally stationary can be used to give a simpler formulation of this problem which doesn't require the wave to be a plane wave.

Conceptually, the model includes the assumption that a point source (one of the pearls on the string) generates a spherical wave which is received as $P(r_1,t)$ at one location and $P(r_2,t)$ at another location. Then if the wind velocity, v_0, is ignored, and $P(r_2,t) = P(r_1,t + \tau)$, once again one can estimate the time lag τ and use the time lag to find the source, using either spherical waves or plane waves. This procedure is discussed in greater detail in the next section.

There are several problems connected with this method. The actual source is not spherical but rather cylindrical. In addition the waves from different locations can interfere with each other leading to some confusion in the estimated time lag. In fact, if two points on the channel are equidistant from the microphone then the signals from those two points are received simultaneously. There may also be some problems with

reflections or echos although one might be able to filter the signal to remove such effects. Finally, as discussed previously, it does not appear that the shock wave is the only component of thunder.

One difficulty with the cross-covariance technique is that the estimated time lags corresponding to peaks in the covariance function are very difficult to study from a statistical point of view. Not only are covariances difficult to treat statistically, but in this method one is actually interested in the time-lag where the covariance function is maximum and this time-lag is difficult to treat statistically.

Few (1970) discusses the errors involved in the cross-covariance procedure but he neglects the fundamental point that the estimate of τ, the time-lag, is a statistical quantity with its own statistical behavior. He really treats his estimate as if it were the true value of τ and only discusses errors due to discretization of the time scale which really ignores part of the problem.

Teer (1973) also claims to treat the statistical problem but he only finds the center of the flash and constructs an elliptical region which will encompass the signal. The validity of this procedure is questionable since once again the statistical behavior of the estimates is not accounted for.

If we examine the simple model where $P(r_2, t + \tau) = P(r_1,t)$ and where the signals are stationary, then we can estimate τ from the cross-spectral density of the two signals. This cross-spectral density is the Fourier transform of the

cross-covariance function. Then, τ can be estimated by examining the angle whose tangent is the ratio of the real and imaginary parts of the cross-spectral density, As we will see in the next section this arctangent, as a function of the frequency, ν, has the form $\tau\ \nu$, so standard regression techniques can be used to estimate τ. In addition, in the frequency domain it is easier to study the statistical properties than in the time domain. Consequently, one can establish confidence limits for the estimate τ, and, by using propagation of error, confidence limits for the source location. In addition the necessary filtering can often be performed more readily in the frequency domain. For these reasons we have selected the cross-spectral procedure and this procedure will be discussed in the next section and in the appendices.

III. CROSS-SPECTRAL ANALYSIS AND LIGHTNING LOCATION

The discussion in this section assumes that the thunder signal is recorded at three locations, where the locations of the recording microphones form a triangular array, (see Figure 1). Microphone i is located at position $P_i = (D_{i1}, D_{i2}, D_{i3})$ and the signal received at microphone i is $X_i(t)$.

Assuming that the signals are stationary, the cross-covariance function between signal i and signal j is defined as:

$$\Gamma_{ij}(s) = \text{cov}[X_i(t), X_j(t + s)] \tag{18.a}$$

$$= E[X_i(t)X_j(t + s)] - E[X_i(t)]\, E[X_j(t + s)]. \tag{18.b}$$

Few's method proceeds by calculating the sample cross-variance function and then letting τ (the time lag between signals $X_i(t)$ and $X_j(t)$) be that point where the covariance function is maximum. The model used assumes that $X_j(t + \tau) = X_i(t)$, as discussed in the previous section of this paper.

If $f_{ij}(u)$ is the cross-spectral density of signals i and j then, as we see in Appendix B, we can estimate $f_{ij}(u)$ by taking the Fourier transforms of $X_i(t)$ and $X_j(t)$ and then multiplying the transforms. Specifically, let

$$F_j(u) = \int_{-\infty}^{\infty} \exp\{2\pi u t i\}\, X_j(t)dt. \tag{19}$$

Then

$$f_{ij}(u) = F_i^*(u)\, F_j(u), \tag{20}$$

where the asterik denotes complex conjugation. In addition if $X_j(t + \tau) = X_i(t)$, a simple change of variables leads to

Figure 1

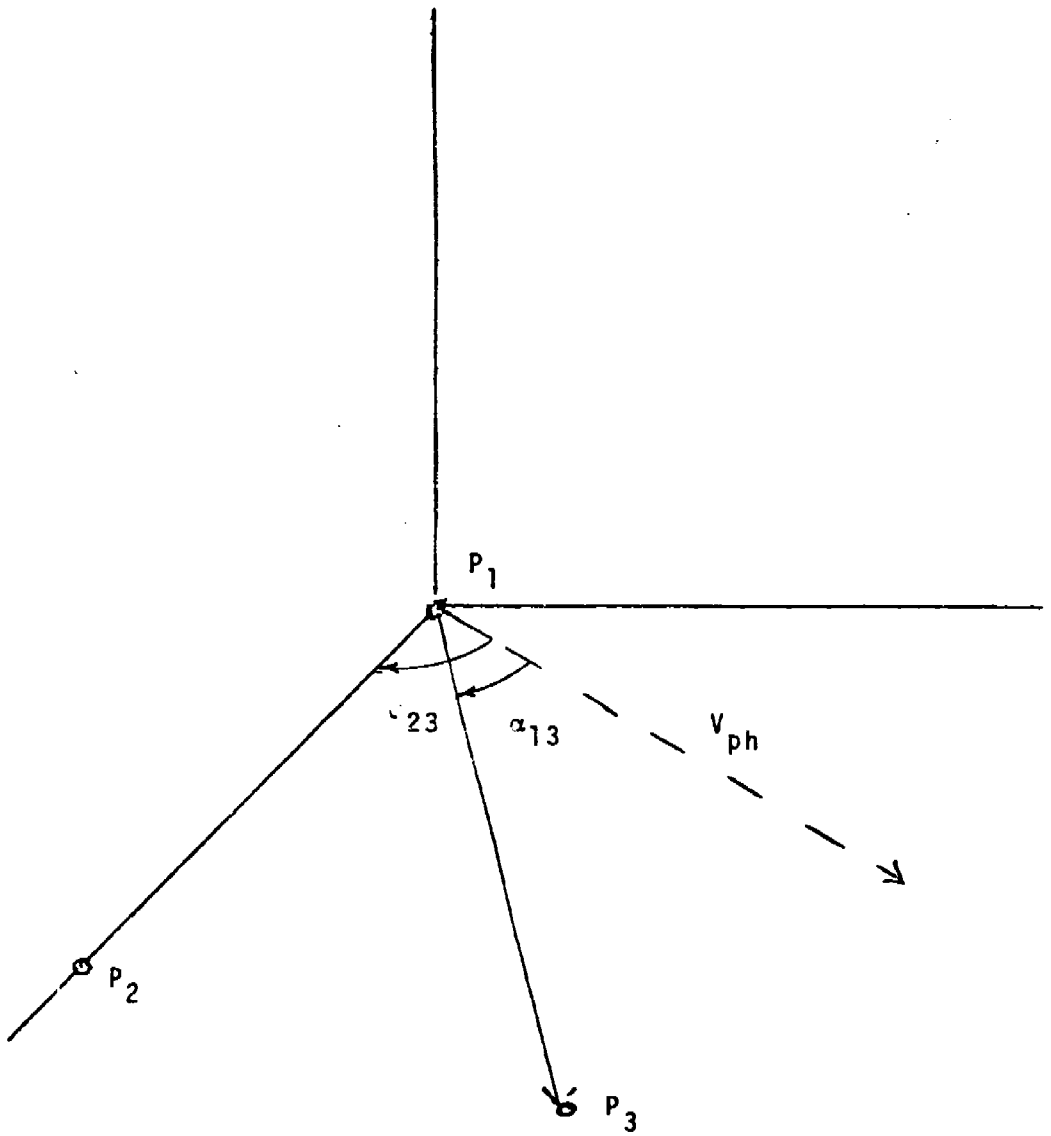

$$F_j(u) = \exp\{2\pi u\tau i\}\, F_i(u), \tag{21}$$

and consequently

$$f_{ij}(u) = \exp\{2\pi u\tau i\}\, |F_i(u)|^2. \tag{22}$$

We next break up $f_{ij}(u)$ into its real and imaginary parts:

$$f_{ij}(u) = [c_{ij}(u) - iq_{ij}(u)]/2. \tag{23}$$

$c_{ij}(u)$ is called the co-spectrum and $q_{ij}(u)$ is called the quadrature spectrum. From eq. (22) it follows that $\Theta_{ij}(u)$, the phase spectrum, is

$$\Theta_{ij}(u) = \arctan(-\, q_{ij}(u)/c_{ij}(u)) = 2\pi\tau u. \tag{24}$$

Hence, the phase spectrum should be a straight line through the origin with slope $2\pi\tau$ if signal j lags signal i by τ units. The phase can be estimated by finding the value of τ that minimizes $\sum_{k=1}^{h} [\Theta_{ij}(u_k) - 2\pi\tau u_k]^2$. Appendix B discusses the cross-spectral calculations in greater detail.

The precision of the estimate of τ can be ascertained by using standard statistical procedures. The necessary calculations are all given in Appendix C.

The cross-spectral approach and the cross-covariance procedure both proceed by partitioning the initial signals into smaller subsignals. After the partitioning, each segment is analyzed as above.

The spectral and cross-spectral estimates are all smoothed in order to stabilize the variance of the estimates. In addition, one can also estimate the cross-spectrum by transforming the cross-covariance function instead of the

original signals. Once again the details are given in Appendices A and B.

a. Spherical location routine

Let S be the time from the initiation of the source until its reception at microphone 1 and let τ_{12} and τ_{13} be the time lags estimated between microphones 1 and 2, and 1 and 3 respectively.

Then, if $\vec{r}' = (r_1', r_2', r_3')$ is the location of the source in a new system of coordinates where microphone 1 has coordinate (0,0,0), microphone 2 is on the x-axis of the primed system and the x-y plane of the primed system contains all 3 microphones, we can obtain the equations

$$\delta_1^2 = (r_1')^2 + (r_2')^2 + (r_3')^2 \tag{25.a}$$

$$\delta_2^2 = (r_1' - x_2')^2 + (r_2')^2 + (r_3')^2 \tag{25.b}$$

$$\delta_3^2 = (r_1' - x_3')^2 + (r_2 - y_3') + r_3'^2. \tag{25.c}$$

Here $\delta_1^2 = (cS)^2$, $\delta_2^2 = [c(S + \tau_{12})]^2$, $\delta_3^2 = [c(S + \tau_{13})]^2$, c is the speed of sound, and x_i', y_i' are coordinates, in the primed system of microphone i.

If equation (25.b) is subtracted from equation (25.a) and similarily if equation (25.c) is subtracted from equation (25.a) one can obtain r_1', r_2', and r_3' in terms of S, τ_{12} and τ_{13}.

Finally, these coordinates can be translated back to the original frame of reference by noting that the primed unit vectors can be expressed as linear combinations of the unprimed unit vectors. The variance and covariance matrix

of the estimated source location can be obtained by using propagation of error. The details of this procedure are given in Appendix D.

If $(1-\alpha) \times 100\%$ confidence intervals are desired for the source location, approximate limits can be obtained by using $\hat{r}_i \pm [\text{var}(\hat{r}_i)]^{1/2} z_{\alpha/6}$, $i = 1,2,3$, where $\hat{r}_i$ is the i^{th} estimated coordinate value, $z_{\alpha/6}$ is the upper $\alpha/6$ point of the standard normal distribution and $\text{var}(\hat{r}_i)$ is the estimated variance of $\hat{r}_i$. More precise estimates can also be obtained by using a chi-square distribution and the covariance matrix of the r-values, but the resulting confidence region is an ellipsoid rather than a box and is somewhat harder to visualize. The above box-like regions are known as Bonferroni confidence regions.

b. Plane wave location

If the received sound wave is a plane wave then one can estimate the velocity vector of the wave by using the lags, τ_{ij}, and then once again trace back to the source.

Here the direction cosines of the angles between the velocity of the wave front and the vectors connecting microphones 2 and 3 to microphone 1 are obtained.

In particular if v is the unit velocity vector of the plane wave, and if α_{ij} is the angle between v and the vector connecting microphone i and j, then

$$\cos \alpha_{ij} = \frac{c\tau_{ij}}{\overrightarrow{P_iP_j}} = \frac{v \cdot \overrightarrow{P_iP_j}}{\overrightarrow{P_iP_j}\,\|v\|} \qquad i,j = 1,2,3.$$

These 2 equations along with $\|\vec{v}\| = 1$ can be used to find v. (Here $\overrightarrow{P_iP_j}$ is the vector connecting microphone i and j.)

The location of the source in this case is $cS\vec{v}$. Once again covariances for the estimates are obtained by propagation of error, after linearizing the resulting expressions in τ_{12} and τ_{13}. Appendix E includes the covariance calculations and a discussion of the plane location procedure.

IV. LOCATION FOR C-4 AND PRIMA-CORD SHOTS

The methods were tested by using experimental explosive charges with point sources (C-4 shots) and line sources (Prima-Cord explosives). The explosives were suspended from balloons and the approximate positions obtained by Theodolite Survey data. The tests were carried out near Langmuir Laboratory in the Magdalena Mountains of New Mexico. The co-ordinates used in this section and the next one are all related to the radar tower at Langmuir Laboratory.

Several different micropnone networks were used in these reconstructions. The three networks used are designated as the Saddle, West Knoll, and Solar Tower networks, corresponding to their locations in South Baldy near the laboratory. However, the spacing between microphones is not the same for all reconstructions as is noted below.

A considerable amount of output is generated by the programs used to do the reconstruction and consequently only one fairly complete set is shown below.

C-4 Shots, Summer 1977:

Two microphone networks were used for these reconstructions - the Saddle and the West Knoll network. Each network consisted of three microphone stations in a triangular array with approximately thirty meters between the stations.

Figures 2-a through 2-ℓ show the output for C-4 shot number one for the Saddle network. Figure 2-a is a graph of three recorded microphone signals for the Saddle network. Figure 2-b summarizes some of the information about the signals and the

FIGURE 2-A

C-4 NUMBER 1, 1977

SADDLE NETWORK

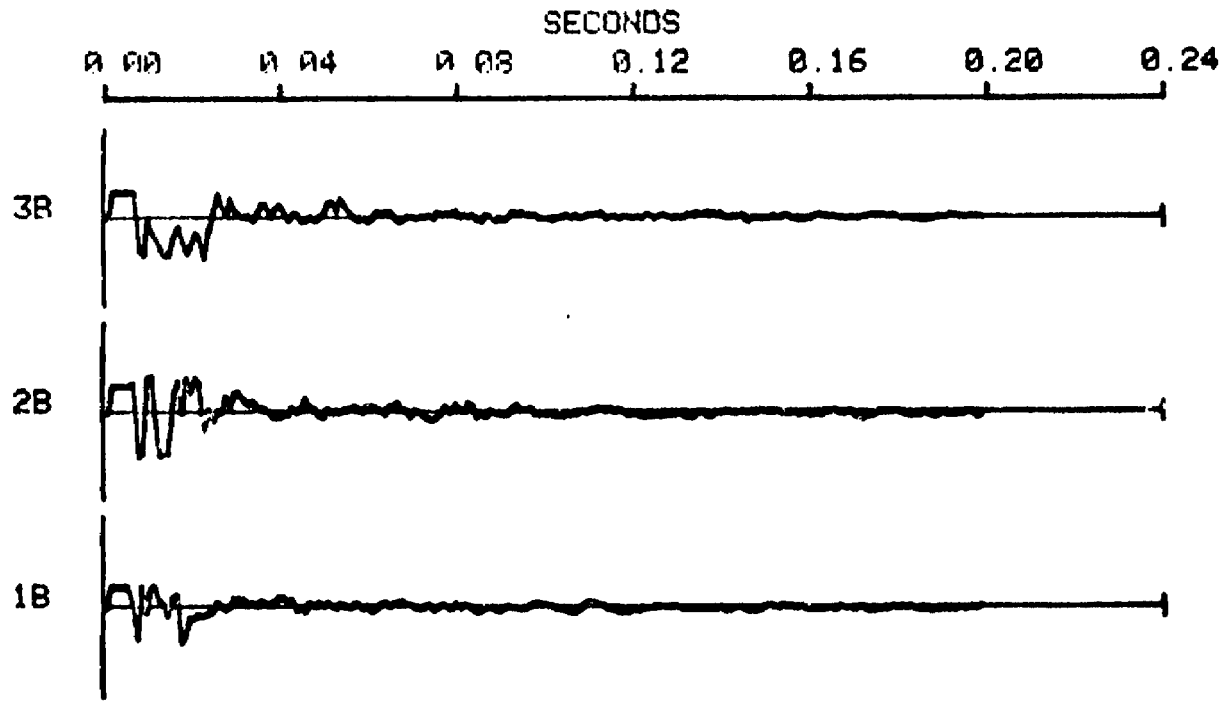

DAY 233,1977 -- PRESSURE SIGNATURE
SIGNAL LENGTH= 0.200 SEC, FULL SCALE DEVIATION=10.000 NEWTON/SQUARE METER
START TIMES:
SIG#1B -- 11:45:20.308
SIG#2B -- 11:45:20.273
SIG#3B -- 11:45:20.243

FIGURE 2-8

C-4 NUMBER 1, 1977

SADDLE NETWORK

DATE:		233/1977		
LIGHTNING		11:45:17.289		
SIG #		1B	2B	3B
START HR		11	11	11
	MN	45	45	45
	SC	20	20	20
	MS	308	273	243
GAIN(N/M/M/U)		1.00	1.00	1.00
LOCATION	X	-568.00	-538.00	-538.00
	Y	311.00	311.00	341.00
	Z	-69.00	-69.00	-68.00
MEAN VALUE		0.3812E-01	0.1883E 00	-0.5337E-01
VARIANCE		0.5374E 00	0.1385E 01	0.1454E 01
JOULES		0.1378E-03	0.3550E-03	0.3728E-03

RECORD LENGTH	0.2000	SECONDS
SPEED OF SOUND	340.00	M/S
SAMPLE RATE	2000.00	/SEC
# SAMPLES	400	
MAXIMUM LAG	16	SAMPLES
CHAR. IMPEDANCE	390.00	NEWTON-SEC/CUBIC METER
DEGREES OF FREEDOM	66	
FREQUENCY SPACING	62.50	HERTZ
EFF. BANDWIDTH	165.00	HERTZ

FIGURE 2-c

C-4 NUMBER 1, 1977

SADDLE NETWORK

DAY 233, 1977 -- SOURCE LOCATION FOR EVENT SPECIFIED BY:

SIG.#1B STARTING AT 11:45:20.308
SIG.#2B STARTING AT 11:45:20.273
SIG.#3B STARTING AT 11:45:20.243

LIGHTNING AT 11:45:17.289

SIGNAL LENGTH= 0.200 SEC

SIG. PAIR	1B,2B	1B,3B	2B,3B
DIF.ARV.(SEC)	-0.03500	-0.06500	-0.03000

SIGNAL	1B	2B	3B
TIME TO SRC	3.11900	3.08400	3.05400
METRES	1060.46	1048.56	1038.36

SPHERICAL WAVE SOLUTION:

	X	Y	Z
SOURCE LOC	-134.71	650.58	837.38

PLANE-WAVE SOLUTION:

	X	Y	Z
SOURCE LOC	-147.35	641.03	846.81

FIGURE 2-D

C-4 NUMBER 1, 1977

SADDLE NETWORK

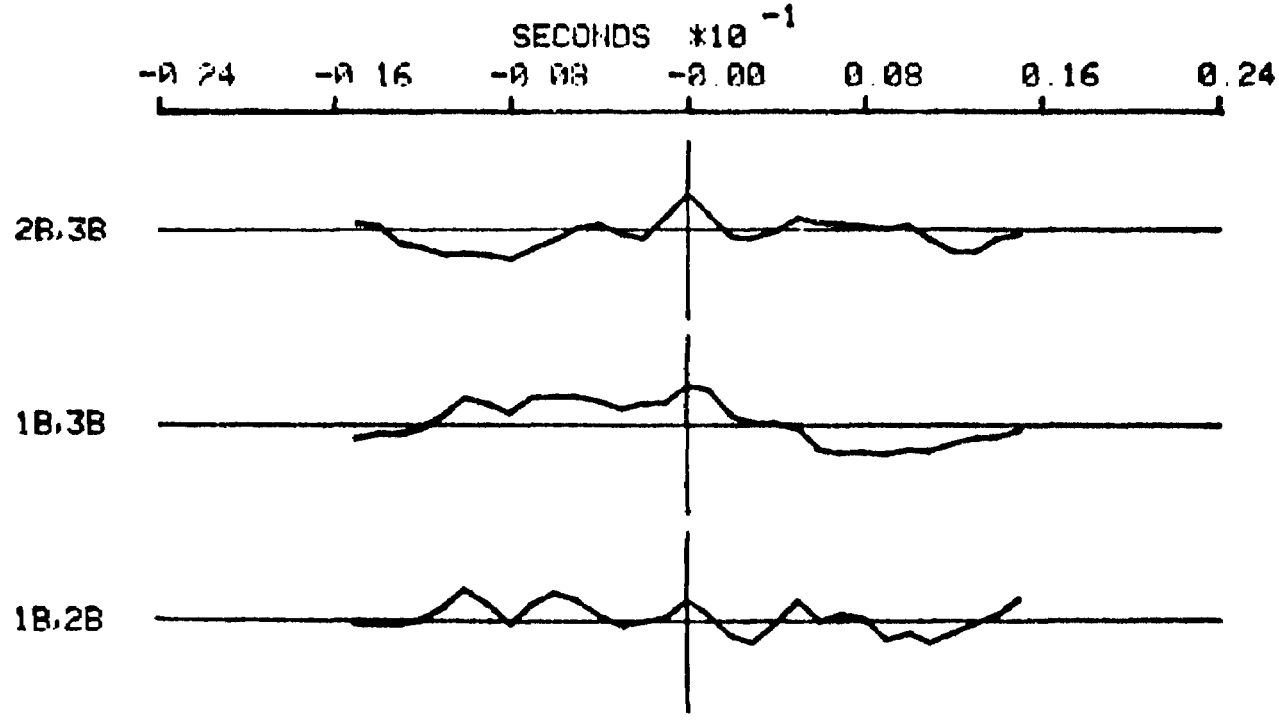

DAY 233, 1977 -- CROSS-CORRELATIONS
SIGNAL LENGTH= 0.200 SEC, MAXIMUM LAG= 0.016 SEC
START TIMES:
SIG#1B -- 11:45:20.308 ABS.MAX. CORR. (1B,2B)= 0.346
SIG#2B -- 11:45:20.273 ABS.MAX. CORR. (1B,3B)= 0.447
SIG#3B -- 11:45:20.243 ABS.MAX. CORR. (2B,3B)= 0.406

FIGURE 2-E

C-4 NUMBER 1, 1977

SADDLE NETWORK

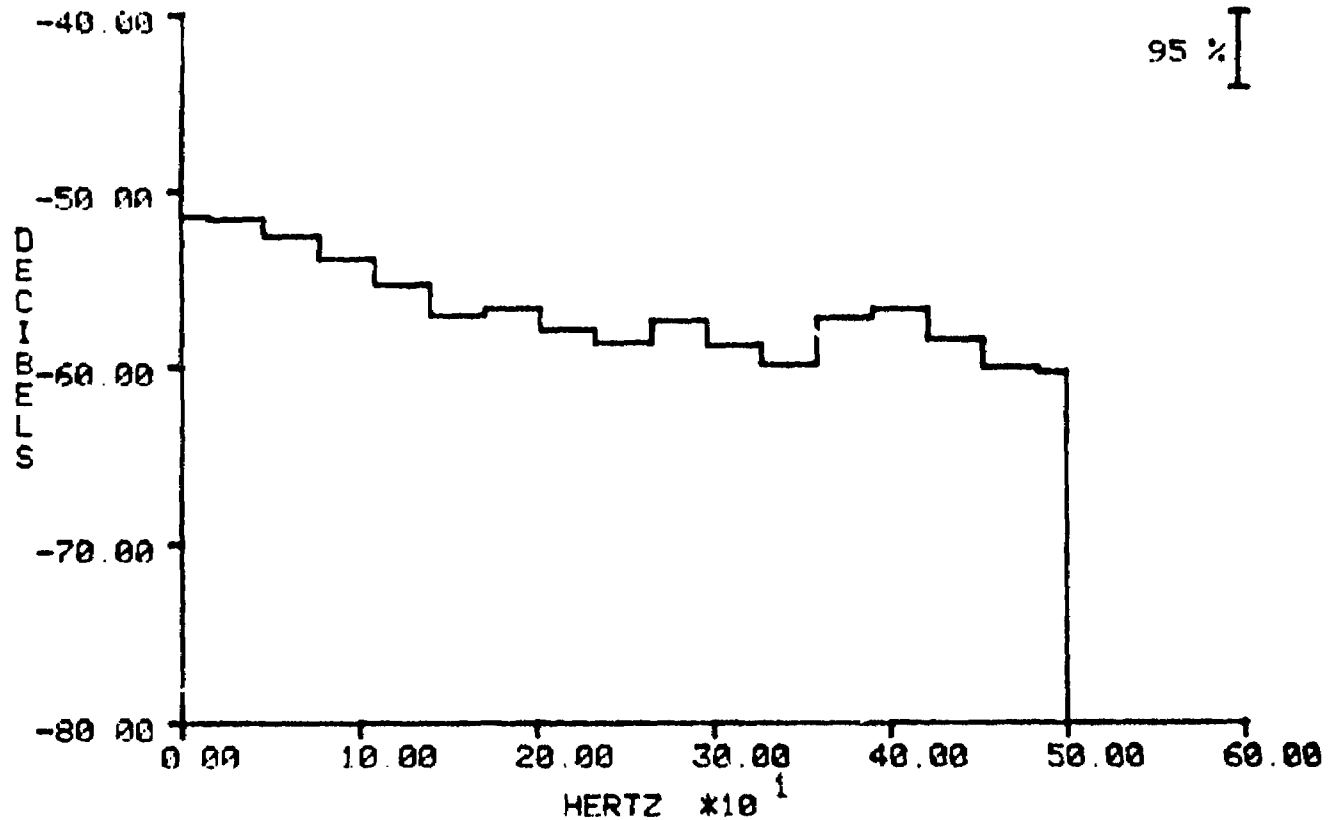

DAY 233, 1977 -- SPECTRAL DENSITY FOR SIGNAL #1B
NU= 33, BW= 82.5, LENGTH= 0.200 SEC.
SIG#1B, STARTS 11:45:20.308 MST.

FIGURE 2-F

C-4 NUMBER 1, 1977

SADDLE NETWORK

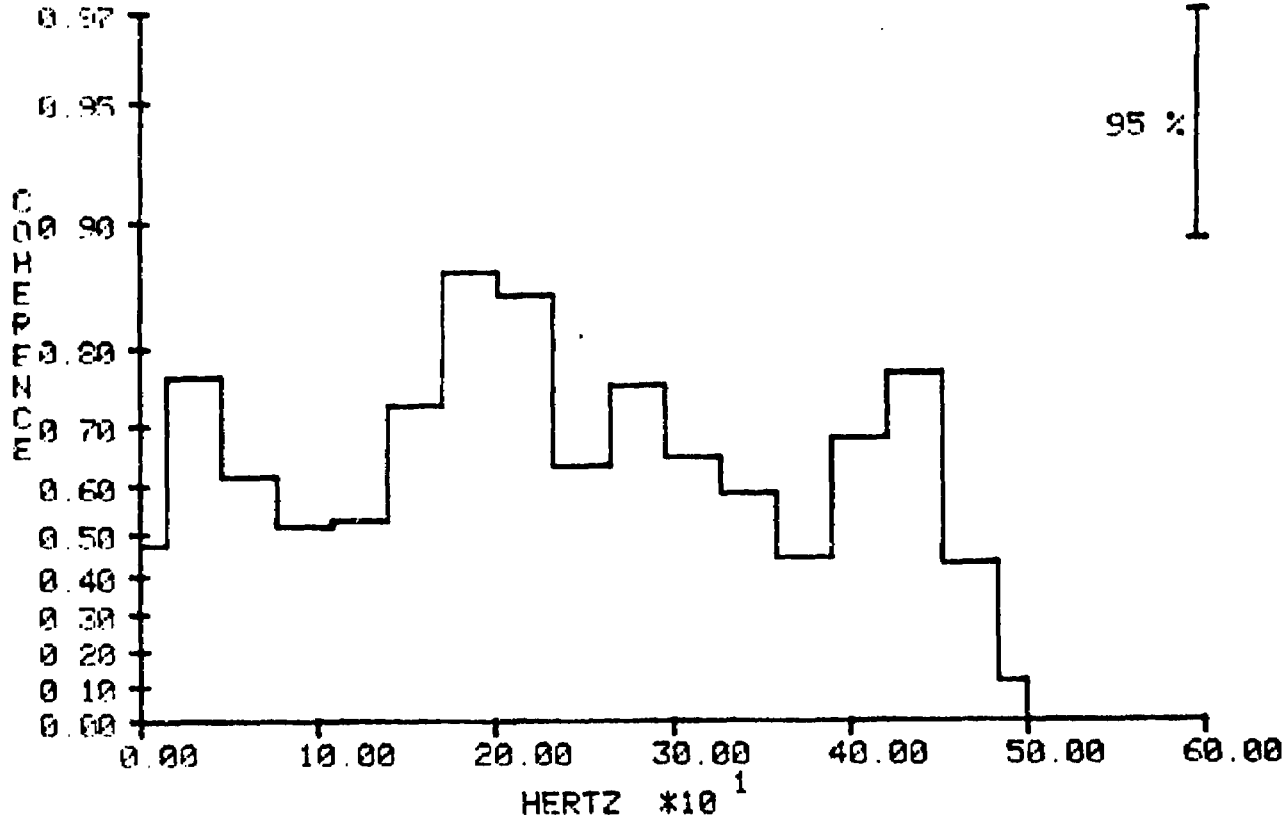

DAY 233, 1977 -- COHERENCY
NU= 33, BW= 82.50 HZ., SIGNAL LENGTH= 0.200 SEC
SIG#1B, AT 11:45:20.308 MST.
SIG#3B, AT 11:45:20.243 MST.

FIGURE 2-G

C-4 NUMBER 1, 1977

SADDLE NETWORK

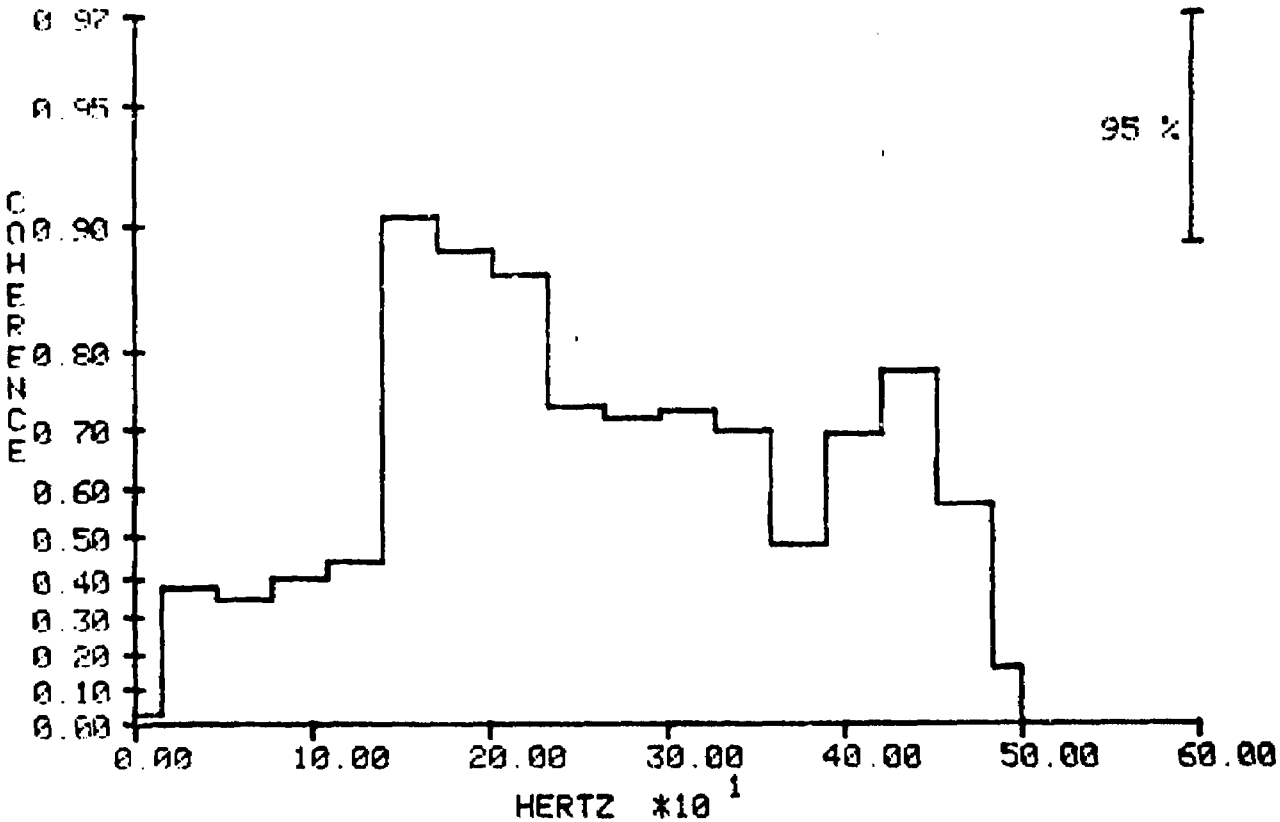

DAY 233, 1977 -- COHERENCY
NU= 33, BW= 82.50 HZ., SIGNAL LENGTH= 0.200 SEC
SIG#2B, AT 11:45:20.273 MST.
SIG#3B, AT 11:45:20.243 MST.

FIGURE 2-H

C-4 NUMBER 1, 1977

SADDLE NETWORK

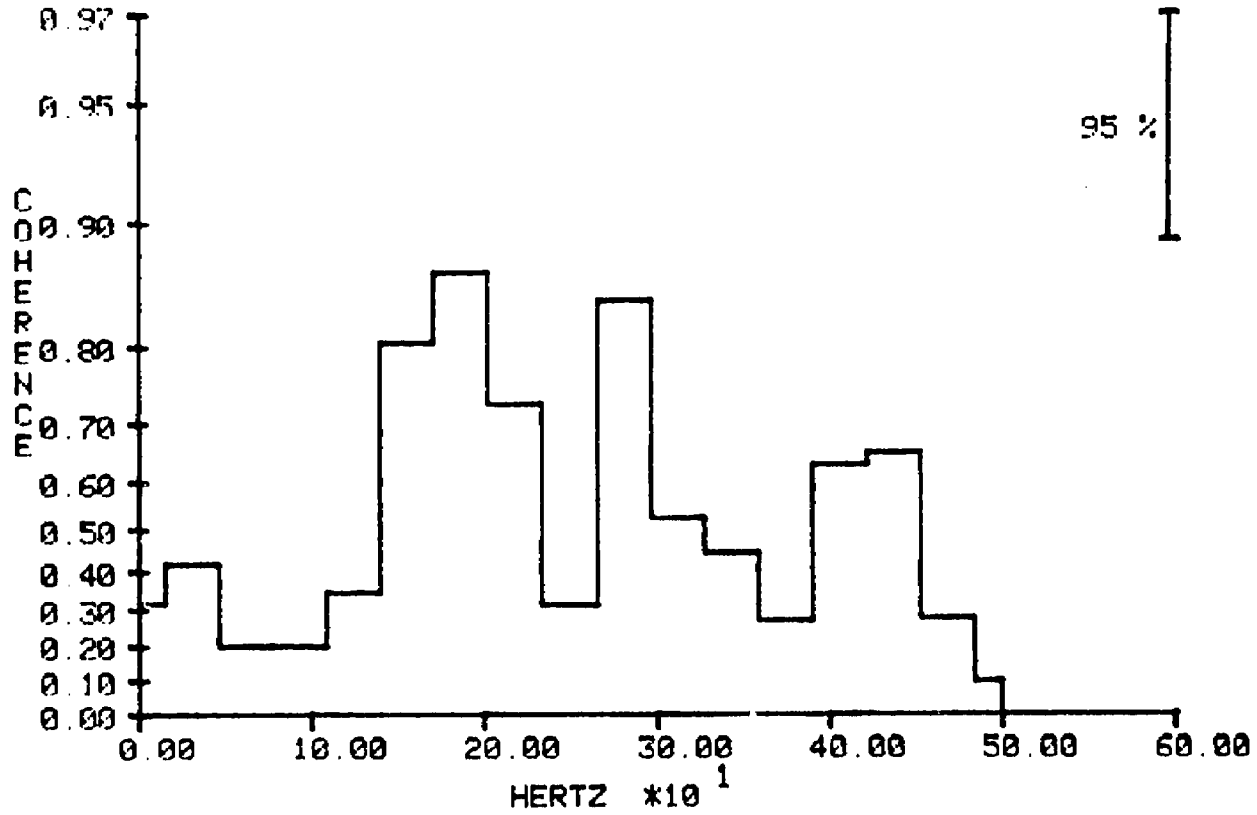

DAY 233, 1977 -- COHERENCY
NU= 33, BW= 82.50 HZ., SIGNAL LENGTH= 0.200 SEC
SIG#1B, AT 11:45:20.308 MST.
SIG#2B, AT 11:45:20.273 MST.

FIGURE 2-1

C-4 NUMBER 1, 1977

SADDLE NETWORK

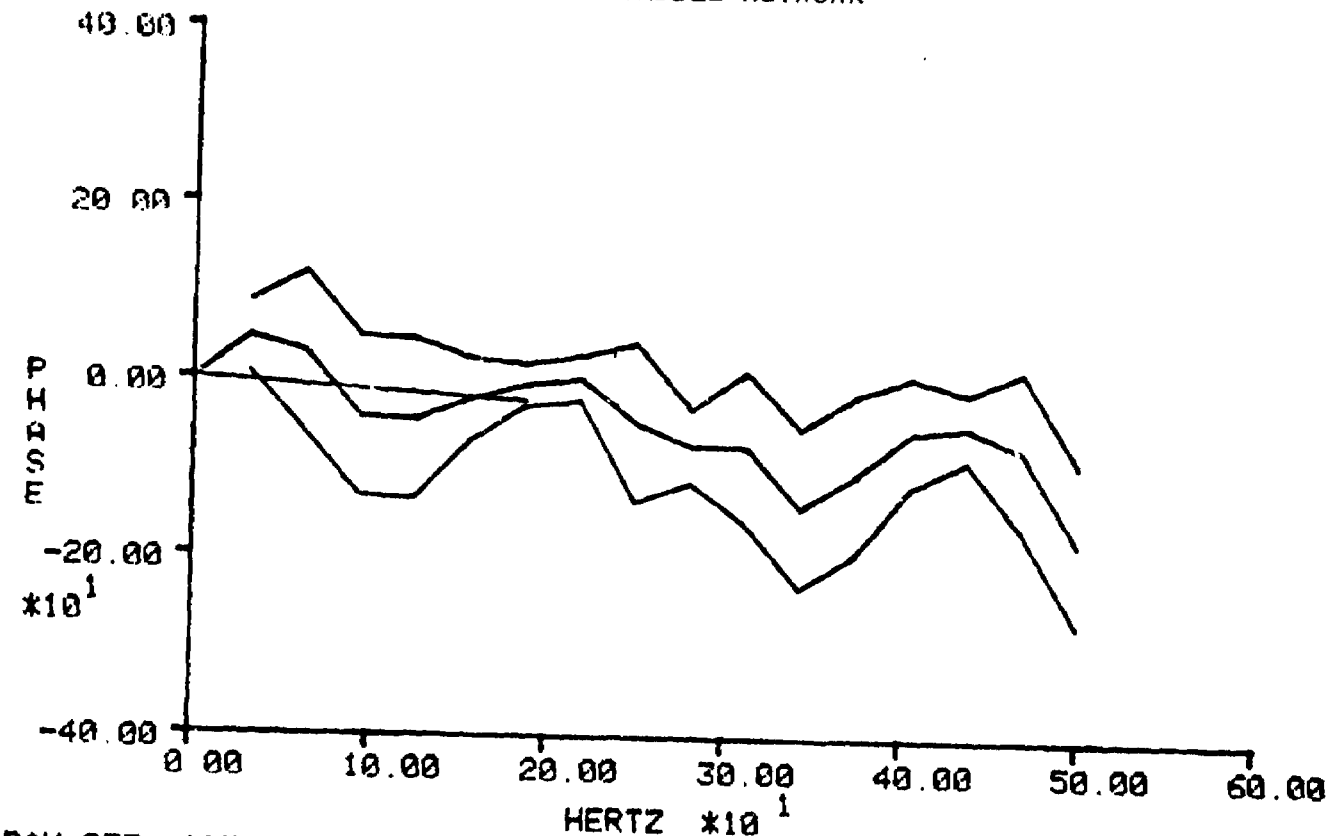

DAY 233, 1977 -- PHASE ESTIMATES
NU= 33, BW= 82.50 HZ., SIGNAL LENGTH= 0.200 SEC, SLOPE= -0.0003 SEC
SIG#1B, AT 11:45:20.308 MST.
SIG#3B, AT 11:45:20.243 MST.

FIGURE 2-J

C-4 NUMBER 1, 1977

SADDLE NETWORK

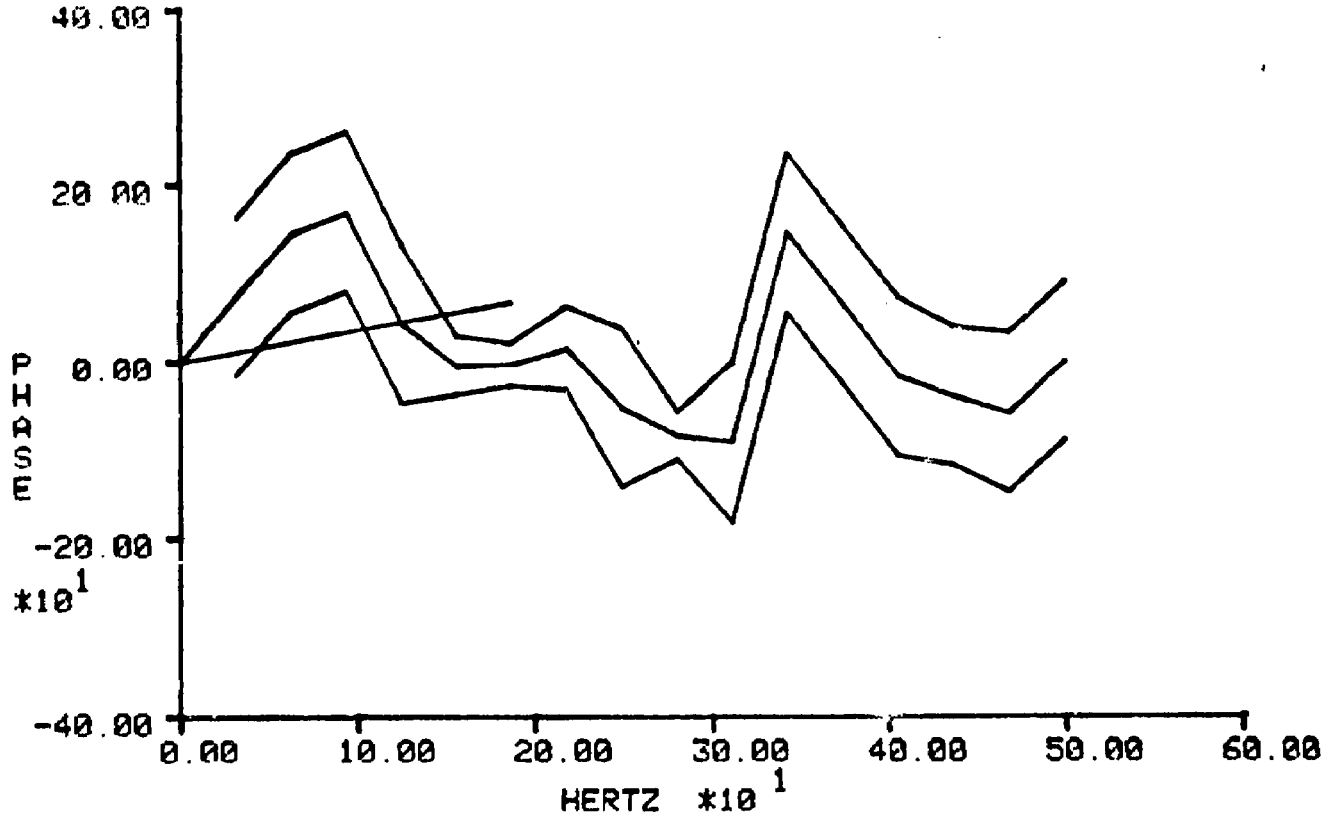

DAY 233, 1977 -- PHASE ESTIMATES
NU= 33, BW= 82.50 HZ., SIGNAL LENGTH= 0.200 SEC, SLOPE= 0.0010 SEC
SIG#1B, AT 11:45:20.308 MST.
SIG#2B, AT 11:45:20.273 MST.

FIGURE 2-K

C-4 NUMBER 1, 1977

SADDLE NETWORK

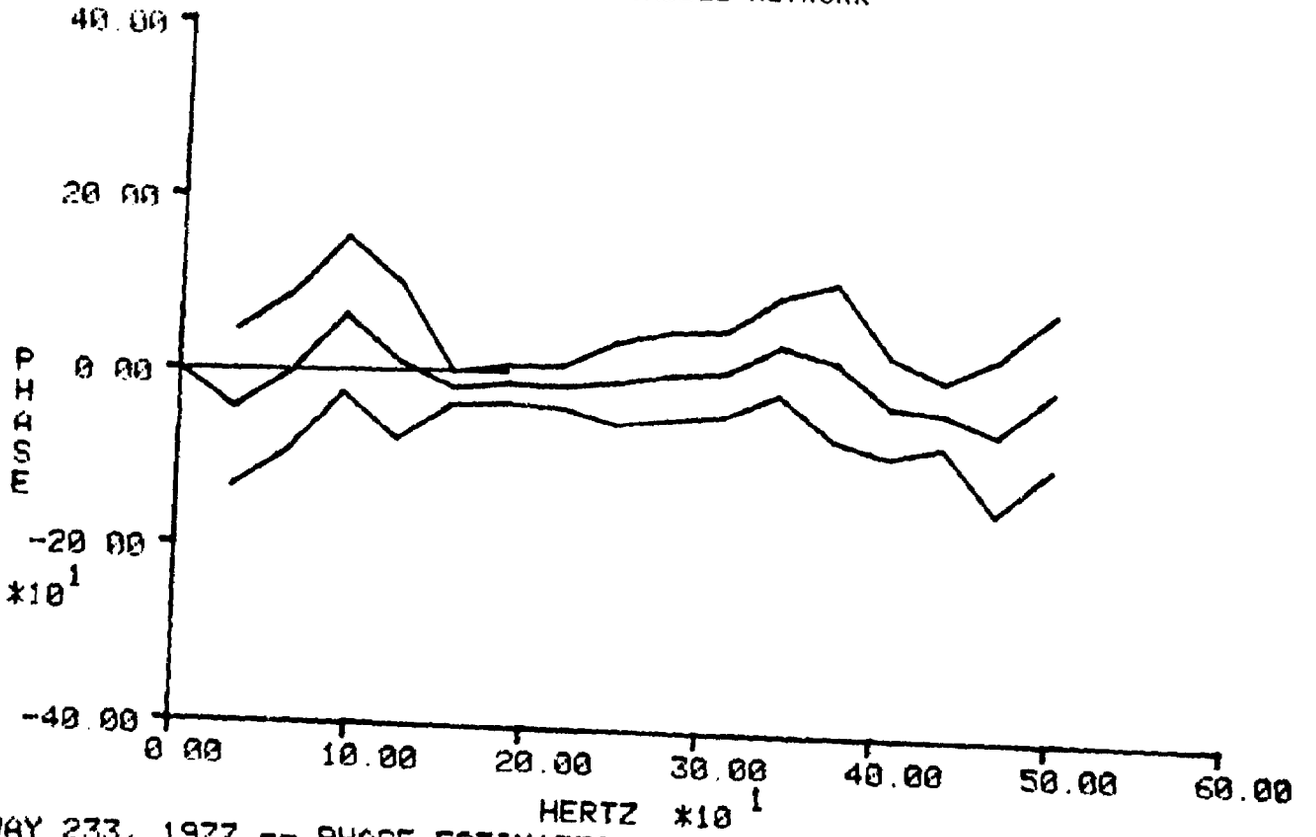

DAY 233, 1977 -- PHASE ESTIMATES
NU= 33, BW= 82.50 HZ., SIGNAL LENGTH= 0.200 SEC, SLOPE= 0.0001 SEC
SIG#2B, AT 11:45:20.273 MST.
SIG#3B, AT 11:45:20.243 MST.

FIGURE 2-L

C-4 NUMBER 1, 1977

SADDLE NETWORK

DAY 233, 1977 -- SOURCE LOCATION FOR EVENT SPECIFIED B

SIG.#1B STARTING AT 11:45:20.308
SIG.#2B STARTING AT 11:45:20.273
SIG.#3B STARTING AT 11:45:20.243

LIGHTNING AT 11:45:17.289

SIGNAL LENGTH= 0.200 SEC MAX FREQUENCY= 200. HERTZ

SIG. PAIR	1B,2B	1B,3B	2B,3B
SLOPE (SEC)	0.00001	-0.00049	-0.00060
DIF.ARV.(SEC)	-0.03581	-0.06451	-0.02940

SUM OF SLOPES= -0.0001013 SEC

SIGNAL	1B	2B	3B
TIME TO SRC	3.01900	2.98399	2.95449
METRES	1026.46	1014.56	1004.53

SOURCE COORDINATES AND 95 % CONFIDENCE INTERVALS

SPHERICAL WAVE SOLUTION	X	Y	Z	
	-171.33	655 45	811 67	
+ OR -	0.00	0.00	0.00	TIME
SOURCE VOLUME=	0.000000E 00 CUBIC METERS			WINDOW
+ OR -	10.61	11.96	2.68	TOTAL
SOURCE VOLUME=	0.271697E 04 CUBIC METERS			VARIANCE

PLANE WAVE SOLUTION	X	Y	Z
	-184 01	645 70	820 99

estimation techniques used. Figure 2-c gives an approximation to the source location using only the starting times of the signals. Figure 2-d indicates the cross-correlation functions. Note that even though (from Figure 2-a) we might guess that the signals are highly correlated the peaks on the cross-correlation functions are not very high. The log of the spectral density at one of the three microphones is shown in Figure 2-e, along with a 95% confidence interval for the estimated spectrum. The flatness of the spectrum suggests that the disturbance is approximately white noise. Figures 2-f through 2-h are coherencies between the signals all of which peak at about 200 Hertz. These coherencies measure the correlation between the various frequency components of the signals. The phase functions, with confidence intervals and a regression line used to estimate the time lags, are shown in Figures 2-i through 2-k. Figure 2-ℓ shows the final output indicating the source location and confidence intervals for the spherical location routine. (The time window line is superfluous - originally one-half the width of the length of record used was added to the times before tracing and the uncertainty introduced by this was included in the variance calculation. However, it appears more accurate estimates are obtained by not including this increment.) Variance estimates (or more precisely confidence intervals) are only shown for the spherical wave solution. The locations are summarized in Table 1 and the computed location contains the surveyed location with its confidence region. The corrections of the program do lead to considerable change in the predicted locations from the initial guess of Figure 2-c which corresponds to a "by eye" alignment.

TABLE 1

1977 C-4 TEST SHOTS

	Co-ordinates (Meters)		
C-4 NO. 1	x	y	z
Survey	-166.7	660.5	812.6
Saddle	-171.3 ± 10.4	655.5 ± 12.1	811.7 ± 3.1
West Knoll	-173.0 ± 16.2	681.9 ± 18.8	818.4 ± 21.4
C-4 NO. 2			
Survey	-213.5	744.0	568.0
Saddle	-229.5 ± 5.4	726.3 ± 6.0	574.5 ± 3.6
West Knoll	-218.6 ± 11.5	726.1 ± 6.6	568.8 ± 6.42

Figures 3-a through 3-g show some of the relevant data for the same event using the West Knoll network. Here the confidence intervals on the spectra and phase are narrower but because of the greater distance from the source, wider on the location. While the confidence region for the source doesn't contain the survey values it just barely misses doing so in the y - co-ordinate only.

The results are presented in Table 1 along with another 1977 C-4 test shot. The confidence regions for the second experiment don't contain the surveyed location with the largest discrepancy appearing in the y - co-ordinate. Since errors also exist in the Theodolite measurements this lack of overlap was not considered to be a serious problem.

Prima-Cord Event 1973:

Some calculations were also made with earlier C-4 and Prima-Cord tests. Only a Prima-Cord test will be discussed here since the C-4 results are similar to those presented above.

For this reconstruction again two networks were used. However, the Saddle network had microphone stations on a one hundred meter spacing rather than a thirty meter spacing.

Some of the output is shown in Figures 4-a through 4-c and the co-ordinate values are given in Table 2. Figure 5 shows two-dimensional views of the reconstruction. The reconstructions agree reasonably well with each other. There was a kink in the cord which appears in one reconstruction but not the other indicating the effect of the aspect angle since this is indeed a real kink. The maximum cross-correlations occur at the ends

FIGURE 3-A

C-4 NUMBER 1, 1977

WEST KNOLL NETWORK

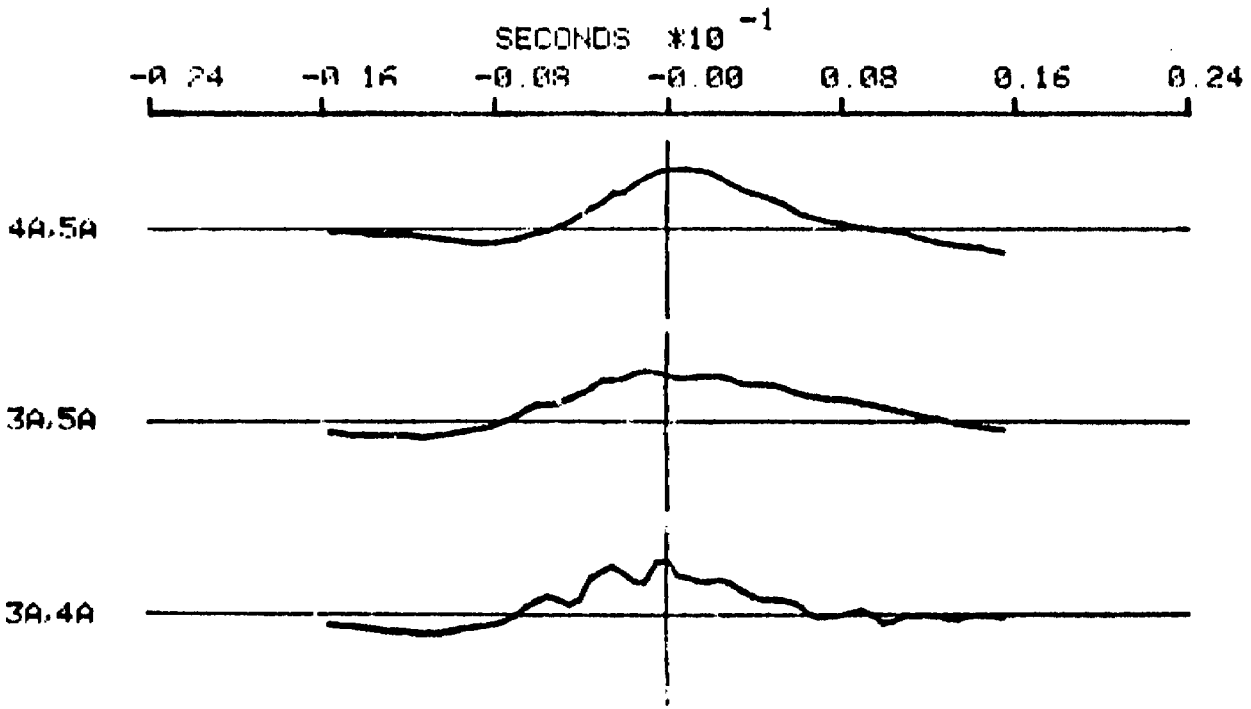

DAY 233, 1977 -- CROSS-CORRELATIONS
SIGNAL LENGTH= 0.200 SEC, MAXIMUM LAG= 0.016 SEC
START TIMES:
SIG#3A -- 11:45:21.372 ABS.MAX. CORR. (3A,4A)= 0.609
SIG#4A -- 11:45:21.309 ABS.MAX. CORR. (3A,5A)= 0.575
SIG#5A -- 11:45:21.324 ABS.MAX CORR. (4A,5A)= 0.698

FIGURE 3-B

C-4 NUMBER 1, 1977

WEST KNOLL NETWORK

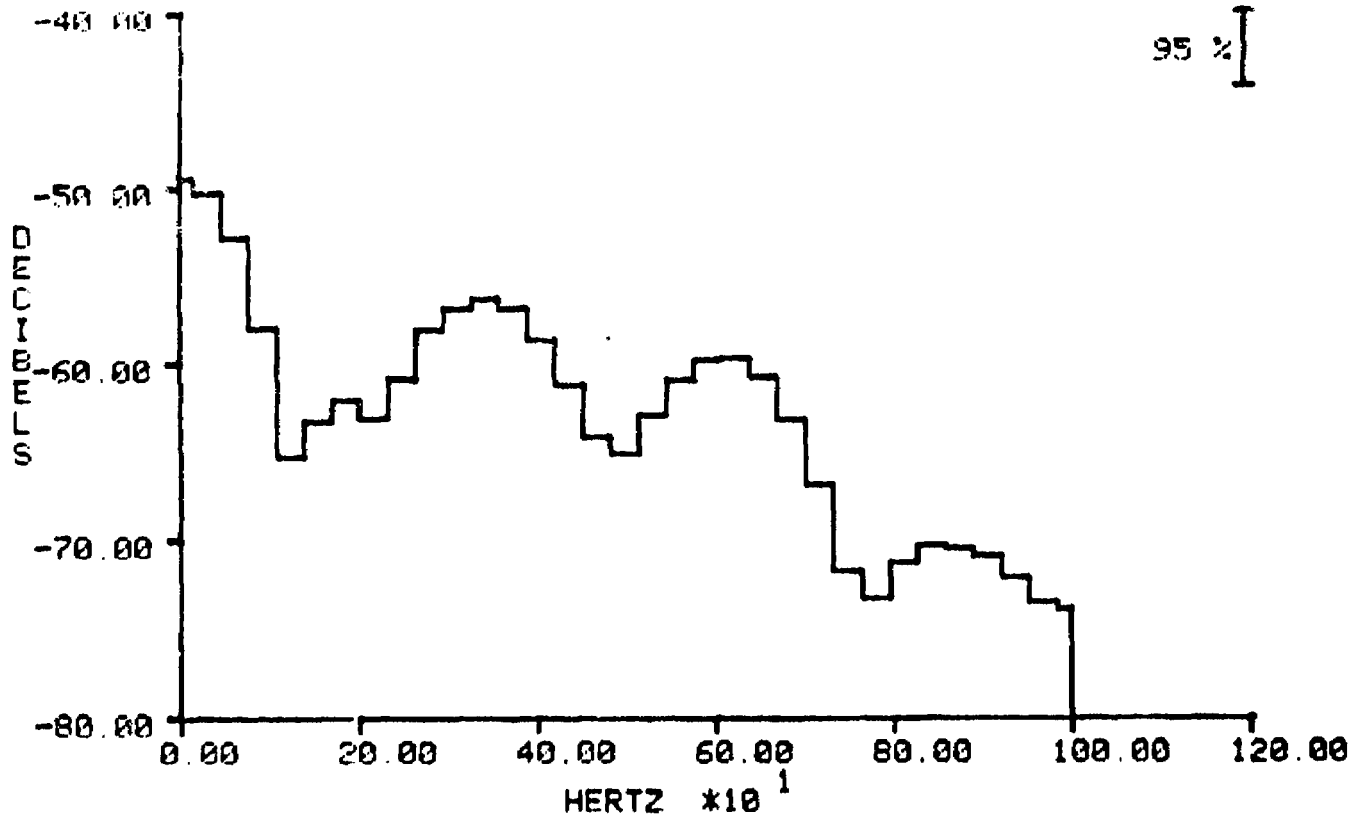

DAY 233, 1977 -- SPECTRAL DENSITY FOR SIGNAL #3A
NU= 33, BW= 82 5, LENGTH= 0.200 SEC.
SIG#3A, STARTS 11:45:21.372 MST.

FIGURE 3-c

C-4 NUMBER 1, 1977

WEST KNOLL NETWORK

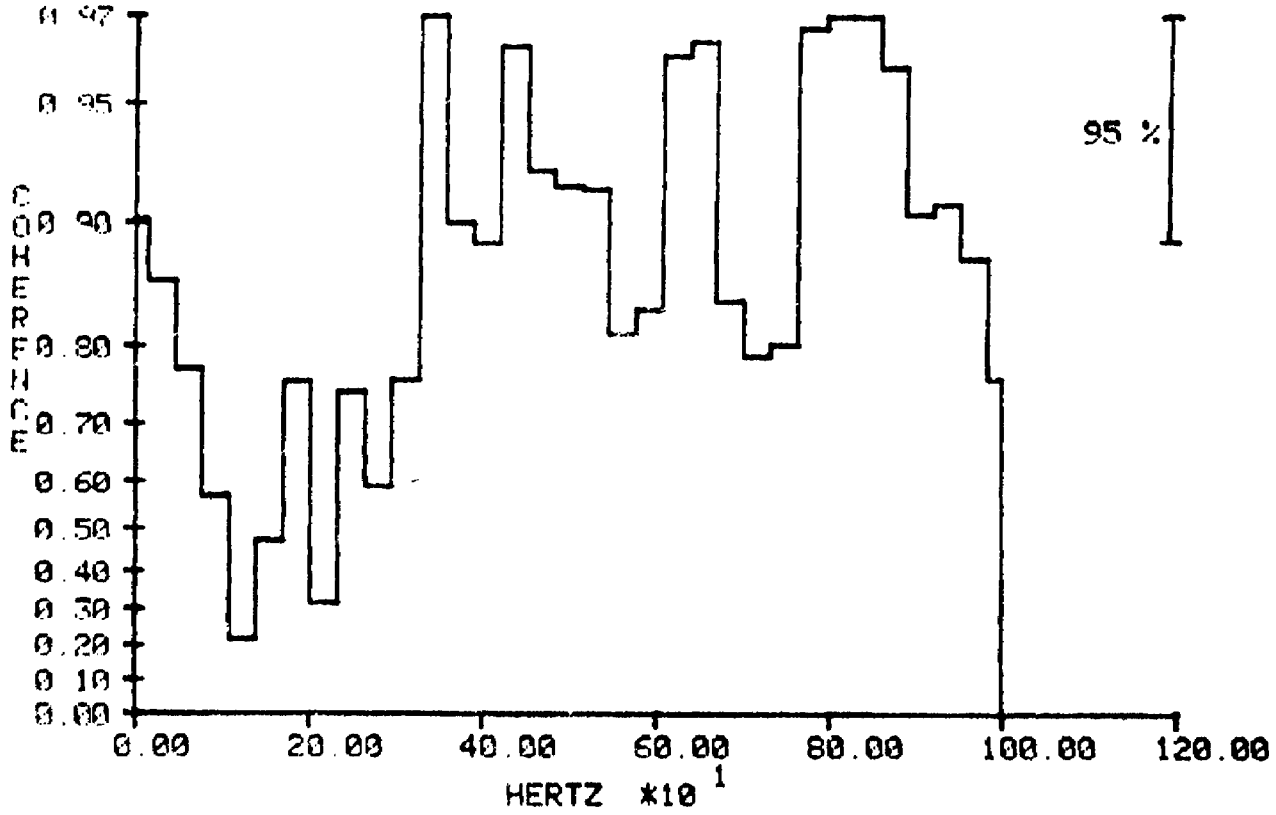

DAY 233, 1977 -- COHERENCY
NU= 33, BW= 82.50 HZ., SIGNAL LENGTH= 0.200 SEC
SIG#3A, AT 11:45:21.372 MST.
SIG#4A, AT 11:45:21.309 MST.

FIGURE 3-D

C-4 NUMBER 1, 1977

WEST KNOLL NETWORK

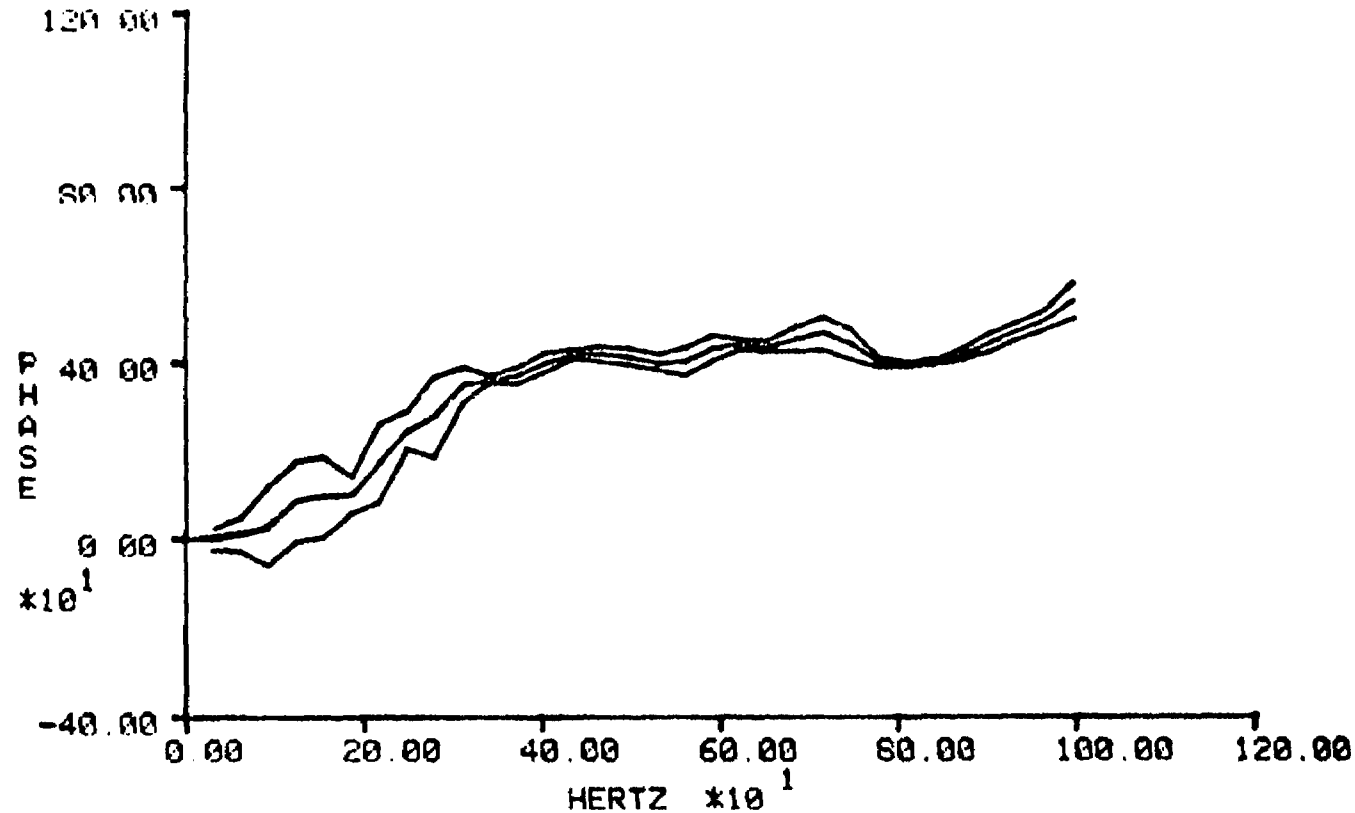

DAY 233, 1977 -- PHASE ESTIMATES
NU= 33, BW= 82.50 HZ., SIGNAL LENGTH= 0.200 SEC, SLOPE= 0.0007 SEC
SIG#3A, AT 11:45:21.372 MST.
SIG#4A, AT 11:45:21.309 MST.

FIGURE 3-E

C-4 NUMBER 1, 1977

WEST KNOLL NETWORK

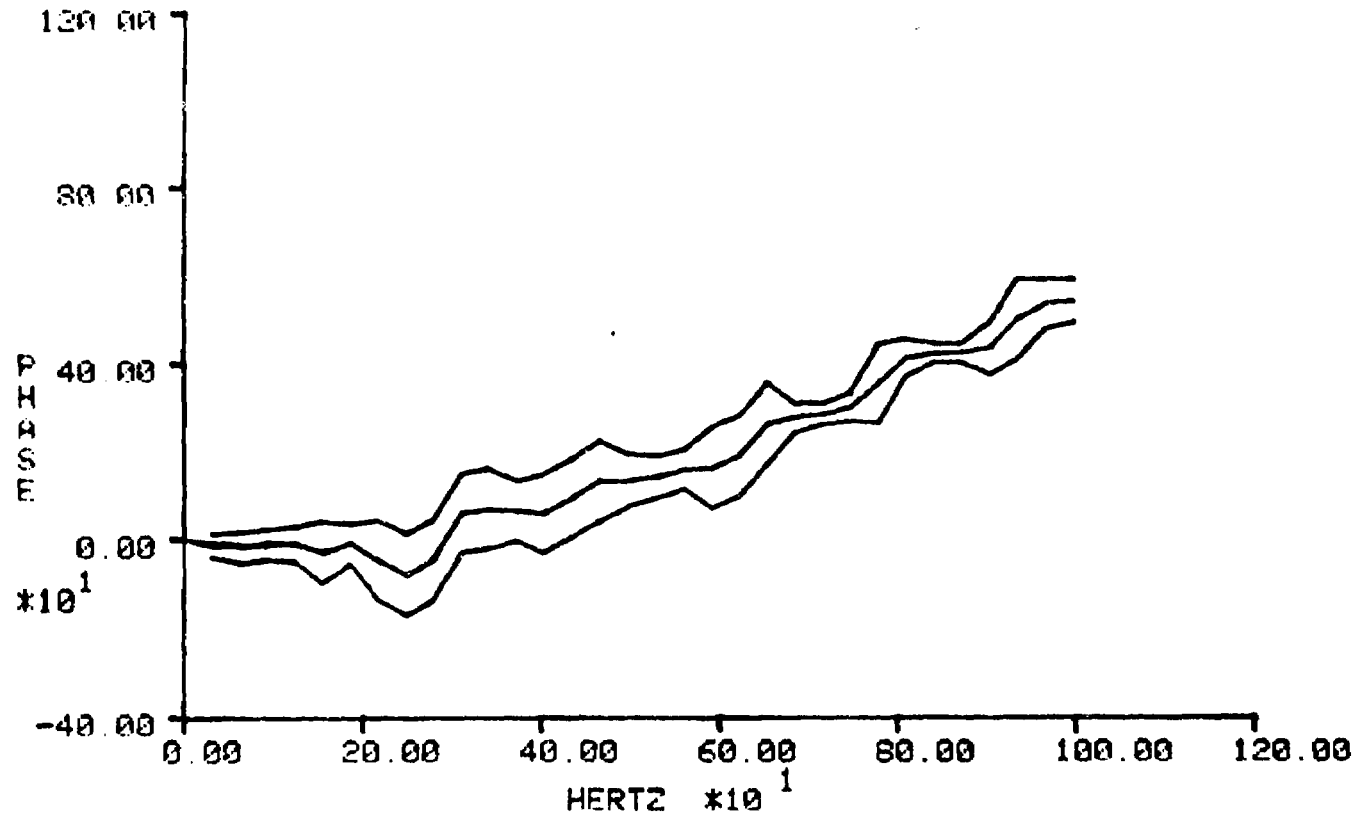

DAY 233, 1977 -- PHASE ESTIMATES
NU= 33, BW= 82.50 HZ., SIGNAL LENGTH= 0.200 SEC, SLOPE= -0.0005 SEC
SIG#4A, AT 11:45:21.309 MST.
SIG#5A, AT 11:45:21.324 MST.

FIGURE 3-F

C-4 NUMBER 1, 1977

WEST KNOLL NETWORK

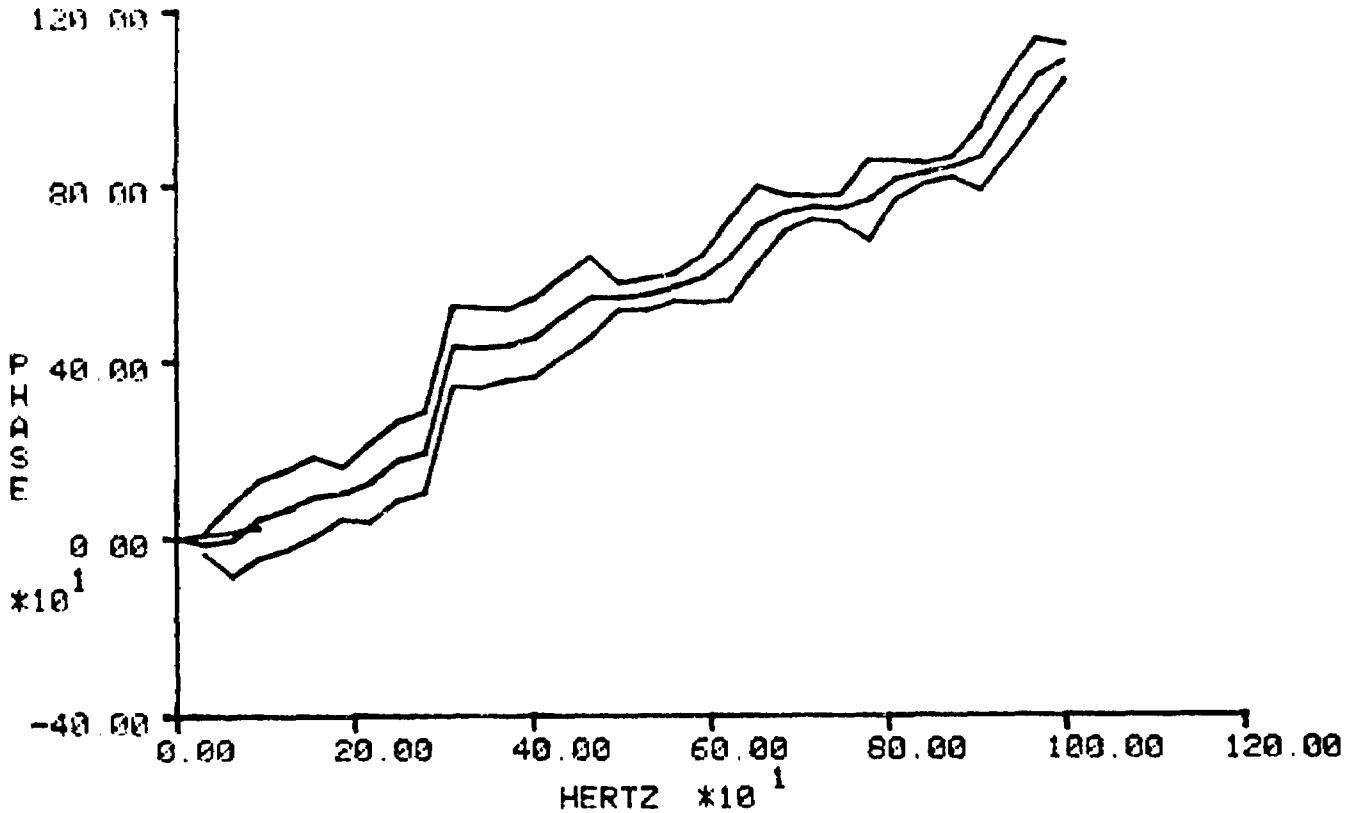

DAY 233, 1977 -- PHASE ESTIMATES
NU= 33, BW= 82.50 HZ., SIGNAL LENGTH= 0.200 SEC, SLOPE= 0.0007 SEC
SIG#3A, AT 11:45:21.372 MST.
SIG#5A, AT 11:45:21.324 MST.

FIGURE 3-G

C-4 NUMBER 1, 1977

WEST KNOLL NETWORK

DAY 233, 1977 -- SOURCE LOCATION FOR EVENT SPECIFIED BY:

SIG.#3A STARTING AT 11:45:21.372
SIG.#4A STARTING AT 11:45:21.309
SIG.#5A STARTING AT 11:45:21.324

LIGHTNING AT 11:45:17.289

SIGNAL LENGTH= 0.200 SEC MAX FREQUENCY= 100. HERTZ

SIG. PAIR	3A,4A	3A,5A	4A,5A
SLOPE (SEC)	0.00069	0.00047	-0.00052
DIF.ARV.(SEC)	-0.06369	-0.04847	0.01552

SUM OF SLOPES= -0.0003020 SEC

SIGNAL	3A	4A	5A
TIME TO SRC	4.08300	4.01931	4.03453
METRES	1388.22	1366.57	1371.74

SOURCE COORDINATES AND 95 % CONFIDENCE INTERVALS

SPHERICAL WAVE SOLUTION	X	Y	Z	
	-173.01	681.94	818.39	
+ OR -	0.00	0.00	0.00	TIME WINDOW
SOURCE VOLUME=	0.000000E 00 CUBIC METERS			
+ OR -	16.20	18.79	21.38	TOTAL VARIANCE
SOURCE VOLUME=	1.520715E 05 CUBIC METERS			

PLANE WAVE SOLUTION	X	Y	Z
	-179.76	672.82	829.34

and at the kink. The smaller spaced network has signals that do not decorrelate as fast as this larger spaced network. The agreement with the surveyed location is not very good at the bottom but the bottom survey was not very accurate so the discrepancy isn't too alarming.

FIGURE 4-A

PRIMA-CORD TEST, 1973

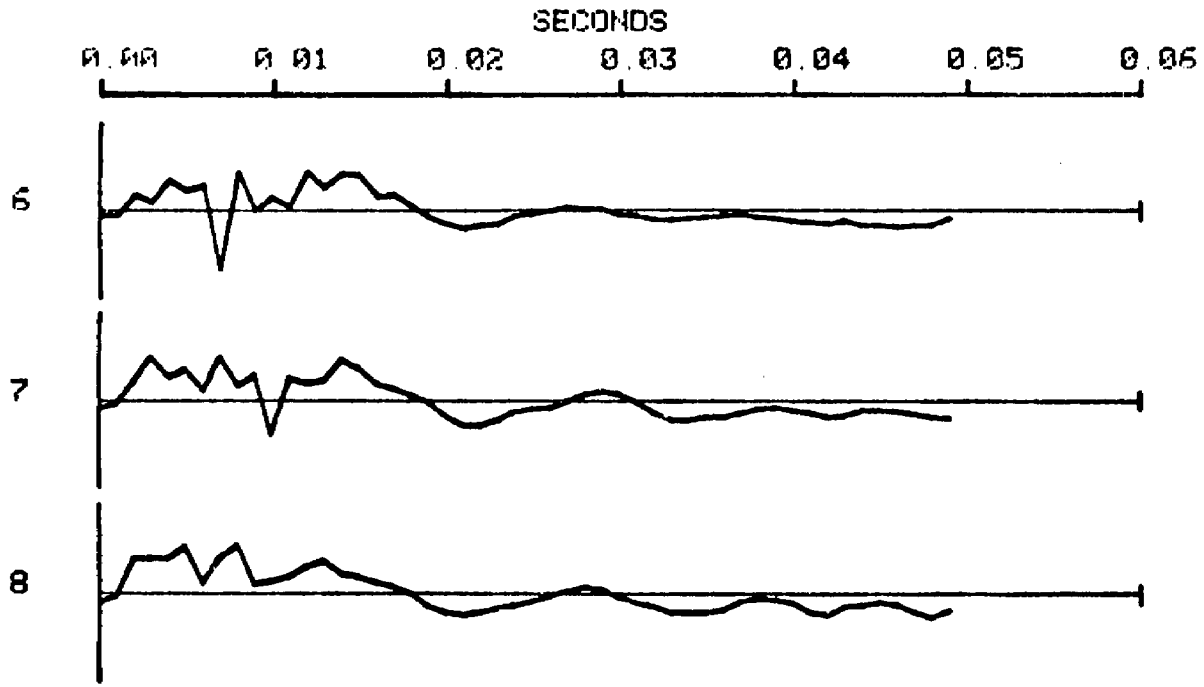

DAY 226,1973 -- PRESSURE SIGNATURE
SIGNAL LENGTH= 0.050 SEC, FULL SCALE DEVIATION= 4.000 NEWTON/SQUARE METER
START TIMES:
MIC# 8 -- 11:50: 2.510
MIC# 7 -- 11:50: 2.549
MIC# 6 -- 11:50: 2.595

FIGURE 4-B

PRIMA-CORD TEST, 1973

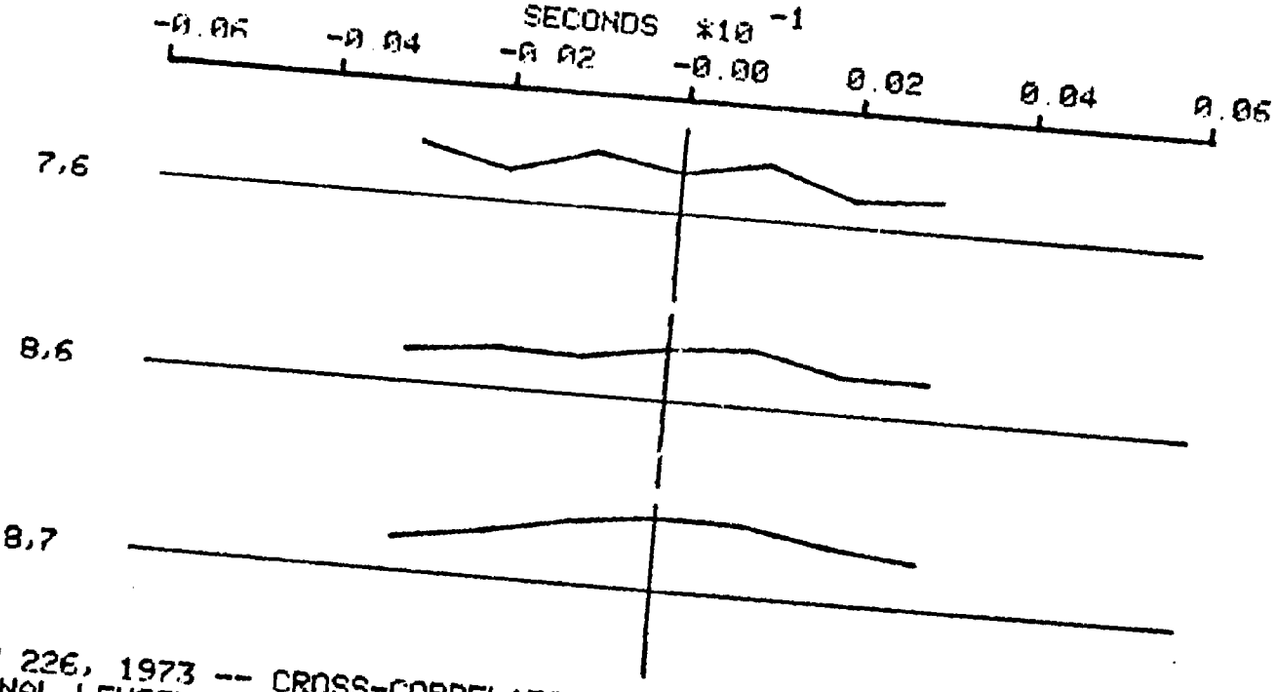

DAY 226, 1973 -- CROSS-CORRELATIONS
SIGNAL LENGTH= 0.050 SEC, MAXIMUM LAG= 0.004 SEC
START TIMES:
MIC# 8 -- 11:50: 2.510
MIC# 7 -- 11:50: 2.549
MIC# 6 -- 11:50: 2.595

ABS.MAX. CORR. (8, 7)= 0.846
ABS.MAX. CORR. (8, 6)= 0.665
ABS.MAX. CORR. (7, 6)= 0.672

FIGURE 4-c

PRIMA-CORD TEST, 1973

DAY 226, 1973 -- SOURCE LOCATION FOR EVENT SPECIFIED BY:

SIG.#3B STARTING AT 11:50: 2.510
SIG.#2B STARTING AT 11:50: 2.549
SIG.#1B STARTING AT 11:50: 2.595

LIGHTNING AT 11:50: 1. 42

SIGNAL LENGTH= 0.050 SEC MAX FREQUENCY= 100. HERTZ

SIG. PAIR	3B,2B	3B,1B	2B,1B
SLOPE (SEC)	-0.00011	-0.00008	0.00006
DIF.ARV.(SEC)	0.03911	0.08508	0.04594

SUM OF SLOPES= 0.0000304 SEC

SIGNAL	3B	2B	1B
TIME TO SRC	1.46800	1.50711	1.55308
METRES	499.12	512.42	528.05

SOURCE COORDINATES AND 95 % CONFIDENCE INTERVALS

	X	Y	Z	
SPHERICAL WAVE SOLUTION	-659.36	380.72	67.33	
+ OR -	0.00	0.00	0.00	TIME WINDOW
SOURCE VOLUME=	0.000000E 00 CUBIC METERS			
+ OR -	4.33	2.78	14.08	TOTAL VARIANCE
SOURCE VOLUME=	0.135740E 04 CUBIC METERS			
PLANE WAVE SOLUTION	-656.83	367.23	64.68	

FIGURE 5

PRIMA-CORD, DAY 226, 1973

x : SADDLE

• : WEST KNOLL

T : TOP

B : BOTTOM

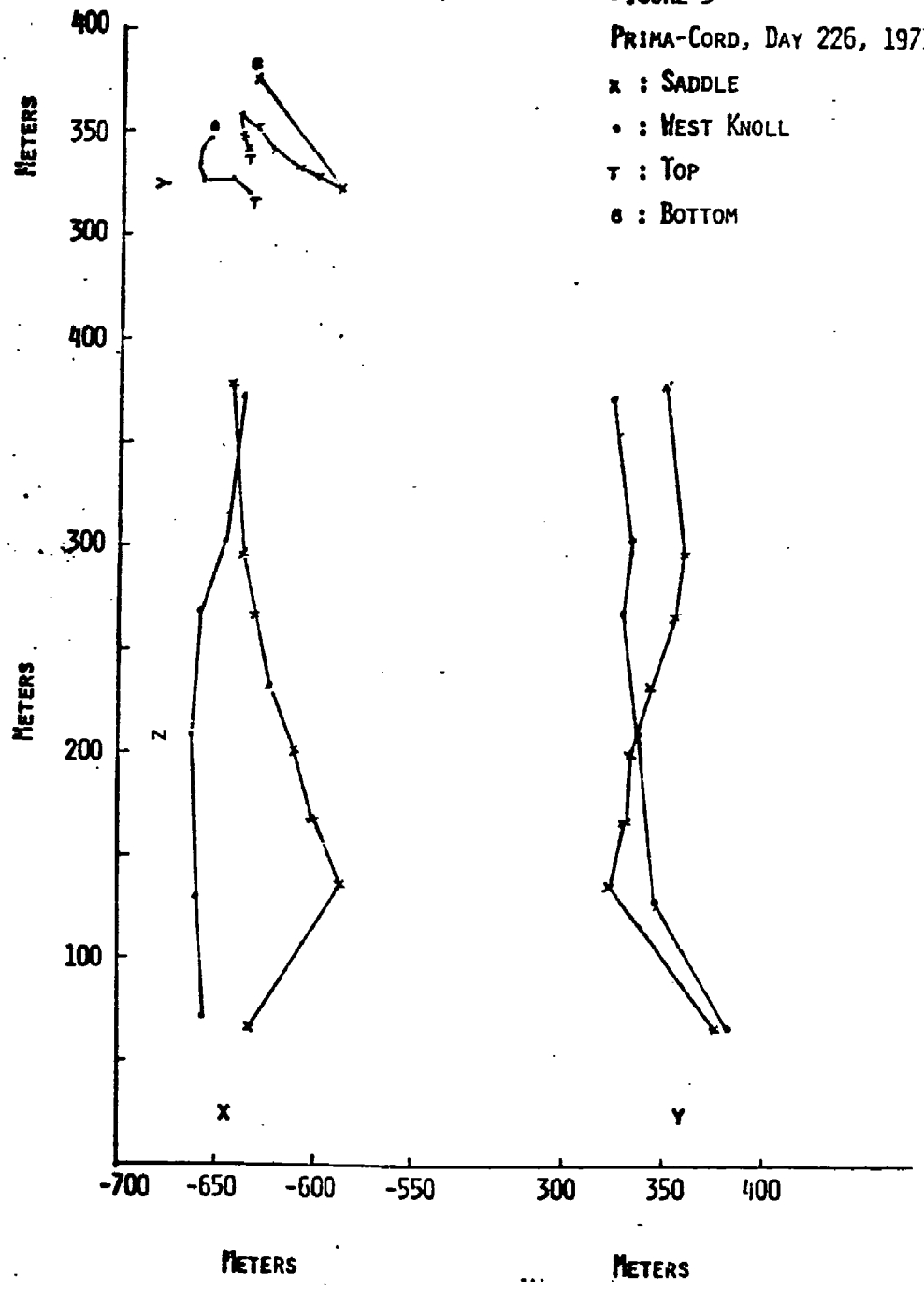

TABLE 2

1973 PRIMA-CORD SHOT

a. Saddle Network	Co-ordinates (Meters)		Maximum Cross-correlation
x	y	z	
-631.7 ± 1.5	376.0 ± 1.4	67.9 ± 1.1	.69
-588.0 ± 3.3	323.1 ± 4.1	135.6 ± .9	.49
-600.1 ± 6.2	331.1 ± 2.7	168.2 ± 1.6	.39
-610.8 ± 3.3	334.6 ± 3.4	200.7 ± .9	.31
-624.0 ± 4.9	342.9 ± 8.7	232.4 ± 1.4	.40
-630.3 ± 12.0	354.4 ± 6.3	265.7 ± 3.2	.21
-640.5 ± 35.0	357.2 ± 7.6	299.1 ± 9.6	.16
-641.0 ± .6	348.6 ± 1.0	379.6 ± .12	.90
b. West Knoll Network			
-659.4 ± 4.3	380.7 ± 2.8	67.3 ± 14	.85
-660.9 ± 7.6	344.1 ± 5.8	130.1 ± 17	.82
-663.9 ± 8.4	332.3 ± 6.9	208.8 ± 13.4	.72
-661.6 ± 7.2	327.3 ± 3.0	269.0 ± 9.5	.86
-646.6 ± 3.7	331.8 ± 3.0	305.0 ± 4.7	.87
-636.4 ± 2.2	324.2 ± 1.6	373.9 ± 2.4	.99
c. Double Theodolyte Survey			
Top: -648	356	385	
Bottom: -723 (Best guess)	385	85	

V. LOCATION FOR SOME LIGHTNING EVENTS

This section includes a few reconstructions for lightning events. The primary purpose is to show some reconstructions and also to discuss procedures and problems associated with reconstruction of lightning paths by the techniques discussed in this report. Note that while the individual points are connected these connections are to a large extent guesses and are made to give some order to the data. The more tortorous parts of the channels may indeed look a lot different than what the figures below show. The examples will be presented first with a few comments. The section closes with some more detailed comments on methods and procedures.

Event 1 - Day 233, 1977

Figures 6-a through 6-f show some results from a lightning event as recorded on the West Knoll network (30 meter spacings). This event was tracked with both the West Knoll and Saddle (30 meter spacings) networks and the results are shown in Table 3. The two-dimensional views of the reconstruction are shown in Figure 7 and a possible channel is indicated. While it is difficult to completely reconstruct the lightning path, the general region of the stroke is fairly clear with both networks agreeing fairly well.

Event 2 - Day 209, 1975

This event was recorded on three networks: Saddle (100 meter spacing), West Knoll (30 meter spacing), and Solar Tower (30 meter spacing).

FIGURE 6-A

EVENT 1, DAY 233, 1977

WEST KNOLL NETWORK

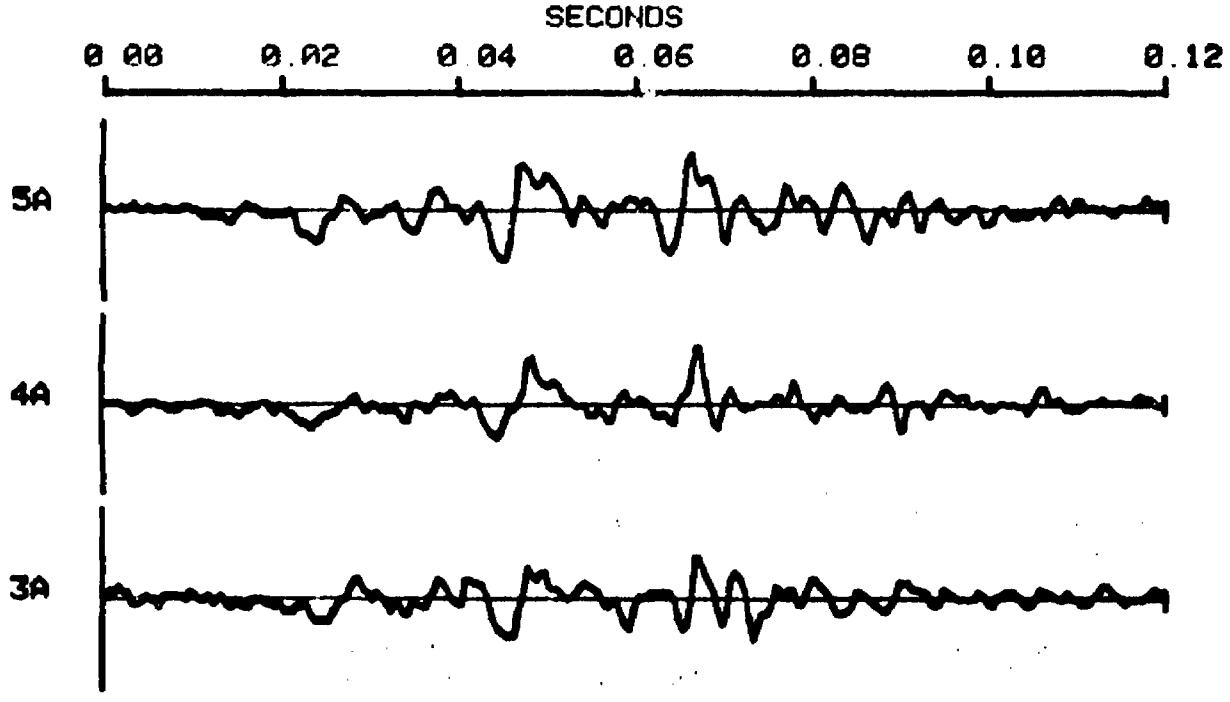

DAY 233,1977 -- PRESSURE SIGNATURE
SIGNAL LENGTH= 0.120 SEC. FULL SCALE DEVIATION= 1.000 NEWTON/SQUARE METER
START TIMES:
SIG#3A -- 14:24: 6. 0
SIG#4A -- 14:24: 6. 88
SIG#5A -- 14:24: 6. 63

FIGURE 6-B

EVENT 1, DAY 233, 1977

WEST KNOLL NETWORK

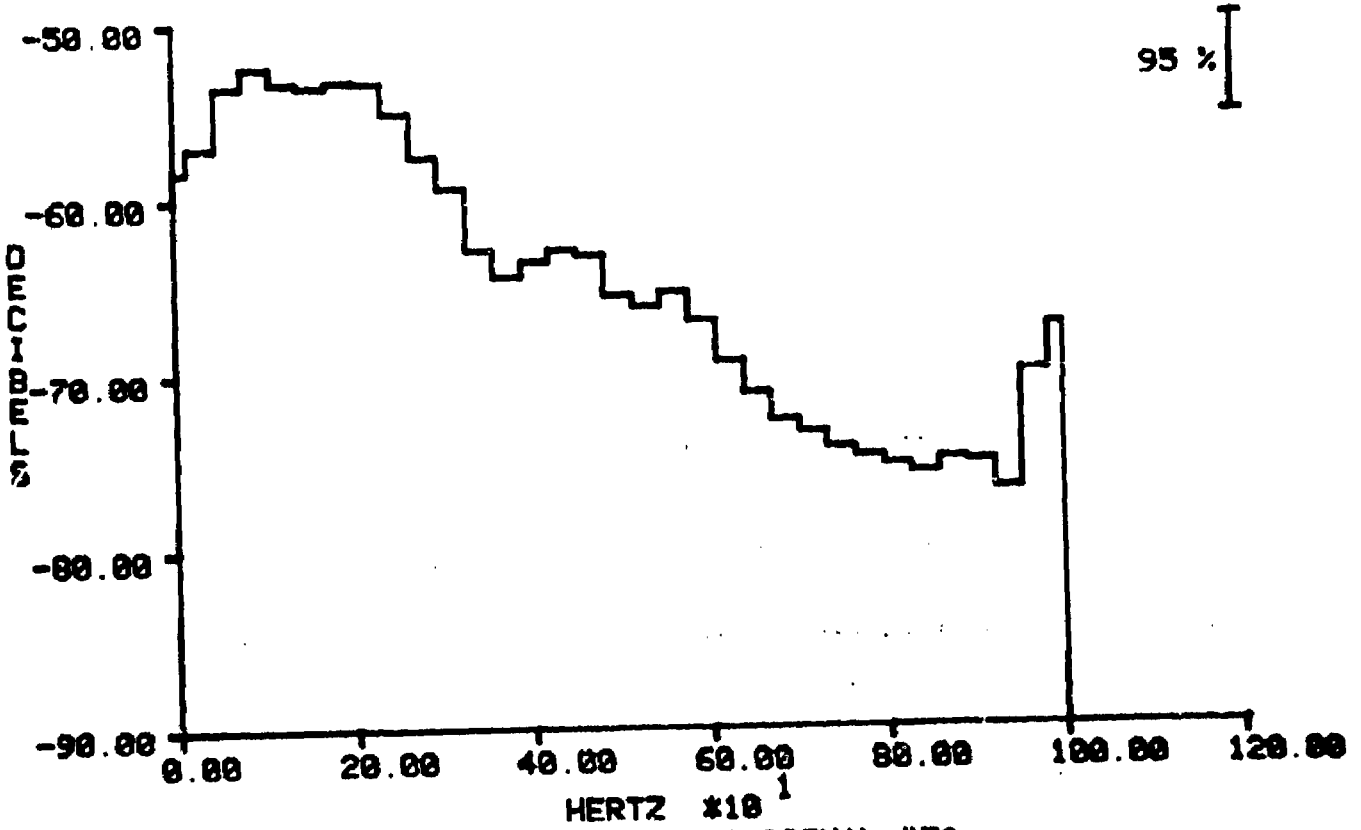

DAY 233, 1977 — SPECTRAL DENSITY FOR SIGNAL #3A
NU= 20, BW= 83.3, LENGTH= 0.120 SEC.
SIG#3A, STARTS 14:24: 6. 0 MST.

FIGURE 6-c

EVENT 1, DAY 233, 1977

WEST KNOLL NETWORK

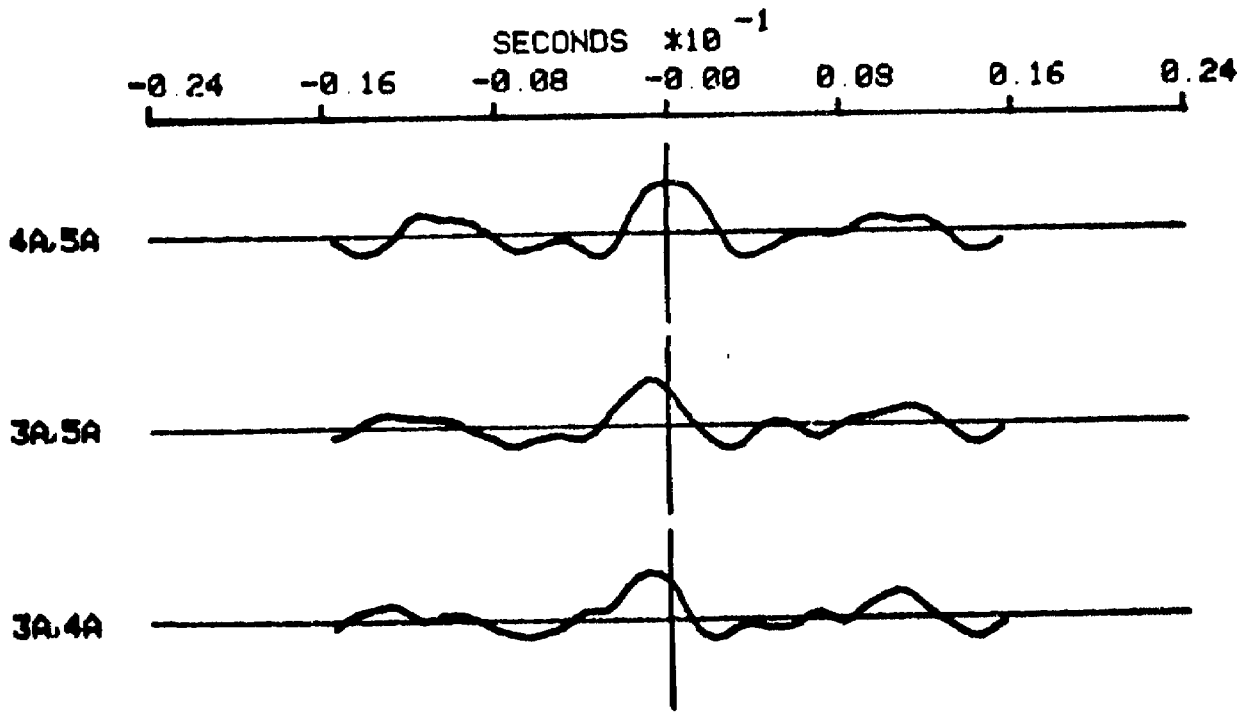

DAY 233, 1977 -- CROSS-CORRELATIONS
SIGNAL LENGTH= 0.120 SEC, MAXIMUM LAG= 0.016 SEC
START TIMES:
SIG#3A — 14:24: 6. 0
SIG#4A — 14:24: 6. 88
SIG#5A — 14:24: 6. 63

ABS.MAX. CORR. (3A,4A)= 0.513
ABS.MAX. CORR. (3A,5A)= 0.526
ABS.MAX. CORR. (4A,5A)= 0.565

FIGURE 6-D

EVENT 1, DAY 233, 1977

WEST KNOLL NETWORK

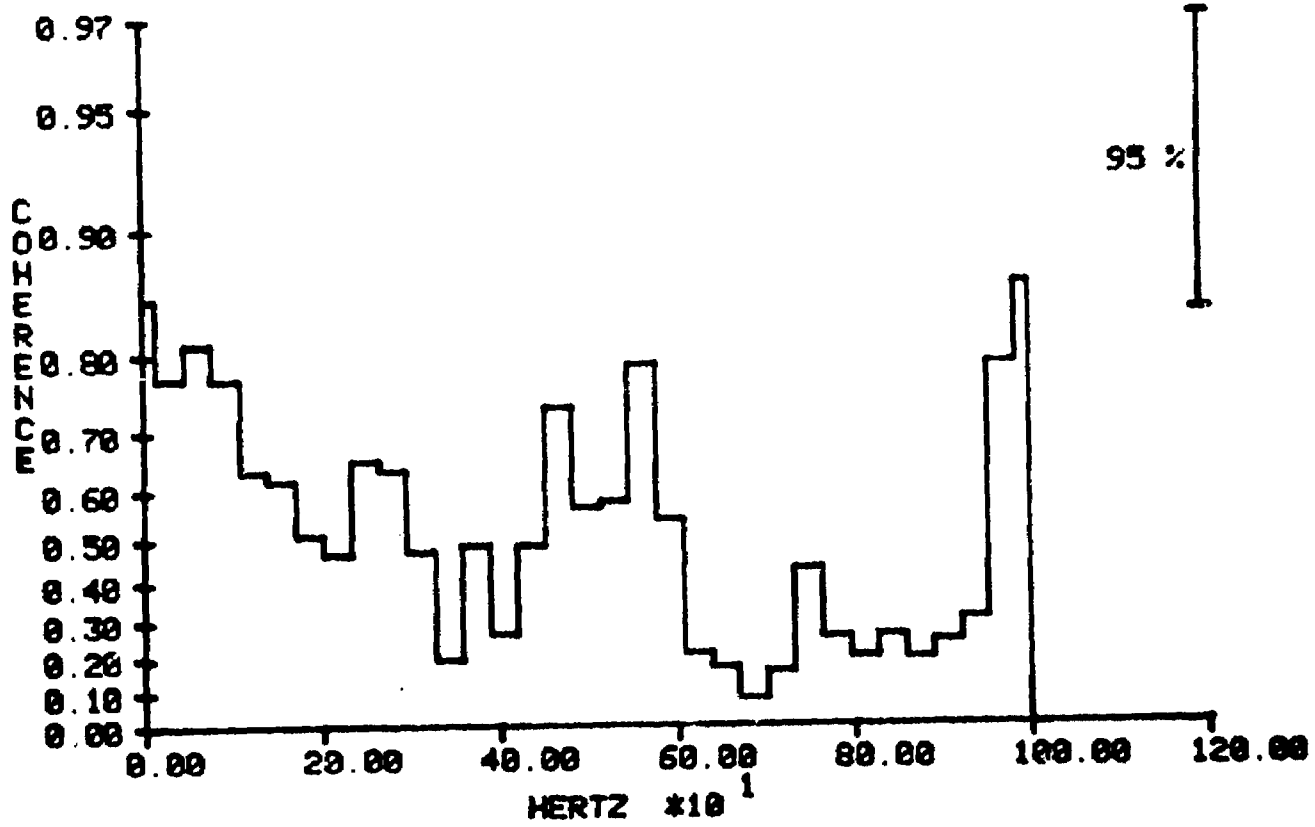

DAY 233, 1977 -- COHERENCY
NU= 20, BW= 83.33 HZ., SIGNAL LENGTH= 0.120 SEC
SIG#3A, AT 14:24: 6. 0 MST.
SIG#4A, AT 14:24: 6. 00 MST.

FIGURE 6-E

EVENT 1, DAY 233, 1977

WEST KNOLL NETWORK

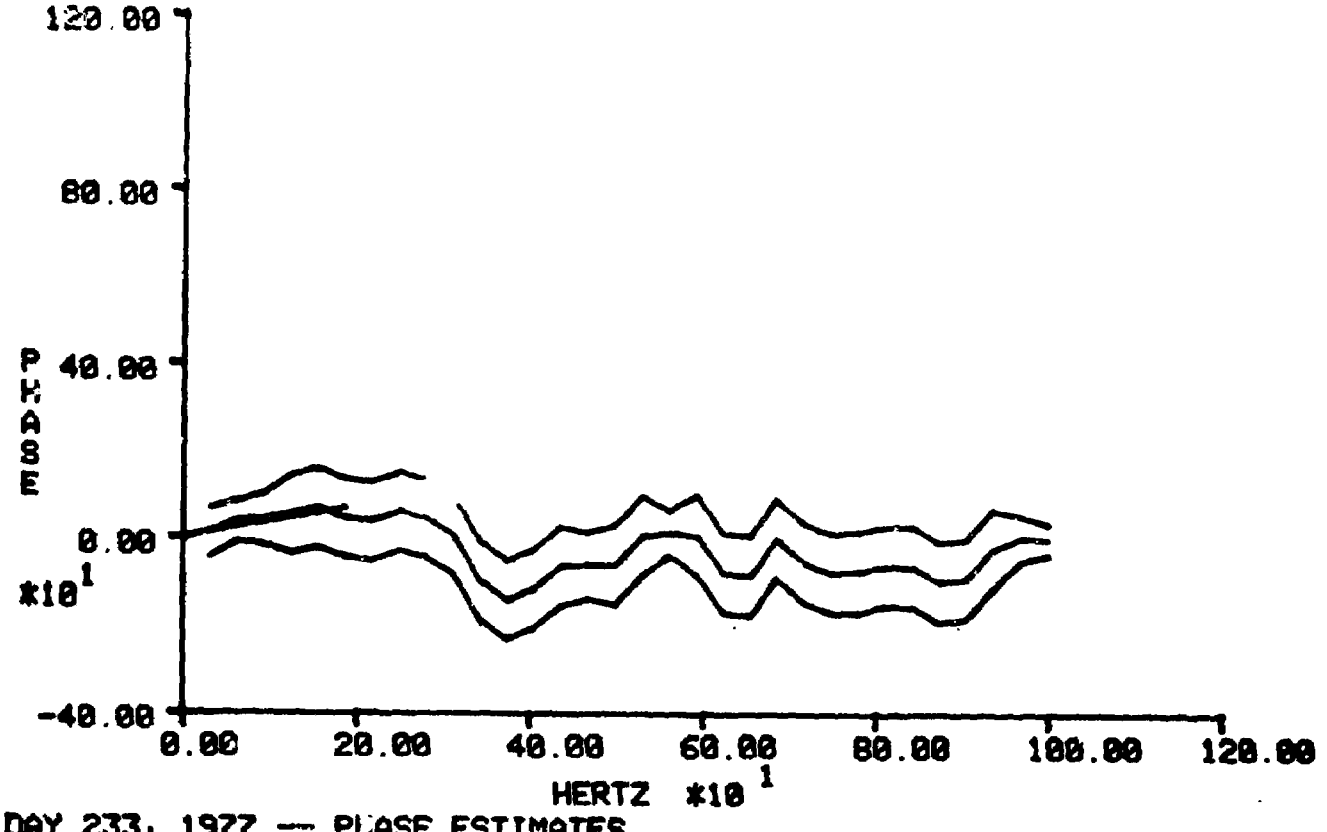

DAY 233, 1977 — PHASE ESTIMATES
NU= 20, BW= 83.33 HZ., SIGNAL LENGTH= 0.120 SEC, SLOPE= 0.0010 SEC
SIG#3A, AT 14:24: 6. 0 MST.
SIG#4A, AT 14:24: 6. 88 MST.

FIGURE 6-F

EVENT 1, DAY 233, 1977

WEST KNOLL NETWORK

DAY 233, 1977 -- SOURCE LOCATION FOR EVENT SPECIFIED BY:

SIG.#3A STARTING AT 14:24: 6. 0
SIG.#4A STARTING AT 14:24: 6. 88
SIG.#5A STARTING AT 14:24: 6. 63

LIGHTNING AT 14:23:59.166

SIGNAL LENGTH= 0.120 SEC MAX FREQUENCY= 200. HERTZ

SIG. PAIR	3A,4A	3A,5A	4A,5A
SLOPE (SEC)	0.00102	0.00084	-0.00023
DIF.ARV.(SEC)	0.08698	0.06216	-0.02477

SUM OF SLOPES= -0.0000620 SEC

SIGNAL	3A	4A	5A
TIME TO SRC	6.83400	6.92098	6.89616
METRES	2323.56	2353.13	2344.69

SOURCE COORDINATES AND 95 % CONFIDENCE INTERVALS

SPHERICAL WAVE SOLUTION	X	Y	Z	
	-3356.18	-348.10	289.75	
+ OR -	0.00	0.00	0.00	TIME WINDOW
SOURCE VOLUME=	0.000000E 00 CUBIC METERS			
+ OR -	28.33	20.31	187.45	TOTAL VARIANCE
SOURCE VOLUME=	0.862701E 06 CUBIC METERS			

PLANE WAVE SOLUTION	X	Y	Z
	-3356.99	-357.81	267.03

TABLE 3

CO-ORDINATES FOR EVENT 1 (Day 233, 1977)

Lightning at 14:23:59.166

a. Saddle Network

	Start Time	Co-ordinates (Meters) x	y	z
	14:24:07.124	-3245 ± 50	-51 ± 92	69 ± 770
	14:24:07.409	-3276 ± 42	-330 ± 56	256 ± 295
*	14:24:07.703	-3221 ± 96	-554 ± 125	726 ± 223
	14:24:08.572	-3602 ± 34	-272 ± 172	752 ± 141
	14:24:08.772	-3664 ± 82	-274 ± 205	786 ± 275
	14:24:09.626	-3713 ± 35	-974 ± 57	981 ± 89

b. West Knoll Network

	14:24:06.00	-3356 ± 28	-348 ± 20	290 ± 187
*	14:24:06.147	-3334 ± 31	-380 ± 21	570 ± 95
	14:24:06.347	-3319 ± 31	-425 ± 36	785 ± 72

*Times indicate these two points are close to each other.

FIGURE 7

EVENT 1, DAY 233, 1977

x : SADDLE

• : WEST KNOLL

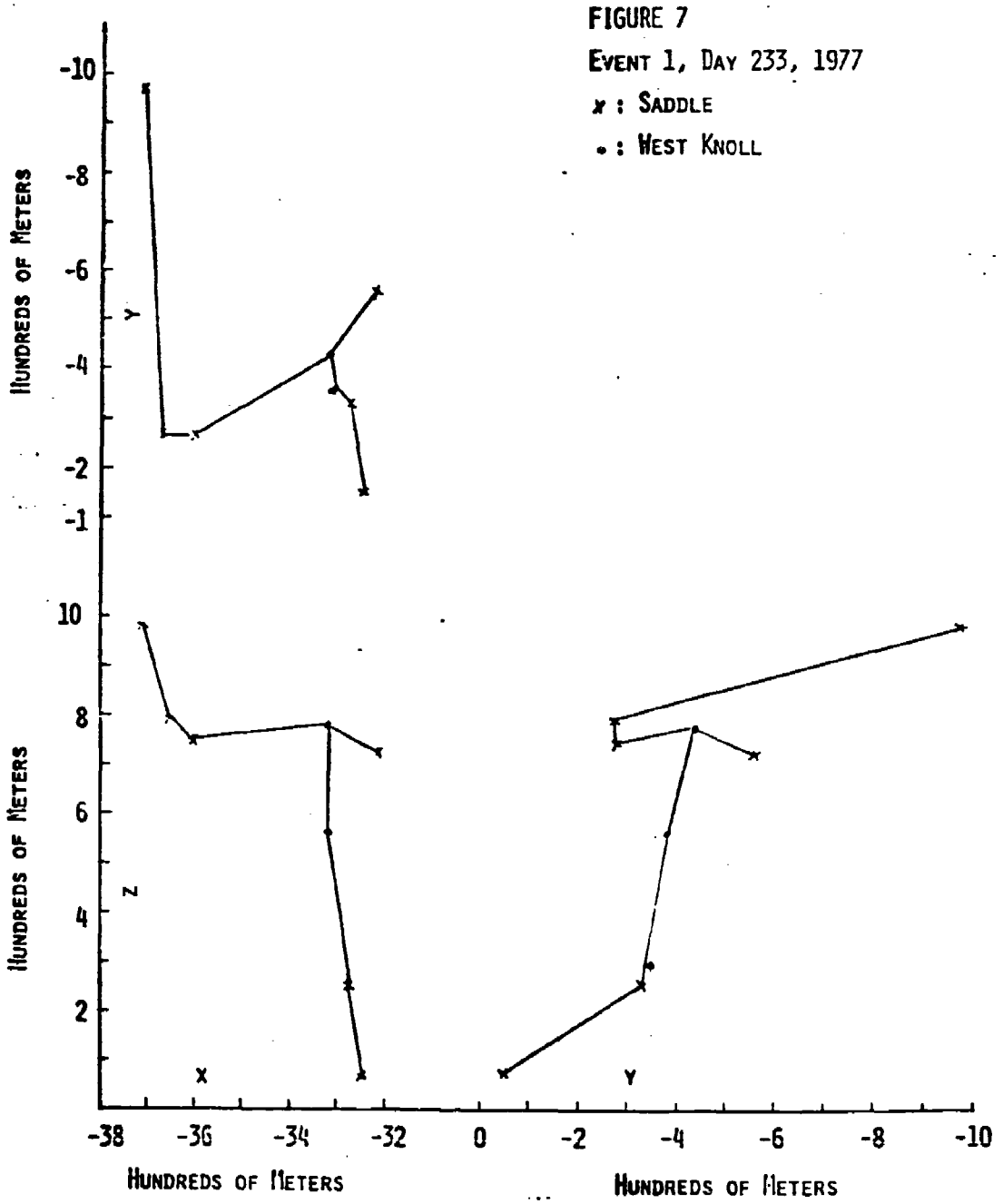

TABLE 4

CO-ORDINATES FOR EVENT (Day 209, 1975)

Lightning at 12:47:07.550

a. Saddle Network

Co-ordinates (Meters)			Maximum Cross-correlation
x	y	z	
-1230	1645	226	.70
-1397	1598	993	.75
-706	1900	2351	.62

b. West Knoll Network

-1151	1705	19	.28
-1332	1721	385	n.a.
-1415	1801	1280	.76
-1489	1814	1500	n.a.
-1084	1762	2135	.74
-803	1775	2339	.54
-688	1858	2395	.71

c. Solar Tower Network

-1317	1660	111	.30
-1387	1622	1156	.78
-1545	1679	1532	.69
-1587	1635	1744	.34
-882	1731	2438	.64
-344	1926	2570	.60

n.a. means not available.

FIGURE 8

EVENT 2, DAY 209, 1975

x : SADDLE

• : WEST KNOLL

o : SOLAR TOWER

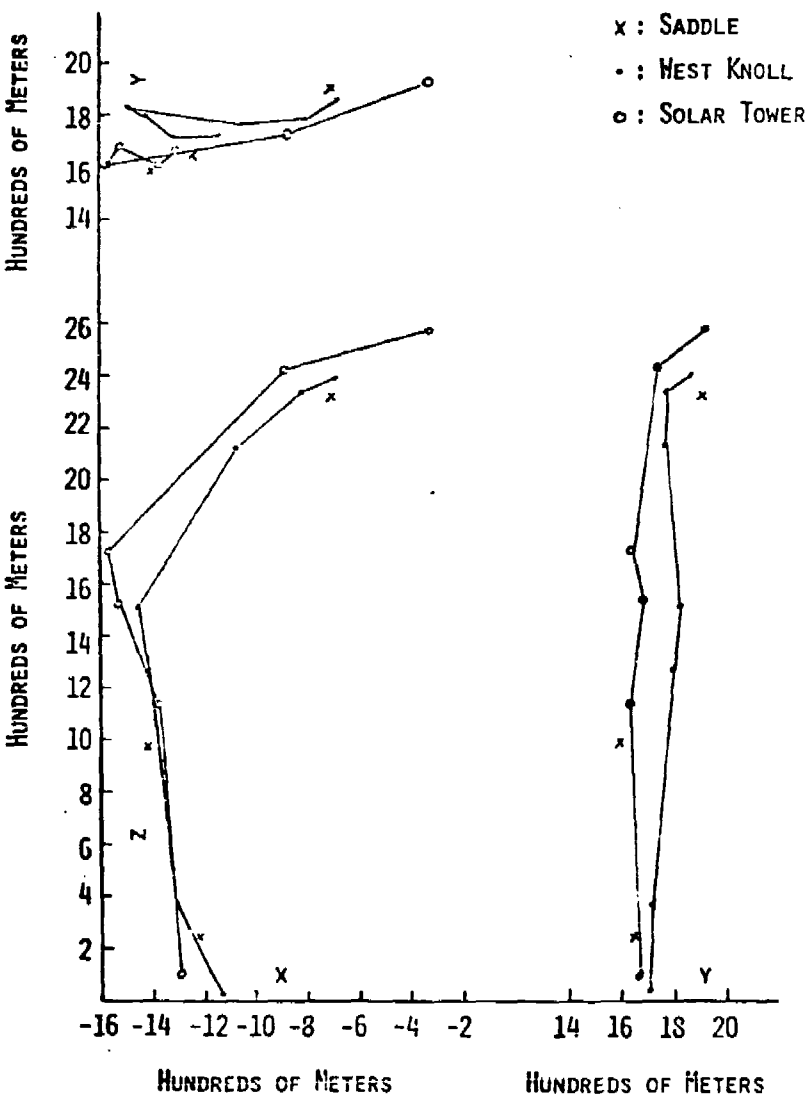

The reconstruction for this (and the following events) was done with an earlier version of the computer program. The earlier version added half the width of the signal to the times of arrival, as indicated above, and also had in error in the confidence interval calculations. Consequently the results in Table 4 don't include any error limits. The graphs for this event are in Figure 8. The three networks give results that agree very well. This appears to be a very clean cloud-to-ground stroke with little evidence of branching.

Event 3 - Day 213, 1976

Figures 9-a and b show a signal at the Solar Tower network (30 meter spacing) for a more complex and long record. Figure 9-a shows one-second of the data and Figure 9-b shows .300 seconds. One can pick out corresponding features from the three signals quite easily and the cross-correlations between various signal segments were quite high.

Figure 10 shows the two-dimensional views with a possible path. In addition the relative maxima of the maximum correlation values are shown along the signal path. Here it would appear that cross-corrections are maximum at corner points or branching points.

Event 4 - Day 210, 1975

Table 5 and Figures 11-a, b, and c show a reconstruction for what would appear to be a cloud-to-cloud stroke. Three networks were used as the figures and table indicate. Again this was done with the early version and consequently no

FIGURE 9-A

EVENT 3, DAY 213, 1976

SOLAR TOWER NETWORK

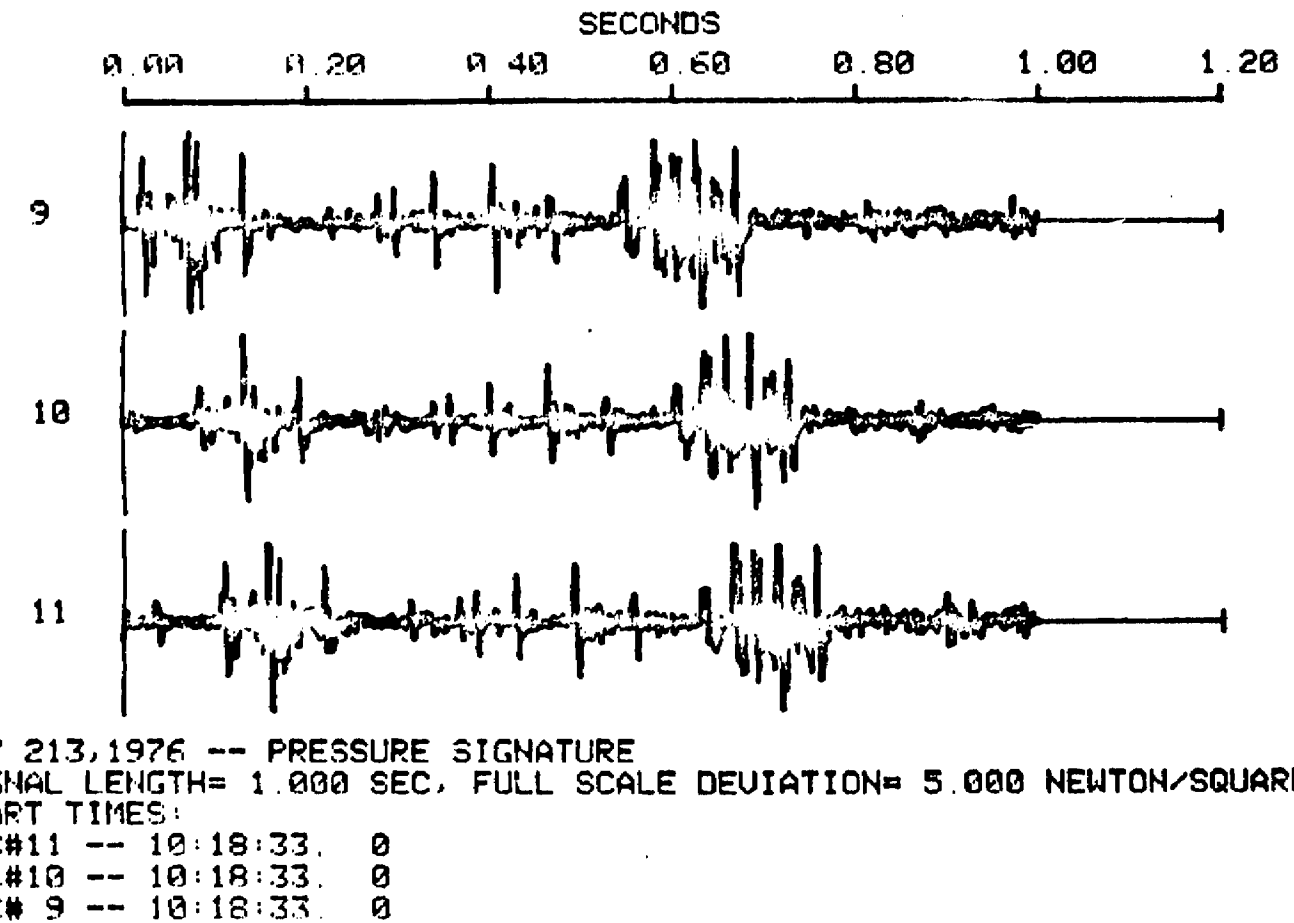

DAY 213,1976 -- PRESSURE SIGNATURE
SIGNAL LENGTH= 1.000 SEC, FULL SCALE DEVIATION= 5.000 NEWTON/SQUARE METER
START TIMES:
MIC#11 -- 10:18:33. 0
MIC#10 -- 10:18:33. 0
MIC# 9 -- 10:18:33. 0

FIGURE 9-B

EVENT 3, DAY 213, 1976

SOLAR TOWER NETWORK

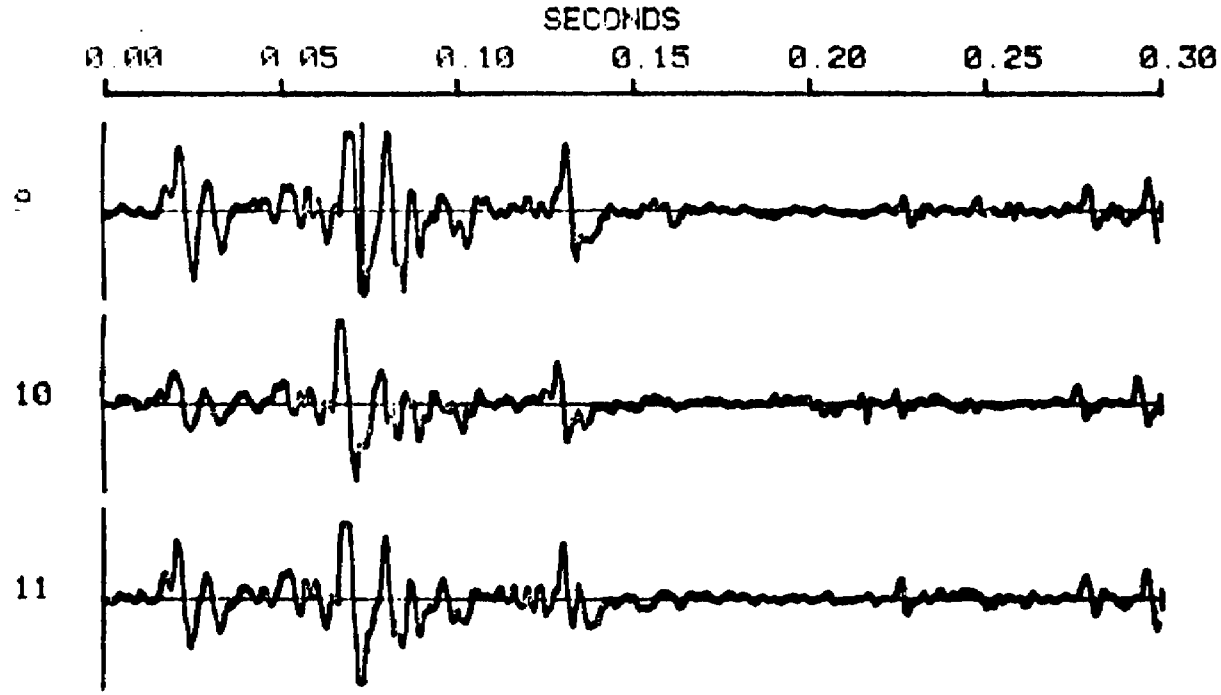

DAY 213.1976 -- PRESSURE SIGNATURE
SIGNAL LENGTH= 0.300 SEC, FULL SCALE DEVIATION= 5.000 NEWTON/SQUARE METER
START TIMES:
MIC#11 -- 10:18:33. 90
MIC#10 -- 10:18:33. 64
MIC# 9 -- 10:18:33. 0

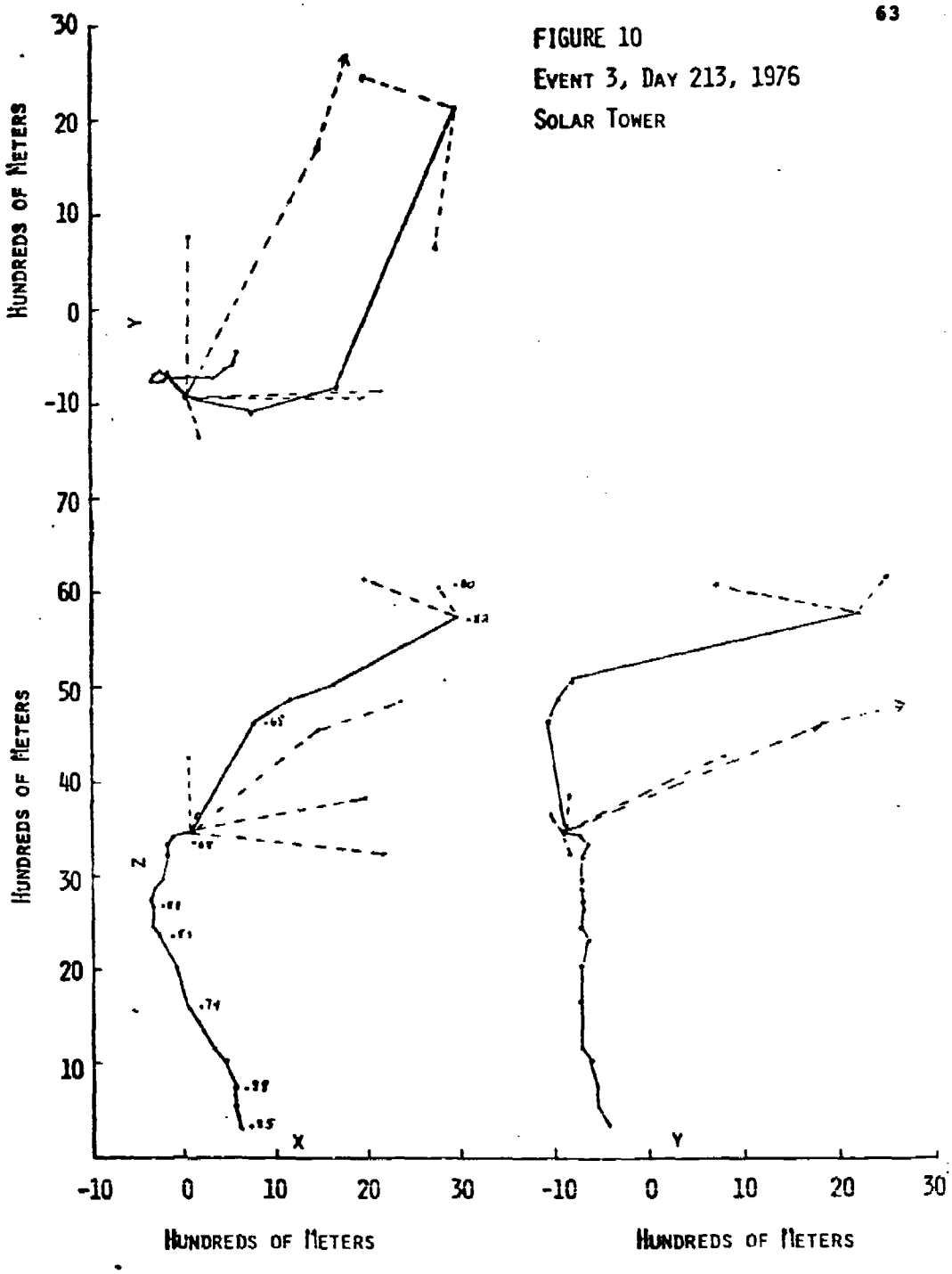

FIGURE 10
EVENT 3, DAY 213, 1976
SOLAR TOWER

TABLE 5

CO-ORDINATES FOR EVENT 4 (Day 210, 1975)

Lightning at 11:29:12.760

	Co-ordinates (Meters)			Maximum Cross-correlation
	x	y	z	
a. Saddle Network				
	942	5529	3146	.72
	-732	4180	2382	.29
	1620	2755	3299	.81
	2361	2199	4069	.71
	816	5303	2773	.74
	185	6011	2736	.74
	680	2549	6435	.68
	-302	4287	6890	.55
	-4818	6899	4154	.84
b. West Knoll Network				
	1404	2247	2979	.63
	1734	2841	3131	.72
	2033	2672	2984	.73
	1884	2067	4397	.60
	1222	3309	5964	.54
	-2532	5537	5267	.59
	-2028	5267	5617	.60
	-641	5258	6065	.32
c. Solar Tower Network				
	-761	2361	2809	.52
	-453	3901	2785	.55
	1457	3754	3185	.50
	1685	2513	4360	.75
	911	3540	5980	.67
	-2508	5350	5447	.45
	-5805	5521	3137	.62
	-5055	7003	3933	.76

FIGURE 11-A

EVENT 4, DAY 210, 1975

x : SADDLE

• : WEST KNOLL

o : SOLOR TOWER

(X - Z VIEW)

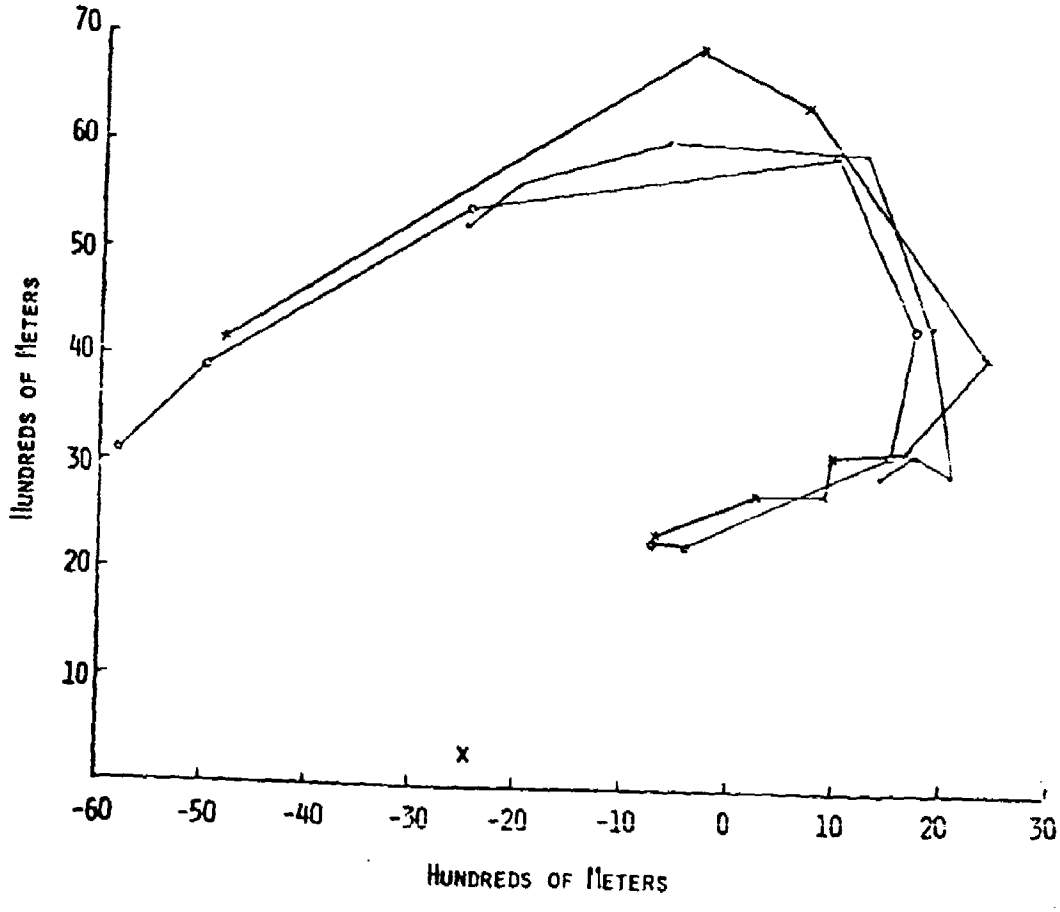

FIGURE 11-B
EVENT 4, DAY 210, 1975
x : SADDLE
• : WEST KNOLL
o : SOLAR TOWER
(Y - Z VIEW)

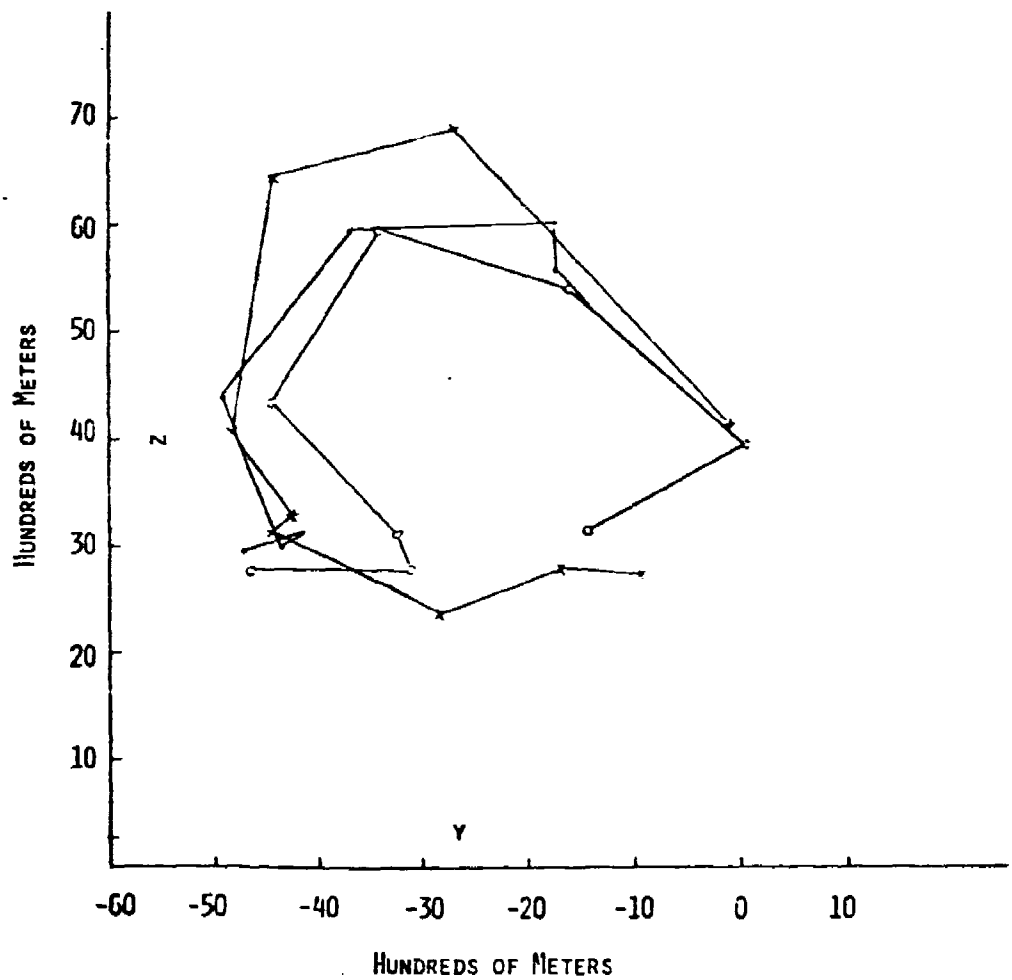

FIGURE 11-c

EVENT 4, DAY 210, 1975

x : SADDLE

· : WEST KNOLL

o : SOLAR TOWERS

(x - y VIEW)

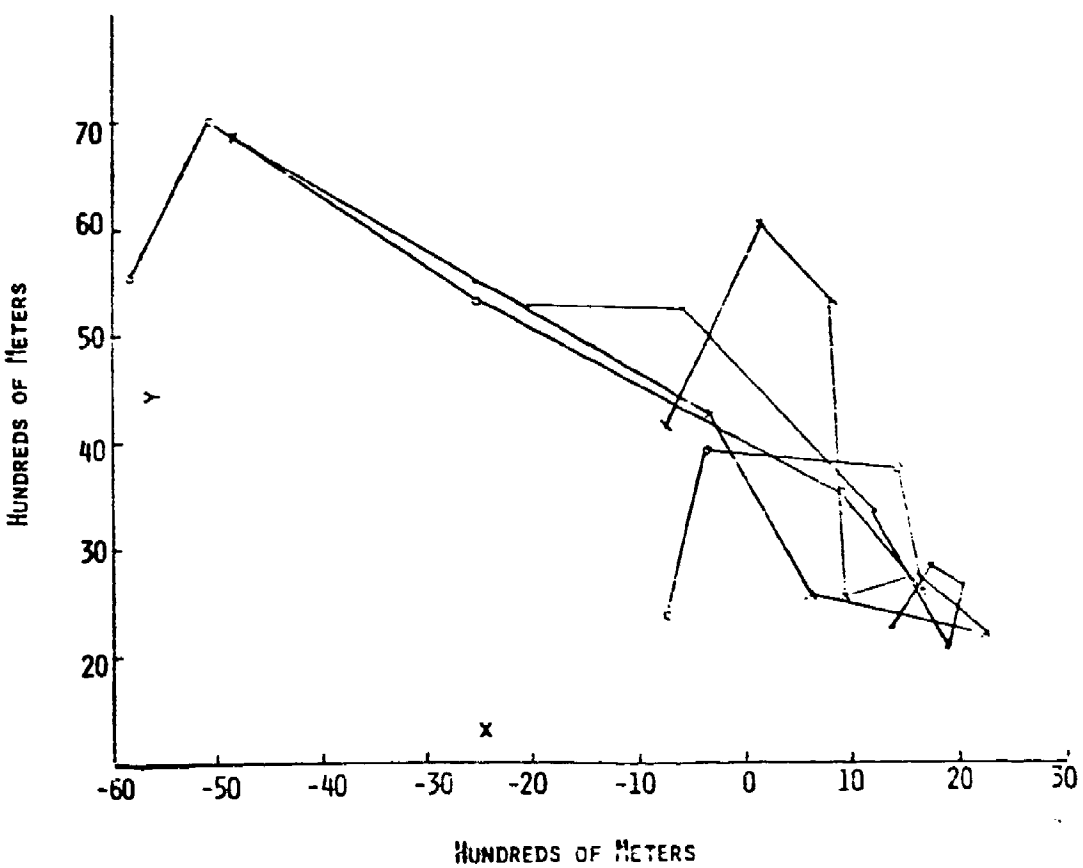

confidence intervals are given in the table. The three reconstructions seem to agree fairly well and once again suggested patterns for the stroke are sketched in the figures. Again higher correlation values seem to be associated with turning points.

Comments on Lightning Channel Reconstruction

The purpose of this report has been primarily to review and present the techniques of lightning channel reconstruction from acoustic data. The following comments pertain to the use of these techniques.

Reconstruction of lightning paths using the acoustic technique is a rather time consuming process. It requires constant operator attention and is rather dependent on a good initial guess regarding signal alignment. A reasonably clean signal (i.e., isolated from other noise sources) is needed in order for the method to succeed. The results presented here and additional confirmatory results using independent radar measurements by Szymanski (1977) do indicate that the technique can, under proper conditions yield a reasonably accurate reconstruction of a channel.

Problems involving the physics of the process need more investigation, however. For example a detailed study of the interference expected between the acoustic signals from different segments of the lightning path should be made to see what effect such interference has on the reconstruction. Higher correlations do appear to occur at branching or turning points suggest such interference or interaction is minimized at these

points. An examination of the relation between tortuosity and correlation is clearly a subject that needs more study. Finally the effect of assuming a spherical rather than a cylindrical wave may also introduce some bias into the reconstruction.

The confidence intervals given in the paper are predicated on an accurate model and pertain primarily to estimation techniques. The fact that for some of the test cases these intervals did not contain the surveyed point does indicate that the model may be biased although not to a very strong degree.

ACKNOWLEDGMENTS

Robert Rogers wrote an initial version of the computer program for the PDP 11. This program was refined and streamlined by James Fordice. This research was supported by ONR Grant # N0014-75-C-0169.

APPENDIX A

Stochastic Analysis and Spectral Analysis

The general time series model deals with second order stationary processes, which we define below.

Definition: $X(t)$ is a second order stationary stochastic process, if

(a) $E(X(t)) = \mu$

(b) $COV(X(t),X(t + s)) = \Gamma(s)$.

Thus, the process must have a constant mean and a covariance function that only depends on the time difference. We use E to denote expected value and COV for covariance.

$$COV(X(t),X(t + s)) = E[X(t) \cdot X(t + s)] - E[X(t)]\, E[X(t + s)] \quad \ldots\ldots (A.1)$$

in case $X(t)$ is a real process.

If Z and W are complex random variables and if W* is the complex conjugate of W*, then

$$COV(Z,W) = E(ZW^*) - E(Z)\, E(W^*). \quad (A.2)$$

Condition (a) in the definition above is not as stringent as condition (b). In particular, if $E(X(t)) = \mu(t)$, then using $X(t) - \mu(t)$ in place of $X(t)$ will eliminate the dependence on t. In addition $E(X(t) - \mu(t)) = 0$, and consequently we often assume without loss of generality that $E(X(t)) = 0$.

For a second order stationary process,

$$VAR(X(t)) = \Gamma(0)$$

and, since $VAR(X(t + s) - X(t)) \geq 0$, $\Gamma(0) \geq \Gamma(s)$ for all s.

In addition $\Gamma(s) = \Gamma(-s)$. Hence, cos(s) is a valid covariance function but sin(s) is not.

If a process is not second-order stationary, very little can be done. (See Hannan, p. 77). Most of the theory for second-order stationary processes relies on the following two representation theorems.

THEOREM I. If X(t) is a second-order stationary process then there exists a complex random process, $Z(\nu)$, such that

$$X(t) = \int_{-\infty}^{\infty} e^{-i\nu t} Z(d\nu) \tag{A.3}$$

where $COV(Z(\Delta\nu_1), Z(\Delta\nu_2)) = 0$ if $\Delta\nu_1$ and $\Delta\nu_2$ are two disjoint intervals and $Z(-\Delta\nu) = Z^*(\Delta\nu)$. ($Z(A) = Z(b) - Z(a)$ if $A = [b,a]$ is an interval on the ν axis).

THEOREM II. If $\Gamma(s)$ is the covariance function of the second-order stationary process X(t), then

$$\Gamma(s) = \int_{-\infty}^{\infty} e^{-i\nu s} F(d\nu) \tag{A.4}$$

where $F(\Delta\nu) > 0$ and $E(|Z(\Delta\nu)|^2) = F(\Delta\nu)$.

A proof of these theroems can be found in Rosenblatt, Chapter VII (1963).

$F(\nu)$ is called the spectral distribution function. If $F(\nu)$ is differentiable then $f(\nu) = \frac{dF}{d\nu}(\nu)$ is called the spectral density for the process.

The ν's correspond to frequencies while the $Z(\nu)$'s assign

complex weights to frequency ν. By Theorem I, a second-order stationary process is a mixture of sines and cosines with random amplitudes at each frequency. The condition that $Z(-\Delta\nu) = Z^*(\Delta\nu)$ ensures a real value for $X(t)$. The usefulness of Theorem I is due to the uncorrelated nature of the random amplitudes, $Z(\Delta\nu)$.

In Theorem II, the definition of $F(\Delta\nu)$ and the fact that $Z(-\Delta\nu) = Z^*(\Delta\nu)$ imply $F(\Delta\nu) = F(-\Delta\nu)$ and hence $f(\nu) = f(-\nu)$ if the spectral density exists. We will assume $f(\nu)$ always exists in the rest of this paper.

From the relationship between a Fourier transform and its inverse, we can obtain $Z(\Delta\nu)$ and $f(\nu)$ by taking the appropriate transform of $X(t)$ and $\Gamma(s)$. In order to make these transform pairs more symmetric in appearance and also to make the results consistent with conventional engineering approaches and computer programs, let $\nu = 2\pi u$. Then

$$Z(\Delta u) = \int_{-\infty}^{\infty} \exp\{-2\pi\Delta u t i\}\, X(t)dt \qquad (A.5)$$

and

$$f(u) = \int_{-\infty}^{\infty} e^{-2\pi i u s}\, \Gamma(s)ds. \qquad (A.6)$$

(In practica' calculation, only positive frequencies are used and the resulting estimate is doubled.)

The results of Theorem I and II show that one can obtain the spectral density in 2 different ways. One way, via equation A.6, is to take the Fourier transform of the covariance function. The other way is to use the fact that

$f(u)\,\Delta u \approx F(\Delta u) = E(|Z(\Delta u)|^2)$ and hence use equation A.5 to obtain $Z(\Delta u)$ and then square the absolute value. Both procedures have been used in theory and in practice and each method leads to insight about the behavior of spectral estimates.

In particular, we will use $f(u)\Delta u = E(|Z(\Delta u)|^2)$ to see why the chi-square distribution is used to set confidence intervals on estimated spectra and also to see why smoothing is desirable when one estimates spectra.

We will start by assuming that $Z(u)$ is a complex Gaussian process. This means $(Re(Z(\Delta u_i)), Im(Z(\Delta u_i)))$ $i = 1,\ldots n$ are jointly normal. This also implies $X(t)$ is a Gaussian process and, since $E(X(t)) = 0$, $E(Z(u)) = 0$. It can be shown (Breiman, Chapter 9, or Hannan, Chapter 2) that

$$COV(Re(Z(\Delta u)), Im(Z(\Delta u))) = 0 \qquad (A.7.a)$$

$$VAR(Re(Z(\Delta u))) = \frac{F(\Delta u)}{2} \qquad (A.7.b)$$

and $$VAR(Im(Z(\Delta u))) = \frac{F(\Delta u)}{2} \; . \qquad (A.7.c)$$

Consequently the real and imaginary parts of $Z(\Delta u)$ are statistically independent, normal random variables, each with mean 0 and variance $\frac{F(\Delta u)}{2}$. Hence

$$\frac{2|Z(\Delta u)|^2}{F(\Delta u)} \qquad (A.8)$$

has a chi-squared distribution with 2 degrees of freedom. In addition, if Δu and $\Delta u'$ are non-overlapping intervals then

$$\frac{2|Z(\Delta u)|^2}{F(\Delta u)} + \frac{2|X(\Delta u')|^2}{F(\Delta u')} \qquad (A.9)$$

will have a chi-squared distribution with 4 degrees of freedom since the 2 terms correspond to independent chi-squared variables, each with 2 degrees of freedom.

If Z(u) is not a Gaussian process one can still obtain an approximate chi-squared distribution as the argument below shows.

Suppose $\Delta u = [a,b)$ is an interval in frequency space. Break up the interval [a,b) into n non-overlapping intervals

$$[a,b) = \bigcup_{i=0}^{n-1} \left[a + i\left(\frac{b-a}{n}\right),\ a + (i+1)\left(\frac{b-a}{n}\right)\right)$$

$$\equiv \bigcup_{i=0}^{n-1} A_i$$

$$Z(\Delta u) = \sum_{i=0}^{n-1} Z(A_i). \qquad (A.10)$$

If $Z(A_i) = Z\left(a + (i+1)\frac{b-a}{n}\right) - Z\left(i + i\left(\frac{b-a}{n}\right)\right)$ and if

$$F(A_0) \approx F(A_1) \approx F(A_2) \ldots \approx F(A_n), \qquad (A.11)$$

where $F(A_i) = E(|Z(A_i)|^2)$, then if the central limit theorem applies, $Z(\Delta u)$ is approximately Gaussian and the previous results apply with $F(\Delta u) = nF(A_0)$.

This approach also shows why the variance of the spectrum doesn't decrease with increasing sample size. For example, if $2|Z(\Delta u)|^2/F(\Delta u)$ has a χ^{-2} distribution with 2 degrees of freedom,

$$\mathrm{VAR}[2|Z(\Delta u)|^2/F(\Delta u)] = 4 \text{ and}$$

$$\mathrm{VAR}(|Z(\Delta u)|^2) = F^2(\Delta u),$$

independent of the sample size. If the spectrum is reasonably flat, one can improve estimates for the spectral density by averaging over several frequency bands and hence improve the accuracy of the estimates without introducing any appreciable bias.

If the covariance function is used in the spectral estimation, a weighting function (called a lag window) $W(t)$ is used to smooth the spectral estimate. $W(t)$ is a function such that:

$$W(o) = 1 \tag{A.12.a}$$

$$W(t) = W(-t) \tag{A.12.b}$$

and $$W(t) = 0 \text{ if } |t| > L. \tag{A.12.c}$$

The smoothed spectrum is

$$f_W(u) = \int_{-\infty}^{\infty} W(t)\, \Gamma(t) e^{-i2\pi ut}\, dt. \tag{A.13}$$

If $w(u)$ is the Fourier transform of $W(t)$ and $f(u)$ is the Fourier transform of $\Gamma(t)$ then by the convolution property of transforms,

$$f_W(u) = \int_{-\infty}^{\infty} w(v)\, f(u-v)dv. \tag{A.14}$$

$w(u)$ is called the spectral window. Thus, one can smooth either before or after transformation of the covariance function.

A lag or spectral window can be used to reduce

the variance of the estimate but it can also lead to biased and correlated estimates. (See Jenkins and Watts, p. 247).

If $u_1 \leq u \leq u_2$,

$$COV(f_W(u_1)\ f_W(u_2)) \approx \frac{f^2(u)}{T} \int_{-\infty}^{\infty} W(u_1-v)\ \{W(u_2+v) + W(u_2-v)\}dv \quad \ldots\ldots (A.15)$$

so the 2 estimates are not independent. Neglecting $\int_{-\infty}^{\infty} W(v)\ W(v + 2v)dv$ which is small compared to the integral of the square, $VAR(f_W(u)) \approx \frac{f^2(u)}{T} \int_{-\infty}^{\infty} W^2(v)dv$.

2T is the length of time over which the signal is recorded. Let

$$I = \int_{-T}^{T} W^2(t)dt. \quad (A.16)$$

Then, $VAR(f_W(u)) \approx f^2(u)\ I/T$ and so I/T is the proportional reduction in the variance due to smoothing when the lag window W(t) is used.

A concept occasionally used is that of band-width for a spectral window. If

$$w(u) = 1/b,\ -b/2 \leq u \leq b/2$$

is a rectangular window, it has a unique band-width, b, in the frequency domain. The variance of an estimator that is smoothed via this window is $f^2(u)/Tb$.

For non-rectangular windows, the equivalent band-width is defined as $b = 1/I$ and the standardized band-width is bT. Note that the variance times band-width is constant and hence large band-width implies small bias. Some common windows and and their properties are discussed in Jenkins and Watts, Chapter 6.

A commonly used window is the Tukey window:

$$W(t) = \frac{1}{2}(1 + \cos(\pi t/L)) \quad |t| \leq L. \tag{A.17}$$

This lag window has the associated spectral window

$$w(u) = [L \sin(2\pi uL)]/(2\pi uL)(1 - (2uL)^2). \tag{A.18}$$

For the Tukey window,

$$I = \int_{-\infty}^{\infty} w^2(u)\, du = 3L/4 \tag{A.19.a}$$

$$\text{d.f.} = 2T/I = 8T/3L \tag{A.19.b}$$

$$\text{band-width} = 4/3L \tag{A.19.c}$$

$$\text{variance ratio} = 3L/4T. \tag{A.19.d}$$

For the truncated estimate the Tukey spectral window corresponds to weighted averages, with weighting factors of (1/4, 1/2, 1/4) for $u - \Delta u$, u and $u + \Delta u$ respectively.

(A-i) Direct Spectral Estimates

Since most observations are digitized the integrals are replaced by sums in the calculations. Suppose $X(t)$ is observed at discrete times $k\Delta t$, $k = -m, -m+1, \ldots, m-1$ ($n = 2m$ observations), then

$$\int_{-m\Delta t}^{(m-1)\Delta t} X(t) e^{i2\pi ut}\, dt \triangleq$$

$$\sum_{k=-m}^{m-1} X(k\Delta t)\, \{\cos(2\pi uk\Delta t) + i \sin(2\pi ku\Delta t)\}\, \Delta t.$$

If $u_k = k/n\Delta t$, $\Delta u = 1/n\Delta t$, $k = -m, \ldots, m$, and if

$$A(u) = \sum_{k=-m}^{m-1} X(k\Delta t)\cos(2\pi uk\Delta t) \qquad (A.20.a)$$

$$B(u) = \sum_{k=-m}^{m-1} X(k\Delta t)\sin(2\pi uk\Delta t), \qquad (A.20.b)$$

then the sample spectrum at u_k is

$$\hat{f}(u_k) = 2[A^2(u_k) + B^2(u_k)]\,\Delta t/n \qquad (A.21.a)$$

at $k = \pm 1, \pm 2, \ldots, \pm (m-1)$.

At the end points, $u_k = 0$ and $u_k = 1/(2\Delta t)$,

$$\hat{f}(u_k) = [A^2(u_k) + B^2(u_k)]\,\Delta t/n \qquad (A.21.b)$$

with a corresponding loss of 1 degree of freedom.

$\frac{\hat{f}(u_k)}{\Delta t f(u_k)}$ has a chi-squared distribution with 2 degrees of freedom, for $k = \pm 1, \pm 2, \ldots, \pm (m-1)$ and 1 degree of freedom for $k = 0$ and $k = m$, for a total of $2(m-1) + 2 = 2m = n$ degrees of freedom. (Note that, by the symmetry of the spectrum, there are only $(m-1) + 1$ independent estimates rather than $2(m)$ independent estimates). These n degrees of freedom are distributed over the various frequency bands. If the true spectrum is reasonably constant over ℓ adjacent bands (say, over $u \pm i\,\Delta u$, $i = 1, \ldots, \ell/2$) and if

$$\overline{\hat{f}(u)} = \sum_{i=1}^{\ell/2} [\hat{f}(u + i\Delta u) + \hat{f}(u - i\Delta u)]/\ell$$

then $\frac{\ell\overline{\hat{f}(u)}}{\Delta t f(u)}$ has a chi-squared distribution with 2ℓ degrees of freedom.

$\mathrm{VAR}[\overline{\hat{f}(u)}] = 4\ell/\ell^2 = 4/\ell$ is now decreased. If successive

bands are averaged without overlapping, $n/2\ell$ independent estimates are obtained, each with 2ℓ degrees of freedom. If overlapping occurs, the estimates will not be statistically independent.

In this direct procedure (known as the Cooley-Tukey procedure) a "fader" or "taper" is usually applied to the original series before transformation in order to reduce bias. This is a function $a(t)$ such that $a(t)$ increases from 0 to 1 in $[0,S_1)$, equals 1 on $[S_1,S_2)$ and decreases to 0 on $[S_2,T)$. Usually $a(t + T/2) = a(T/_2 - t)$.

A typical fader, with $S_1 = T/10$, is

$$a(t) = \begin{cases} \frac{1}{2}[1 - \cos(\pi t/S_1)] \equiv \sin^2(\pi t/2\ S_1), & 0 \le t \le S_1 \\ 1 & S_1 \le t \le T - S_1 \\ \frac{1}{2}[1 - \cos(\pi(T-t)/S_1)] \equiv \sin^2(\pi(T-t)/2\ S_1), & T - S_1 \le t \le T \end{cases} \quad \ldots\ (A.22)$$

The signal $X(t)$ is first multiplied by $a(t)$, where now we assume $X(t)$ is observed on $[0,T]$. After multiplication, $a(t)\ X(t)$ is transformed and then averaged as above. To see the effect of the "taper", let $u(x) = a(t/T)$ so that $u(x)$ is defined on $[0,1]$. If $Z(u)$ is the transform of $a(t)\ X(t)$ then the direct estimate of the spectrum is $|Z(u)|^2\ (2\Delta t/n)$ at frequency u (where $n\Delta t = T$).

However,

$$E(|Z(u)|^2) \approx \left[\sum_{k=1}^{n} a^2(k)\right] f(u) = \left[\int_0^1 u^2(x)dx\right] f(u). \quad (A.23)$$

Hence, the true spectral estimate becomes

$$2\Delta t|Z(u)|^2/(n\int_0^1 u^2(x)dx). \qquad (A.24)$$

For the cosine taper above,

$$\int_0^1 u^2(x)dx = 2\int_0^{.1} \sin^4(\pi x/.2)dx + .8$$

$$= 2(\tfrac{3}{4})(\tfrac{\pi}{4})(\tfrac{.2}{\pi}) + .8 \tilde{=} .875.$$

The smoothed (averaged) estimates are weighted chi-squared variables, after division by f(u). The distribution of these estimates is approximated by a constant times a chi-squared variable, where the constant and degrees of freedom are obtained by equating means and variances.

$$d = 2f^2(u)/VAR(\overline{\hat{f}(u)}) \qquad (A.25.a)$$

$$c = E(\overline{\hat{f}(u)})/d \qquad (A.25.b)$$

If m + 1 final estimates are obtained the degrees of freedom become

$$= 2n\,[\int_0^1 u^2(x)dx]^2/(m+1)[\int_0^1 u^4(x)dx]. \qquad (A.26.a)$$

For the cosine taper,

$$\int_0^1 u^4(x)dx = .8 + 2\int_0^{.1} \sin^8(\tfrac{\pi x}{.2})dx = .8055 \qquad (A.26.b)$$

The band width is d/2N.

The above is true for non-overlapping bands. If averaging occurs in overlapping bands, the degrees of freedom are

$$(2L + 1)[\int_0^1 u^2(x)dx]^2/[\int_0^1 u^4(x)dx] \qquad (A.26.c)$$

where 2L + 1 is the number of elementary bands averaged. In either case, the degrees of freedom at each end point are half the figures given above.

The computer routine uses a fast Fourier transform coded in a subroutine called NLOGN. If Z(I), I=1, ..., N is a (complex) input array, NLOGN, produces an output array

$$\tilde{Z}(K) = \sum_{J=1}^{N} \exp\{2\pi i(K-1)(J-1)\} Z(J) \qquad (A.27)$$

K = 1, ..., N. The number of entries in the input and output array are equal.

X(k) ≡ X(kΔt), k = 0,1, ..., n-1 is the original data array, k = 0, ..., n-1 and N = n.

The steps in the computer analysis are

1. Taper X(k) with the cosine taper by multiplying the taper and the series. Load the result into the Z array.
2. Fill out the Z array with zeroes in order to get NN = 2M(2L + 1) - 1 points if M + 1 estimates are desired.
3. Call NLOGN to get $\tilde{Z}(I)$, I=1, 2, ..., NN.

The elementary spectral estimates are

$$F(I) = 2|\tilde{Z}(I)|^2 \Delta t/.875\ NN \qquad (A.28)$$

4. Average the elementary estimates,

(a) $\sum_{I=1}^{L} F(I)/L$ is the estimate at frequency 0.

(b) $\{\sum_{I=(2K-1)L+K}^{(2K+1)L+K} F(I)\}/2L + 1$ is the estimate at frequency $(2L + 1)K/2\Delta t$.

(c) $\sum_{I=(2M-1)L+M}^{M(2L+1)-1} F(I)$ is the estimate at frequency $1/2\Delta t$.

More closely spaced estimates could be obtained by allowing the bands to slide across the entire frequency band - in this case the estimates would not be independent.

Thus, for example, the first non-zero frequency could be $(L + 2)/2\Delta t$ and could involve elementary estimates 2 through $2L + 3$, the next frequency could be $(L + 3)/2\Delta t$, etc. Confidence intervals for the estimates would be obtained by using the chi-squared distribution and the appropriate d.f. ($2L + 1$ for the center estimates, L for the end points).

(A-ii) Indirect Spectral Estimates

Suppose $X(j) \equiv X(j\Delta t)$, $j=0, \ldots, n$ is a zero-mean process.

Let $\hat{\Gamma}(k) = \frac{1}{n} \sum_{j=0}^{n-k-1} X(j)\, X(j+k)$ for $k=0, \ldots, m$ (or $\hat{\Gamma}'(k) = \hat{\Gamma}(k)\, n/(n-k)$). Then

$$\hat{f}(u) = \Delta t \sum_{k=-m}^{m} \hat{\Gamma}(k) e^{-i2\pi uk\Delta t}, \quad -1/2\Delta t \leq u \leq 1/2\Delta t$$

is another estimator of the true spectrum, based on a covariance function with maximum lag m. As discussed previously the estimates must be smoothed with either a lag or spectral window. In addition, the spectrum is only computed for positive frequencies so the estimates are doubled to obtain

$$\hat{f}(u) = 2\Delta t[\hat{\Gamma}(0) + 2 \sum_{k=1}^{m-1} \hat{\Gamma}(k) W(k) \cos(2\pi uk\Delta t)] \qquad (A.29)$$

for $0 \leq u \leq 1/(2\Delta t)$. Here $W(k) \equiv W(k\Delta t)$ and the maximum lag is m.

APPENDIX B

Cross-Spectral Analysis

When two or more time series are observed, one can study their inter-relationship by using cross-spectral analysis. Subscripts will be used to indicate the different series and only the case of two series will be discussed.

Suppose $X_1(s)$ and $X_2(s)$ are two zero-mean time series and let $X(s) = (X_1(s), X_2(s))$. $X(s)$ is a second-order stationary vector process if the covariance matrix, $\Gamma_{12}(u) = E(X^t(s)\, X(s+u))$ only depends on u (the superscript t indicates the vector transpose here). $\Gamma_{12}(u)$ is called the cross-covariance function. Note that $\Gamma_{21}(u) = \Gamma_{12}(-u)$.

There are two representation theorems that correspond to Theorems I and II of Appendix A, with scalers replaced by vectors and matrices.

In particular, for a second-order stationary vector process

$$X_j(t) = \int \cos(\nu t)\, \alpha_j(d\nu) + \int \sin(\nu t)\, \beta_j(d\nu) \qquad \text{(B.1)}$$

where $COV(\alpha_j(d\nu)\, \alpha_k(d\nu)) = COV(\beta_j(d\nu)\, \beta_k(d\nu)) = c_{jk}(d\nu)$ $- COV(\alpha_j(d\nu)\, \beta_k(d\nu)) = COV(\beta_j(d\nu)\, \alpha_k(d\nu)) = q_{jk}(d\nu)$ and all other covariances are 0.

$$\Gamma(t) = \int e^{it\nu}\, dF(\nu) = \int \cos(t\nu)\, c(d\nu) - \int \sin(t\nu)\, q(d\nu) \qquad \text{.... (B.2),}$$

where $F(\nu)$ is a matrix with Hermitian non-negative increments

in ν, $c(\nu)$ is a real symmetric matrix with entries $c_{jk}(\nu)$ and $q_{jk}(\nu)$ is a real, skew-symmetrix matric with entries $q_{jk}(\nu)$. $c(\nu)$ is called the co-spectral distribution and $q(\nu)$ is called the quadrature spectral distribution.

$$\rho^2_{jk}(\nu) = [c^2_{jk}(\nu) + q^2_{jk}(\nu)]/[c_{jj}(\nu)\, c_{kk}(\nu)]$$

is the co-herence spectrum and

$\theta_{jk}(\nu) = \arctan(-q_{jk}(\nu)/c_{jk}(\nu))$ is the phase-spectrum.

We will again replace ν by $2\pi u$ and use capital letters to denote the various entries, so that

$$F_{jk}(u) = \frac{1}{2}(C_{jk}(u) - i\, Q_{jk}(u))$$

$$\theta_{jk}(u) = \arctan[-Q_{jk}(u)/C_{jk}(u)].$$

Once again one can either estimate the cross spectral densities directly by transforming the original series or by calculating cross-covariances and then transforming the cross-covariances.

(B.i) Direct Estimation

The computer analysis for direct estimation is outlined below.

1. Let $X_1(k)$, $k=0, \ldots, n-1$ and $X_2(k)$, $k=0, \ldots, n-1$ be the 2 original series. Taper each series with the $\sin^2$ taper.
2. Let $Z_i(k) = X_i(k-1)$, $k=1, \ldots, n$ and fill out the Z-arrays to get $NN = 2M(2L + 1) - 1 \geq n$ points if $M + 1$ estimates are desired (each based on $2L + 1$ elementary estimates).
3. Transform each series to get $\tilde{Z}_i(k)$, $i = 1,2$, $k = 1, \ldots, NN$.
4. The elementary estimate of the cross spectrum is

$$F_{12}(I) = [2\, \tilde{Z}_1(I)\ \ \tilde{Z}^*_2(I)]\Delta t/(.875)NN$$

5. Average the elementary estimates over 2L + 1 points (except for the first and last estimates which are obtained by averaging over L points) to get estimates M + 1 estimates, with the middle estimates centered at $(2L + 1)K/2\Delta t$, k=1, ..., M.

6. The real part of the above average is half of the co-spectrum and the imaginary part is half of the quadrature spectrum, $(F_{12} = (C_{12} - i\, Q_{12})/2)$ omitting the frequency argument.

7. The coherence spectrum is

$$\rho_{12}^2 = (C_{12}^2 + Q_{12}^2)/F_1 \cdot F_2$$

where F_1 and F_2 are the individual spectra and the coherence spectrum is calculated after averaging (else it will be identically one).

The phase spectrum is $\theta_{12} = \arctan(-Q_{12}/C_{12})$ which can be made continuous by "guessing" so that the true arctangent rather than the principal value is obtained.

(B.ii) Indirect Spectral Estimates

If $\Gamma_{12}(k)$ is the estimated covariance with M lags (k=0, ± 1, ± 2, ..., ± M) then the indirect approach is outlined below.

1. Let $\Gamma^e(k) = \frac{1}{2}[\Gamma_{12}(k) + \Gamma_{12}(-k)]$

$$\Gamma^o(k) = \frac{1}{2}[\Gamma_{12}(k) - \Gamma_{12}(-k)].$$

2. Form

$$Z_1(k) = \Gamma^e(k-1)\, W(k-1) \quad k=1, \ldots, L + 1$$

$$Z_2(k) = \Gamma^o(k-1)\, W(k-1) \quad k=1, \ldots, L + 1$$

where W(k) is the lag window, $(L \leq M)$.

3. If the cross spectrum is desired at frequency spacing $1/(N_2\ \Delta t)$ from 0 to $1/2\Delta t$ where $N_2 > N$, add zeroes to the arrays to get N_2 entries. Once again, if $N_2 = 2L$, estimates are obtained at frequencies $i/2L\Delta t$, $i=0, 1, \ldots, L$.

4. Fourier transform, via FOURT, the Z arrays to get $\tilde{Z}_i(k)$. The smoothed estimates of the co- and quadrature spectrum are

$$C_{12}(k) = [2\ \mathrm{Re}(Z_1(k)) - r^e(0)]2\Delta t$$

and $Q_{12}(k) = 4\Delta t\ \mathrm{Im}(\tilde{Z}_2(k))$ at frequencies $(k-1)/(2L\Delta t)$, $k=1, \ldots, L+1$.

(B.iii) Other comments on Cross-Spectra

If both series are subjected to the same linear filters the coherence and phase spectra are unaffected. If a trend is suspected one can difference the 2 series and improve the final estimates (see Jenkins and Watts, Sec. 8.4.5).

One can also re-align the 2 series to get better estimates of the coherence. The raw estimates of the cross-spectrum can be obtained without recalculation by multiplying the original cross-spectrum by $\exp\{-i2\pi\tau u\}$ where τ is the time shift. For the estimates based on the cross-covariance, new even and odd estimates are needed (see Jenkins and Watts, Sec. 9.3.4).

APPENDIX C

Variance and Covariance Calculations

Throughout this appendix, we assume we have N observations, M estimates and d degrees of freedom. The variance and covariance calculations are based on the treatment in Hannan, Chapter V. Carats will be used to denote estimates and frequency will be measured in radians. The proofs of the main theorems can be carried out by using multivariate analysis (including complex multivariate analysis). Jenkins and Watts, Chapter 9, pp. 372-373 and appendix A.9.1 present an alternative approach.

The following theorem is the key theorem for practical covariance calculation.

THEOREM I. (Hannan, Theorem 9, p. 280). Under suitable conditions on the moments of X(t),

$$\lim_{N\to\infty} \frac{N}{M} \operatorname{COV}[\hat{f}_{ij}(\nu_1), \hat{f}_{k\ell}(\nu_2 + \pi P/M)] = 0, \qquad \text{(C.1.a)}$$

for $\nu \neq \pi/2 (\mathrm{mod} 2\pi)$.

$$\lim_{N\to\infty} \frac{N}{M} \operatorname{COV}[\hat{f}_{ij}(\nu), \hat{f}_{k\ell}(\nu)] = \frac{2N}{dM} f_{ik}(\nu)\, f_{\ell j}(\nu), \qquad \text{(C.1.b)}$$

for $\nu \neq 0, 2\pi$.

$$\lim_{N\to\infty} \frac{N}{M} \operatorname{COV}[\hat{f}_{ij}(\nu_1), \hat{f}_{k\ell}(\nu_2)] =$$

$$(2N/dM)[f_{ik}(\nu_1)\, f_{\ell j}(\nu_2) + f_{i\ell}(\nu_1)\, f_{kj}(\nu_2)], \qquad \text{(C.1.c)}$$

for $\nu_1 = \pm \nu_2 = 0, 2\pi$.

Since most other estimates in cross-spectral analysis are functions of f_{ij} and $f_{k\ell}$, one can derive the desired covariances quite readily.

For example, for N/M large (omitting the dependence on ν) we have (for N large)

$$\begin{aligned}(N/M)\ VAR(\hat{C}_{ij}) &= (N/M)\ VAR(\hat{f}_{ij} + \hat{f}_{ji}) \\ &= [N/M][VAR(\hat{f}_{ij}) + VAR(\hat{f}_{ji}) + 2\ COV(\hat{f}_{ij},\hat{f}_{ji})] \\ &= [2N/Md][f_{ii}f_{jj} + 2f_{ij}f_{ji} + f_{jj}f_{ii}] \\ &= [4N/Md][f_{ii}f_{jj}\ (1 - \rho_{ij}^2) + C_{ij}^2/2] \end{aligned} \qquad \ldots\ldots\ (C.2)$$

Note that $f_{ii} = 2\ C_{ii}$ is the spectrum of $X_i(t)$, and recall that $COV(ZW) = E(ZW^*)$, assuming $E(Z) = E(W) = 0$.

Similarly[+], since $\hat{C}_{k\ell} = (\hat{f}_{k\ell} + \hat{f}_{\ell k})$ and $\hat{Q}_{k\ell} = i[\hat{f}_{k\ell} - \hat{f}_{\ell k}]$ we have

$$\begin{aligned}COV(\hat{C}_{ij},\hat{C}_{k\ell}) &= COV[(\hat{f}_{ij} + \hat{f}_{ji})(\hat{f}_{k\ell} + \hat{f}_{\ell k})] \\ &= E(\hat{f}_{ij}\ \hat{f}_{k\ell} + \hat{f}_{ji}\ \hat{f}_{k\ell} + \hat{f}_{ij}\ \hat{f}_{\ell k} + \hat{f}_{ji}\ \hat{f}_{\ell k}) \\ &= 2[f_{ik}\ f_{\ell j} + f_{jk}\ f_{\ell i} + f_{i\ell}\ f_{kj} + f_{j\ell}\ f_{ki}]/d \\ &= [C_{ik}\ C_{\ell j} - Q_{ik}\ Q_{\ell j} + C_{i\ell}\ C_{kj} - Q_{i\ell}\ Q_{kj}]/d \end{aligned} \qquad \ldots\ldots\ (C.3)$$

$$\begin{aligned}VAR(\hat{Q}_{ij}) &= VAR\ (\hat{f}_{ij} - \hat{f}_{ij}) \\ &= E(\hat{f}_{ij}^2 - 2\hat{f}_{ij}\ \hat{f}_{ij} + \hat{f}_{ij}^2) \\ &= 4\{f_{ii}f_{jj}[1 - \rho_{ij}^2] + \tfrac{1}{2}\ Q_{ij}^2\}/d \end{aligned} \qquad (C.4)$$

[+]Assume, without loss of generality, that $E(\hat{f}\ \ ) = 0$ for the following calculations.

$$\begin{aligned}
\mathrm{COV}(\hat{Q}_{ij},\hat{Q}_{k\ell}) &= -\,\mathrm{COV}\,(\hat{f}_{ij} - \hat{f}_{ji})(\hat{f}_{k\ell} - \hat{f}_{\ell k})\} \\
&= -\quad E[\hat{f}_{ij}\,\hat{f}_{k\ell} - \hat{f}_{ij}\,\hat{f}_{\ell k} - \hat{f}_{ji}\,\hat{f}_{k\ell} + \hat{f}_{ji}\,\hat{f}_{\ell k}] \\
&= [C_{ik}\,C_{\ell j} - Q_{ik}\,Q_{\ell j} - C_{i\ell}C_{kj} + Q_{i\ell}\,Q_{kj}]/d
\end{aligned}$$

..... (C.5)

$$\mathrm{COV}(\hat{Q}_{ij},\hat{C}_{ij}) = 2C_{ij}\,Q_{ij}/d \qquad \text{(C.6)}$$

$$\begin{aligned}
\mathrm{COV}(\hat{C}_{ij},\hat{Q}_{k\ell}) &= \mathrm{COV}\{(\hat{f}_{ij} + \hat{f}_{ji}\ ,\ i(\hat{f}_{k\ell} - \hat{f}_{\ell k})\} \\
&= -\quad iE\{\hat{f}_{ij}\,\hat{f}_{k\ell} - \hat{f}_{ij}\,\hat{f}_{\ell k} + \hat{f}_{ji}\,\hat{f}_{k\ell} - \hat{f}_{ji}\,\hat{f}_{\ell k}\} \\
&= -\,[Q_{\ell j}\,C_{ik} + Q_{ik}\,C_{\ell j} + Q_{\ell i}\,C_{ji} + Q_{jk}\,C_{\ell i}]/d
\end{aligned}$$

..... (C.7.a)

$$\begin{aligned}
\mathrm{COV}(\hat{Q}_{k\ell},\hat{C}_{ij}) &= -i\mathrm{COV}((\hat{f}_{k\ell} - \hat{f}_{\ell k})(\hat{f}_{ij} + \hat{f}_{ji})) \\
&= -iE\{\hat{f}_{k\ell}\,\hat{f}_{ij} - \hat{f}_{\ell k}\,\hat{f}_{ij} + \hat{f}_{k\ell}\,\hat{f}_{ji} - \hat{f}_{\ell k}\,\hat{f}_{ji}\} \\
&= \mathrm{COV}(\hat{C}_{ij}\,\hat{Q}_{k\ell}) \qquad \text{(C.7.b)}
\end{aligned}$$

The covariance of the θ's and ρ's can be approximated by using propagation of error - namely by expanding in a Taylor series and dropping higher order terms.

Thus, for $\hat{\theta}_{ij} = \arctan(-\hat{Q}_{ij}/\hat{C}_{ij})$ we have

$$\begin{aligned}
\theta_{ij} - \arctan[\hat{\theta}_{ij}/\hat{C}_{ij}] &= \frac{\partial\hat{\theta}_{ij}}{\partial C_{ij}}\,(C_{ij} - \hat{C}_{ij}) + \frac{\partial\hat{\theta}_{ij}}{\partial Q_{ij}}\,[Q_{ij} - \hat{Q}_{ij}] \\
&= \{Q_{ij}/(\hat{C}_{ij}^2 + \hat{Q}_{ij}^2)\}\{C_{ij} - \hat{C}_{ij}\} \\
&\quad -\{C_{ij}/(C_{ij}^2 + Q_{ij}^2)\}\{Q_{ij} - \hat{Q}_{ij}\}
\end{aligned}$$

..... (C.8)

$$\begin{aligned}\mathrm{VAR}(\hat{\theta}_{ij}) &= \{Q_{ij}/(C_{ij}^2 + Q_{ij}^2)\}^2\ \mathrm{VAR}(\hat{C}_{ij}) \\ &+ \{C_{ij}/(C_{ij}^2 + Q_{ij}^2)\}^2\ \mathrm{VAR}(\hat{Q}_{ij}) \\ &- 2\{C_{ij}\ Q_{ij}/(C_{ij}^2 + Q_{ij}^2)^2\}\ \mathrm{COV}(\hat{C}_{ij}\ \hat{Q}_{ij}) \\ &= (1 - \rho_{ij}^2)/d\rho_{ij}^2 \qquad \text{(C.9)}\end{aligned}$$

Similarily,

$$\mathrm{VAR}(\hat{\rho}_{ij}^2) = (1 - \rho_{ij}^2)^2/d \qquad \text{(C.10)}$$

Covariances can also be obtained by multiplying the appropriate expansions and then taking expected values. In particular $\mathrm{COV}(\hat{\theta}_{ij},\hat{\theta}_{k\ell})$ will be required for confidence interval construction in the location routines.

$$\begin{aligned}\mathrm{COV}(\hat{\theta}_{ij},\hat{\theta}_{k\ell}) &= [Q_{ij}\ \hat{Q}_{k\ell}\ \mathrm{COV}(\hat{C}_{ij}\ \hat{C}_{k\ell}) - C_{ij}\ Q_{k\ell}\mathrm{COV}(\hat{C}_{k\ell}\ \hat{Q}_{ij}) \\ &- Q_{ij}\ C_{k\ell}\ \mathrm{COV}(\hat{C}_{ij}\ \hat{Q}_{k\ell}) \\ &+ C_{ij}\ C_{k\ell}\ \mathrm{COV}(\hat{Q}_{ij}\ \hat{Q}_{k\ell})]/\{(C_{ij}^2 + Q_{ij}^2)(C_{k\ell}^2 + Q_{k\ell}^2)\} \\ &\qquad \text{..... (C.11)}\end{aligned}$$

The time lags estimated are linear combinations of the θ_{ij}'s, if the estimates are least squares estimates. Thus,

$$\tau_{ij} = \sum_{p=1}^{N} \theta_{ij}(p)\ p(\Delta\nu)/\sum_{p=1}^{N} p^2(\Delta\nu)^2$$

$$\mathrm{VAR}(\tau_{ij}) = \sum_{p=1}^{N} p^2(\Delta\nu)^2\ \mathrm{VAR}(\hat{\theta}_{ij}(p))/(\sum_{p=1}^{N} p^2(\Delta\nu)^2)^2$$

$$\begin{aligned}\mathrm{COV}(\tau_{ij}\tau_{k\ell}) &= \sum_{p=1}^{N}\sum_{q=1}^{N} pq\ \mathrm{COV}(\hat{\theta}_{ij}(p),\hat{\theta}_{k\ell}(q))(\Delta\lambda)^2/[\sum_{p=1}^{N} p^2(\Delta\lambda)^2]^2 \\ &= \sum_{p=1}^{N} p^2\ \mathrm{COV}(\hat{\theta}_{ij}(p),\hat{\theta}_{k\ell}(p))(\Delta\nu)^2/[\sum_{p=1}^{N} p^2(\Delta\nu)^2]^2 \\ &= \sum_{p=1}^{N} p^2\ \mathrm{COV}(\theta_{ij}(p),\theta_{k\ell}(p))/(\sum_{p=1}^{N} p^2)^2\ (\Delta\nu)^2.\end{aligned}$$

For spherical location,

$\delta_1 = (CS)$,

$\delta_2 = C(S + \tau_{12})$ and

$\delta_3 = C(S + \tau_{13})$

are used.

Assuming S and τ_{ij} are independent, and using propagation of error, we have

$$VAR(\delta_1) = C^2\ VAR(S)$$

$$VAR(\delta_2) = C^2[VAR(S) + VAR(\tau_{12})]$$

$$VAR(\delta_3) = C^2[VAR(S) + VAR(\tau_{13})]$$

$$COV(\delta_1,\delta_2) = C^2\ VAR(S)$$

$$COV(\delta_1,\delta_3) = C^2\ VAR(S)$$

$$COV(\delta_2,\delta_3) = C^2[VAR(S) + COV(\tau_{12},\tau_{13})].$$

This covariance matrix is required in Appendix D.

For plane location, the required covariance matrix is given in Appendix E.

APPENDIX D

Spherical Location

The equations used for spherical location are (c.f. eqns. 25 - primes are dropped for typographical convenience).

$$\delta_1^2 = r_1^2 + r_2^2 + r_3^2 \tag{D.1}$$

$$\delta_2^2 = (r_1 - x_2)^2 + r_2^2 + r_3^2 \tag{D.2}$$

$$\delta_3^2 = (r_1 - x_3)^2 + (r_2 - y_3)^2 + r_3^2 \tag{D.3}$$

In these equations,

(i) $\delta_1^2 = (cS)^2$, $\delta_2^2 = [c(S + \tau_{12})]^2$, $\delta_3 = [c(S + \tau_{13})]^2$,

(ii) c is the speed of sound,

(iii) S is the time from initiation at the source to its reception at microphone 1.

(iv) τ_{1j} (j = 1,2) are time lags between reception at microphone 1 and j.

(v) r_1, r_2, r_3 are co-ordinates of the source in a co-ordinate system with origin at microphone 1, and x-y plane in the plane of the three microphones.

(vi) microphone 1 is at location (0,0,0), microphone 2 is at location $(x_2,0,0)$ and microphone 3 is at location $(x_3,y_3,0)$.

Subtracting D.2 from D.1 and D.3 from D.1, we obtain

$$\delta_1^2 - \delta_2^2 = 2x_2 r_1 - x_2^2 \tag{D.4}$$

$$\delta_1^2 - \delta_3^2 = 2x_3 r_1 + 2y_3 r_2 - x_3^2 - y_3^2. \tag{D.5}$$

Hence,

$$r_1 = (\delta_1^2 - \delta_2^2 + x_2^2)/(2x_2) \tag{D.6}$$

$$r_2 = (\delta_1^2 - \delta_3^2 + x_3^2 + y_3^2 - 2x_3\, r_1)/(2y_3) \tag{D.7}$$

$$r_3 = (\delta_1^2 - r_1^2 - r_2^2)^{1/2}. \tag{D.8}$$

These locations have to be converted back to coordinates in the original frame of reference. Suppose the microphones are at P_1, P_2 and P_3, respectively, in the original frame of reference.

Let $D_1 = P_2 - P_1$ (D.9)

and $D_2 = P_3 - P_1$. (D.10)

$(D_2 \cdot D_1)D_1/(D_1 \cdot D_1)$ is the projection of D_2 onto D_1. The un-normalized co-ordinate vectors in the new frame of reference (the one containing the microphones in the x-y plane) are

$$\alpha_1 = D_1 \tag{D.11}$$

$$\alpha_2 = D_2 - (D_2 \cdot D_1)D_1/(D_1 \cdot D_1) \tag{D.12}$$

$$\alpha_3 = D_1 \times D_2. \tag{D.13}$$

The corresponding unit vectors are ($\|\beta\|$ denotes the length of β)

$$U_1 = \alpha_1/\|\alpha_1\| \tag{D.11.a}$$

$$U_2 = \alpha_2/\|\alpha_2\| \tag{D.12.a}$$

$$U_3 = \alpha_3/\|\alpha_3\| \tag{D.13.a}$$

Microphone 1 is at (0,0,0), microphone 2 is at ($\|D_1\|$,0,0) ($x_2 = \|D_1\|$, $y_2 = 0, z_2 = 0$) and microphone 3 is at $((D_2 \cdot D_1)/\|D_1\|, (D_2^2 - (D_2 \cdot D_1)^2/\|D_1\|^2)^{1/2}, 0)$, $(x_3 = (D_2 \cdot D_1)/\|D_1\|, y_3 = (D_2^2 - (D_2 \cdot D_1)^2/\|D_1\|^2)^{1/2}, z_3 = 0$.

Ignoring the translation by P_1, the new co-ordinate vectors can be expressed as a linear combination of the old co-ordinate vectors, e_1, e_2, e_3

$$U_i = \sum_{j=1}^{3} g_{ij} e_j. \qquad (D.14)$$

In matrix notation,

$$U = Ge. \qquad (D.14.a)$$

The source is at $\sum_{j=1}^{3} r_i U_i$ and hence in the old co-ordinate system the source is located at

$$\sum_{i=1}^{3} r_i g_{ij}, \quad j = 1,2,3, \qquad (D.15)$$

or, in matrix notation at

$$G^t r \qquad (D.15.a)$$

where G^t is the transpose of G.

Element (i,j) of G is the $j^{\underline{th}}$ element of vector U_i, so that

$$G = \begin{pmatrix} U_1^t \\ U_2^t \\ U_3^t \end{pmatrix} \qquad (D.16)$$

and $G^t = (U_1, U_2, U_3)$. $\qquad (D.16.a)$

Finally, adding the translation P_1 back in, the source is located at

$$\hat{r}^* = P_1 + G^t r. \tag{D.17}$$

We next obtain approximate confidence limits for the predicted position by linearizing D.6, D.7, and D.8 with respect to δ_1, δ_2, and δ_3.

$$r_j - E(r_j) = \sum_{k=1}^{3} \frac{\partial r_j}{\partial \delta_k} [\delta_k - E(\hat{\delta}_k)] \tag{D.18}$$

$$= \sum_{k=1}^{3} a_{jk} [\delta_k - E(\hat{\delta}_k)], \tag{D.18.a}$$

for $j = 1,2,3$, where

$$a_{11} = \frac{\partial r_1}{\partial \delta_1} = \delta_1/x_1$$

$$a_{12} = \frac{\partial r_1}{\partial \delta_2} = -\delta_2/x_1$$

$$a_{13} = \frac{\partial r_1}{\partial \delta_3} = 0$$

$$a_{21} = \frac{\partial r_2}{\partial \delta_1} = (\delta_1/y_3) - (x_3/y_3)\frac{\partial r_1}{\partial \delta_1} = (\delta_1/y_3) - (x_3/y_3)a_{11}$$

$$a_{22} = \frac{\partial r_2}{\partial \delta_2} = (-x_2/y_2)\frac{\partial r_1}{\partial \delta_2} = -(x_3/y_3)a_{12}$$

$$a_{23} = \frac{\partial r_2}{\partial \delta_3} = -(\delta_3/y_3)$$

$$a_{31} = \frac{\partial r_3}{\partial \delta_1} = (\delta_1 - r_1 a_{11} - r_2 a_{21})/r_3$$

$$a_{32} = \frac{\partial r_3}{\partial \delta_2} = -(r_1 a_{12} + r_2 a_{22})/r_3$$

$$a_{33} = -r_2\, a_{23}/r_3.$$

In vector-matrix notation

$$[r - E(r)] = A[\delta - E(\hat{\delta})], \qquad (D.18.b)$$

where A is a matrix with elements a_{ij}.

The covariance matrix for r is

$$COV(r,r) = E\{[r - E(r)][r - E(r)]^t\}$$

$$= A\ COV(\hat{\delta},\hat{\delta})\ A^t. \qquad (D.19)$$

The covariance matrix for $\hat{r}^*$, the co-ordinates of the source in the original frame of reference, is

$$\Sigma = COV(\hat{r}^*\ \hat{r}^*) = G\ COV(r,r)\ G^t.$$

Hence, an approximate $(1 - \alpha)$ x 100% confidence region for the source r^* is given by

$$(r^* - \hat{r}^*)\ \Sigma^{-1}\ (r^* - \hat{r}^*) \leq \chi^2_3\ (\alpha/2).$$

A simpler procedure is to use a Bonferroni confidence region of the form

$$\hat{r}^*_i \pm z_{\alpha/6}\ [VAR(\hat{r}^*_i)]^{1/2}.$$

Since this gives a confidence box rather than an ellipsoid.

APPENDIX E

Plane Wave Location

Here we will use the definitions given in Appendix D.

$D_1 = P_2 - P_1$, $D_2 = P_3 - P_1$.

$$\cos \alpha_{12} = \frac{c\tau_{12}}{\|D_1\|} \tag{E.1}$$

$$\cos \alpha_{13} = \frac{c\tau_{13}}{\|D_2\|} \tag{E.2}$$

$$v = 1. \tag{E.3}$$

v is the unit velocity vector of the plane wave and the τ's are time lags.

If $D_i = (d_{i1}, d_{i2}, d_{i3})$ then

$$\sum_{k=1}^{3} v_k d_{ik} = c\tau_{12} \tag{E.4}$$

$$\sum_{k=1}^{3} v_k d_{2k} = c\tau_{13} \tag{E.5}$$

$$\sum_{k=1}^{3} v_k^2 = 1. \tag{E.6}$$

These equations must be solved to obtain (v_1, v_2, v_3).

$$v_1 d_{11} + v_2 d_{12} = c\tau_{12} - v_3 d_{13} \tag{E.7}$$

$$v_1 d_{21} + v_2 d_{22} = c\tau_{13} - v_3 d_{23}. \tag{E.8}$$

Hence,

$$v_1 = [(c\tau_{12} - v_3 d_{13})d_{22} - (c\tau_{13} - v_3 d_{23})d_{12}]/[d_{11}d_{22} - d_{12}d_{21}]$$

$$v_2 = [(c\tau_{13} - v_3 d_{23})d_{11} - (c\tau_{12} - v_3 d_{13})d_{21}]/[d_{11}d_{22} - d_{12}d_{21}]$$

or

$$v_1 = b_{11} + b_{12}v_3 \qquad \text{(E.9.a)}$$

$$v_2 = b_{21} + b_{22}v_3 \qquad \text{(E.9.b)}$$

where

$$b_{11} = [c\tau_{12}d_{22} - c\tau_{13}d_{12}]/[d_{11}d_{22} - d_{12}d_{21}] \qquad \text{(E.10.a)}$$

$$b_{12} = [d_{12}d_{23} - d_{13}d_{22}]/[d_{11}d_{22} - d_{12}d_{21}] \qquad \text{(E.10.b)}$$

$$b_{21} = [c\tau_{13}d_{11} - c\tau_{12}d_{21}]/[d_{11}d_{22} - d_{12}d_{21}] \qquad \text{(E.10.c)}$$

$$b_{22} = [d_{23}d_{11} - d_{13}d_{21}]/[d_{11}d_{22} - d_{12}d_{21}]. \qquad \text{(E.10.d)}$$

$v_1^2 + v_2^2 + v_3^2 = 1$ implies

$$(b_{12}^2 + b_{12}^2 + 1)v_3^2 + (2b_{11}b_{12} + 2b_{21}b_{22})v_3 + (b_{11}^2 + b_{21}^2 - 1) = 0$$

or

$$A\,v_3^2 + 2B\,v_3 + C = 0.$$

Hence,

$$v_3 = \frac{-2B \pm \sqrt{4B^2 - 4AC}}{2A} = \frac{-B \pm \sqrt{B^2 - AC}}{A} \qquad \text{(E.11)}$$

where $A = b_{12}^2 + b_{22}^2 + 1$, $B = b_{11}b_{12} + b_{21}b_{22}$ and $C = b_{11}^2 + b_{21}^2 - 1$.

To resolve the sign ambiguity, note v_3 must be negative - the solution with the plus sign on the radical appears because the observed time lags theoretically could arise from a wave traveling orthogonal to the true wave. Hence,

$$v_3 = (- B - \sqrt{B^2 - AC})/A \qquad (E.12)$$

where $A = b_{12}^2 + b_{22}^2 + 1$, $B = b_{11}b_{12} + b_{21}b_{22}$ and $C = b_{11}^2 + b_{21}^2 - 1$.

$$\frac{\partial v_3}{\partial \tau_{12}} = - \left[\frac{\partial B}{\partial \tau_{12}} + \{2B \frac{\partial B}{\partial \tau_{12}} - A \frac{\partial C}{\partial \tau_{12}}\} \frac{1}{\sqrt{B^2 - AC}}\right]/A$$

where $$\frac{\partial B}{\partial \tau_{12}} = [b_{12}\, cd_{22} - b_{22}\, cd_{12}]/(d_{11}d_{22} - d_{12}d_{21})$$

$$\frac{\partial C}{\partial \tau_{12}} = [2b_{11}\, cd_{22} - 2b_{21}\, cd_{21}]/(d_{11}d_{22} - d_{12}d_{21})$$

$$\frac{\partial v_3}{\partial \tau_{13}} = -\left[\frac{\partial B}{\partial \tau_{13}} + \{2B \frac{\partial B}{\partial \tau_{13}} - A \frac{\partial C}{\partial \tau_{13}}\} \frac{1}{\sqrt{B^2 - AC}}\right]/A$$

$$\frac{\partial B}{\partial \tau_{13}} = (- cd_{12}\, b_{12} + cd_{11}\, b_{22})/(d_{11}d_{22} - d_{12}d_{21})$$

$$\frac{\partial C}{\partial \tau_{13}} = (cd_{11}\, b_{21} - cd_{12}b_{11})/(d_{11}d_{22} - d_{12}d_{21}).$$

The covariance matrix for (v_1, v_2, v_3) is

$$VAR(v_3) \begin{bmatrix} b_{12}^2 & b_{12}b_{22} & b_{12} \\ b_{12}b_{22} & b_{22}^2 & b_{22} \\ b_{12} & b_{22} & 1 \end{bmatrix}$$

and $$VAR(v_3) = \left(\frac{\partial v_3}{\partial \tau_{12}}\right)^2 VAR(\tau_{12}) + \left(\frac{\partial v_3}{\partial \tau_{13}}\right)^2 VAR(\tau_{13}) + 2\, COV(\tau_{12}, \tau_{13}) \frac{\partial v_3}{\partial \tau_{12}} \frac{\partial v_3}{\partial \tau_{13}}.$$

The source is located at $- (v_1, v_2, v_3)cS$ where S is the time from initiation of the source until its reception at

microphone 1. The approximate covariance matrix for the source is

$$\mathrm{VAR}(T)c^2 \begin{bmatrix} v_1^2 & v_1v_2 & v_1v_3 \\ v_1v_2 & v_2^2 & v_2v_3 \\ v_1v_3 & v_2v_3 & v_3^2 \end{bmatrix} + (cS)^2\ \mathrm{COV}(v,v),$$

where COV(v,v) is the covariance matrix of the v_i's, (assuming S is independent of τ_{12} and τ_{13}).

Once again one can construct either more exact ellipsoidal confidence regions or box-like Bonferroni confidence regions.

APPENDIX F

Additional Remarks on Spectra and Covariances

One can also estimate auto and cross covariances by transforming twice - this can actually save computer time if the covariance functions are required. (See Enochson and Ottnes, pp. 247-248).

The procedure to obtain the auto-covariance is as follows:

1. Augment the original series $X(1) \ldots, X(n)$ with n zeroes.
2. Obtain the FFT of the 2n-length sequence, $\tilde{Z}(k)$, $k=1, \ldots, 2n$.
3. Compute the raw spectrum $\tilde{Z}(k) = (\Delta t/N) |\tilde{Z}(k)|^2$, $k=1, \ldots, 2n$.
4. Obtain the inverse FFT of $\tilde{Z}(k)$.
5. Discard the last n points of the inverse transform and multiply the $r^{\underline{th}}$ term by (n/n-r) to get the covariance function.

For cross-covariances the following procedure can be used:

1. Augment $X_i(k)$, $k=1, \ldots, n$, with n zeroes.
2. Obtain the FFT of both sequences, $\tilde{Z}_1(k)$ and $\tilde{Z}_2(k)$.
3. Multiply the 2 sequences term by term, to get $Z_3(k) = \tilde{Z}_1(k)\ \tilde{Z}_2^*(k)\ (\Delta t/N)$.
4. Compute the inverse transform of $Z_3(k)$. Then the first n points will be $COV(X_1X_2)$ in reverse order and the last n points will be $COV(X_2X_1)$ in reverse order, after multiplication by (n/n-r).

References

1. Bendat, J.S. and A.G. Piersol, Random data: analysis and measurement procedures, John Wiley and Sons Inc., New York, 1971.

2. Breiman, L., Probability and stochastic processes, with a view toward applications, Houghton-Miflin, Boston, 1969.

3. Colgate, S.A., Enchanced drop coalescence by electric fields in equilibrium. J. Geophys. Rsch. 72 479, 1967.

4. Colgate, S.A. and C. McKee, Electrostatic sound in clouds and lightning, J.Geophys. Rsch. 74, 5379, 1969.

5. Enochson, L.E. and R.K. Ottnes; Digital time series analysis, John Wiley and Sons Inc., 1972.

6. Few, A.A., A.J. Dessler, D.J. Latham and M. Brook, A dominant 200 hertz peak in the acoustic spectrum of thunder; J.Geophys. Rsch. 72, 6149, 1967.

7. Few, A.A., Thunder, Ph.D. Thesis, Rice University, 1968.

8. Few, A.A., Power Spectrum of thunder, J.Geophys. Rsch. 74, 6929, 1969.

9. Few, A.A., Lightning channel reconstruction from thunder measurements, J. Geophys. Rsch., 75, 7517, 1970.

10. Grenander, V. and M. Rosenblatt; Statistical analysis of stationary time series, John Wiley and Sons Inc., New York, 1957.

11. Hannan, E.J.; Multiple time series, John Wiley and Sons, New York, 1970.

12. Holmes, C.R., M. Brook, P. Krehbiel and R. McCrory, On the power spectrum and mechanism of thunder. J. Geophys. Rsch., 76, 2106, 1971.

13. Jenkins, G.M. and D.G. Watts, Spectral analysis and its applications, Holden-Day, San Francisco, 1968.

14. Miller, R.G. Jr., Simultaneous statistical inference Mc-Graw Hill, 1966.

15. McCrory, R., Thunder and its relationship to the structure of lightning, Ph.D. Dissertation, New Mexico Institute of Mining and Technology, May 1971.

16. Rosenblatt, M., Random processes, Oxford University Press, New York, 1962.

17. Szymanski, E.W., Lightning studies with ten centimeter radar, Ph.D. Dissertation, N.M. Inst. of Mining and Tech, May, 1977.

18. Tatarski, V.I., (Translated by R.A. Silverman), Wave propagation in a turbulent medium, McGraw-Hill, New York, 1961.

19. Teer, T.L., Lightning channel structure inside an Arizona thunderstorm, Ph.D. Thesis, Rice University, August, 1973.

20. Uman, M.A., Lightning, McGraw-Hill, New York, 1969.

21. Wilson, C.T.R., Investigations on lightning discharges and the electric field of thunderstorms, Phil. Trans. Roy. Soc. (London) A. 221, 73, 1920.